Scalar fields in cosmology: a dynamical systems approach

G14GDP

MSc Dissertation in

Gravity, Particles and Fields

2017/2018

School of Mathematical Sciences

University of Nottingham

Erik Jensko

Supervisor: Prof. Edmund J. Copeland

I have read and understood the School and University guidelines on plagiarism. I confirm that this work is my own, apart from the acknowledged references.

Abstract

By taking a dynamical systems approach, we show how scalar field quintessence models can be compared with and constrained by observational data. Mathematical methods such as linear stability theory and Lyapunov functions are introduced and then used to analyse the fixed points of cosmological systems. With this technology we are able to deduce the evolutionary behaviour of the different scalar field models, which display a range of phenomenologically interesting properties. We obtain late-time attractor solutions corresponding to the accelerating expansion of the universe, as well as scaling solutions where the barotropic equation of state defines how the universe evolves. The combination of both of these behaviours is achieved for certain quintessence models, which can then satisfy observational constraints. As an example of the power of the dynamical systems approach, we explore current areas of research in string theory as a testing ground for our applications.

Contents

1 Introduction

Since the advent of modern cosmology and the discoveries of the late twentieth century, our view of the Universe has been firmly shifted. The observed accelerated expansion of the Universe has fundamentally changed the way we view many areas of physics, such as with the predicted existence of dark energy, which goes beyond the Standard Model of particle physics. From the Big Bang model of cosmology that describes how the universe evolves, to the theory of inflation that aims to explain the origins of the universe, pioneering research at the frontiers of physics has arisen out of the necessity to understand cosmological observations.

Scalar fields are likely to play an important role in cosmology, already being crucial in both particle physics and quantum field theory. In the early Universe they may describe the inflaton field responsible for inflation or be linked to the spontaneous breaking of symmetries which give particles their mass. They also arise naturally in string theory and can be realised in the compactifications from higher dimensional theories down to four-dimensional spacetime. In quintessence, however, scalar fields are what drive the accelerated expansion of the Universe in present to late times. Because scalar fields evolve with time, they present a possible dynamic explanation for dark energy.

In this work we shall focus on the cosmological applications of quintessence in the form of canonical scalar fields. In particular we will be taking a dynamical systems approach and using methods such as linear stability theory to investigate the dynamics of our models. In recent years, the use of these dynamical system techniques has become increasingly popular due to the qualitative pictures that they can paint (though they date back to the early 1970's [1]-[3]). We will be providing a comprehensive overview of how dynamical systems are employed for scalar field quintessence models, following the work of Bahamonde et al. in [4], and also exploring areas of string theory that are inherently related to scalar fields. String theory, being a strong contender as a consistent framework in which quantum gravity arises, predicts the existence of scalar fields in the Universe which could be the same as those involved in quintessence. Additionally, we will use the same dynamical systems approach to investigate recent claims in string theory [5], which have direct cosmological implications [6].

In Section 2 we begin by covering the basic mathematical tools used when studying dynamical systems. We will introduce linear stability theory and the classifications of fixed

points, treating examples in two-dimensions. A technique used for assessing the stability of fixed points that are non-hyperbolic, meaning one cannot rely on linear stability theory, will also be introduced with an accompanying example. This is called the Lyapunov method. In Section 3 we move on to summarising the relevant aspects of modern cosmology, with a particular emphasis on the most recent observations of the 21^{st} century. We will also introduce Einstein's famous cosmological constant and the cosmological model associated with it, concluding with a discussion of its problems. Section 4 will be devoted to the study of string theory compactifications, revealing how scalar fields are integral to these compactification methods. This will provide the link between string theory and cosmology and introduce the mathematical tools that will be necessary for the topical examples treated in Section 6. Appendix A also contains relevant calculations to accompany the Kaluza-Klein compactification example in Section 4.3.

Section 5 contains the main body of work, where we will apply the dynamical systems techniques to canonical scalar fields in cosmology. Using a change of variables we are able to transform the cosmological equations into a dynamical system defined by a set of coupled autonomous equations. We treat the models associated with three different scalar potentials: the single exponential potential, the double exponential potential and the inverse power-law potential. In all of these examples we assume that the matter content of the universe can be described by a single barotropic equation of state. By analysing the phase space associated with each of these models we can deduce their fundamental properties, such as how a universe would evolve based on different initial conditions. In Section 6 we move on to the topical example in string theory, drawing upon the background knowledge covered in Section 4. We explore the cosmological implications of the claims made in [5] and [6] and see how they impact our quintessence models. Crucially, we use the dynamical systems analysis of Section 5 to determine whether the claims can be satisfied by scalar field quintessence models which also satisfy observational constraints.

In Section 7 we briefly summarise the results from the previous sections and note the utility of the dynamical systems approach. By the end of the work the reader should have a clear understanding of both the roles of scalar fields in cosmology and the applicability of the mathematical methods used. One would also hope that the connections with string theory are not only evident, but that the use of dynamical systems in those regimes also prove to be effective.

1.1 Conventions and Formulas

Here we note some of general conventions that we will adopt throughout. We will be working in natural units where the speed of light c and the reduced Planck constant $\hbar$ are set to one. The constant G refers to Newton's gravitational constant in four spacetime dimensions. Unless stated otherwise, indices with Greek characters μ and ν will run over the full spacetime dimensions and indices with Latin characters i and j will be used for labelling spatial components. We will be using the metric convention $(-,+,\ldots,+)$ and assuming that we are working with a Levi-Cevita connection (zero torsion).

The formulas that will be used throughout the work, but not always explicitly defined, are given by:

$$\Gamma^{a}_{bc} = \frac{1}{2} g^{ad}\big(g_{cd,b} + g_{bd,c} - g_{bc,d}\big) \qquad \text{Christoffel Symbols} \quad (1.1)$$

$$R_{abc}{}^{d} = -2\partial_{[a}\Gamma^{d}{}_{b]c} + 2\Gamma^{\rho}{}_{c[a}\Gamma^{d}{}_{b]\rho} \qquad \text{Riemann Tensor} \quad (1.2)$$

$$R_{ab} = R_{acb}{}^{c} \qquad \text{Ricci Tensor} \quad (1.3)$$

$$R = R_{a}{}^{a} \ . \qquad \text{Ricci Scalar} \quad (1.4)$$

2 Dynamical Systems

Dynamical systems theory is an area of mathematics which has been applied in a wide range of disciplines, from molecular biology to economics to fluid mechanics. It is a crucial tool when wanting to consider the long-term behaviour of any system. In cosmology we are often interested in the asymptotic states of the systems we're modelling, at both the early and late times. Dynamical systems theory presents us a way of characterising that behaviour. For two prominent reviews on dynamical systems in cosmology we refer the reader to [7] and [4].

In this section we will cover the mathematical techniques related to dynamical systems, which will be used throughout this work. In particular we will be focussing on the analysis of fixed points in two dimensions and the behaviour of trajectories in phase space. We will begin with a brief introduction on dynamical systems and fixed points before outlining linear stability theory. For further general reading on these topics see [8]-[10], or [11] for applications in cosmology. We will then move on to some more advanced treatments of dynamical systems to study fixed points that are non-hyperbolic, going beyond linear stability theory. Examples for both cases will be included. In the later sections, these techniques will be employed when considering cosmological models that can be framed as a set of autonomous differential equations, giving useful insight into the dynamics and stability of each model.

2.1 Introduction to Dynamical Systems

Dynamical systems can be classified into two main groups: *differential equations* and *iterated maps*. Systems in which time is continuous are described by differential equations, which is usually the case in cosmology. Iterated maps treat time as a discrete variable, so we shall not be focussing on them here. The class of differential equations that will be of particular importance to us will have just one independent variable, time being a key example. These are known as *ordinary differential equations* (ODE's).

Let us begin by defining the set of variables $x_1, ..., x_n \in X \subseteq \mathbb{R}^n$, which represent coordinates in n dimensional *phase space*. Let us also formally define our independent variable, $t \in \mathbb{R}$, which does not necessarily represent time. As a general framework, a set of

ordinary differential equations describing a dynamical system can be written as [8]

$$\begin{aligned} \dot{x}_1 &= f_1(x_1, ..., x_n) \\ &\vdots \\ \dot{x}_n &= f_n(x_1, ..., x_n) \ , \end{aligned} \tag{2.1}$$

where the overdot represents the derivative with respect to t, such that $\dot{x}_i \equiv \frac{dx_i}{dt}$, and the function f_i is the map $f_i : X \to X$. The system can be described as *autonomous* if there is no explicit dependence on the independent variable t. Writing (2.1) in a more concise, but equivalent way,

$$\dot{\mathbf{x}} = \mathbf{f}(\mathbf{x}) \quad , \tag{2.2}$$

where $\mathbf{x} = (x_1, ..., x_n)$, and the function

$$\mathbf{f}(\mathbf{x}) = \big(f_1(\mathbf{x}), ..., f_n(\mathbf{x})\big) \tag{2.3}$$

can be viewed as a vector field on $\mathbb{R}^n$. We shall restrict ourselves to the case where $\mathbf{f}(\mathbf{x})$ is both smooth and real-valued. If there are areas of the phase space where this does not hold, then the following methods will not be applicable there. For our cosmological examples in later sections, there are some cases where divergences appear in $\mathbf{f}(\mathbf{x})$ for some values of $\mathbf{x}$ and these must be treated with care.

Any particular solution to (2.2) for some initial condition $\mathbf{x_0}$ will correspond to a point moving along a curve in the phase space, which we will label $\psi(t)$. This curve, or solution, $\psi(t)$ is known as the *trajectory* or *orbit*. Hence the phase space is filled with trajectories all starting from different initial conditions. Using this geometric picture we can extract information about the system just by examining the flows of trajectories in the phase space.

2.1.1 Fixed points and stability

Definition 1. *Fixed Point* or *Critical Point* or *Equilibrium Point.* A fixed (or critical or equilibrium) point exists at $\mathbf{x} = \mathbf{x}_*$ if and only if it satisfies $\mathbf{f}(\mathbf{x}_*) = 0$ for an autonomous system of the form (2.2) [10].

If a dynamical system represented by a set of autonomous equations has a fixed point, as defined in Definition 1, then any trajectories originating exactly from that point will be stationary and not evolve in time. To consider what happens under the influence of small

perturbations around this point, or the evolution of trajectories passing close by, we must define its stability.

Definition 2. *Stable Fixed Point* or *Lyapunov Stable Fixed Point.* A fixed point $\mathbf{x}_*$ is considered stable (or Lyapunov stable) if for every $\epsilon > 0$ where ϵ is small, their exists $\delta > 0$ such that $||\psi(t_0) - \mathbf{x}_*|| < \delta$. The solution $\psi(t)$ then satisfies $||\psi(t) - \mathbf{x}_*|| < \epsilon$ for all later times, $t \geq t_0$ [4].

If there exists a stable fixed point, as defined in Definition 2, then all trajectories passing close to the fixed point within some well defined radius will continue to stay within that radius forever (as $t \to \infty$). However, points within that radius need not converge on the stable fixed point. To meet that criteria a stronger definition is needed.

Definition 3. *Asymptotically Stable Fixed Point.* A fixed point $\mathbf{x}_*$ is considered asymptomatically stable if it is stable and their exists a δ such that $||\psi(t_0) - \mathbf{x}_*|| < \delta$. The solution $\psi(t)$ then satisfies $\lim_{t\to\infty} \psi(t) = \mathbf{x}_*$.

If a fixed point is asymptotically stable, as defined in Definition 3, trajectories passing close enough to it will eventually converge on that point. This type of equilibrium point is most relevant for cosmology, with most stable fixed points also being asymptotically stable. Note though that Definition 3 makes no mention of how long it takes for a trajectory to converge on the asymptotically stable fixed point[1]. And finally, an *unstable fixed point* is an equilibrium point which is not stable.

Let us mention a few important things about the phase space of an autonomous dynamical system and the fixed points within it. Ignoring periodic orbits, different trajectories within the phase space cannot cross each other. This is just another way of saying that the solutions to the autonomous ODE are unique, assuming $\mathbf{f}(\mathbf{x})$ is smooth. An orbit between two fixed points is called a *heteroclinic orbit*; these will be of particular importance.

If all of the solutions $\psi(t)$ within a well defined subspace S of the full phase space, $S \subset X \subseteq \mathbb{R}^n$, stay within that subspace for all $t \in \mathbb{R}$, then we call the set of points $\mathbf{x} \in S$ the *invariant set* and the subspace S the *invariant manifold*. In other words, the invariant manifold is not connected to the rest of the phase space by any orbits. A similar concept is that of the *invariant submanifold*: an invariant manifold with dimension one or more less

[1] A further condition known as *exponential stability* gives an estimate on the time taken to converge on the fixed point.

than that of the phase space. Invariant submanifolds separate the phase space into smaller, independent sections which are not connected by any orbits.

Let us give an example in two dimensions, where the invariant submanifold will be a one-dimensional line. Consider the autonomous system

$$\dot{x} = 2x^2 - 3xy^2 + x \tag{2.4}$$

$$\dot{y} = x^3 + 2xy + y \ . \tag{2.5}$$

We can rewrite the first equation (2.4) as

$$\dot{x} = x(2x - 3y^2 + 1) \ . \tag{2.6}$$

Any orbit with the initial condition $x_0 = 0$ will continue to stay on the $x = 0$ line. Likewise, any orbit in the phase space which comes to the $x = 0$ line, say at $t = t_0$, will continue to stay on this line for all $t \geq t_0$. The phase space is divided into points above the $x = 0$ line and points below it, over which no orbit can cross. An important consequence is that only fixed points on this line can have incoming (or outgoing) trajectories that span the whole phase space.

2.2 Linear Stability Theory

To understand the dynamics of trajectories close to a critical point we look to linear stability theory. We can approximate the non-linear dynamics of complicated systems, still of the form $\dot{\mathbf{x}} = \mathbf{f}(\mathbf{x})$, by linearising about a critical point $\mathbf{x}_*$. This approximation works if we assume $\mathbf{f}(\mathbf{x})$ to be sufficiently regular. Taylor expanding $\mathbf{f}(\mathbf{x})$ around the critical point $\mathbf{x}_*$ gives

$$\mathbf{f}(\mathbf{x}) = \mathbf{f}(\mathbf{x}_*) + (\mathbf{x} - \mathbf{x}_*)\frac{\partial \mathbf{f}}{\partial \mathbf{x}}\bigg|_{\mathbf{x}=\mathbf{x}_*} + \ldots \ , \tag{2.7}$$

where we will only need to consider the first partial derivatives [8]. By definition $\mathbf{f}(\mathbf{x}_*) = 0$, so the evolution of the points $(\mathbf{x} - \mathbf{x}_*)$ are governed by the Jacobian matrix evaluated at the critical points,

$$J|_{\mathbf{x}=\mathbf{x}_*} = \frac{\partial \mathbf{f}}{\partial \mathbf{x}}\bigg|_{\mathbf{x}=\mathbf{x}_*} = \begin{bmatrix} \frac{\partial f_1}{\partial x_1} & \cdots & \frac{\partial f_1}{\partial x_n} \\ \vdots & \ddots & \vdots \\ \frac{\partial f_n}{\partial x_1} & \cdots & \frac{\partial f_n}{\partial x_n} \end{bmatrix}_{\mathbf{x}=\mathbf{x}_*} \ . \tag{2.8}$$

The Jacobian matrix is also called the *stability matrix*, and the eigenvalues of (2.8) contain information about the stability of the critical points $\mathbf{x}_*$. The eigenvalues can be found either

by hand, as we will see shortly in the next example, or with computational methods when the system of equations are more complicated. The same can be said for the fixed points of the system.

Let us briefly run through the classification of fixed points for linear systems, which depend on the eigenvalues of its Jacobian matrix at the critical point (2.8). If all the eigenvalues have positive real parts then the point is an *unstable point* (or *repeller*) and trajectories are repelled from it. If all the eigenvalues have negative real part then we have a *stable point* (or *attractor*) and trajectories are attracted to it. If at least two of the eigenvalues have opposite signs then we have a *saddle node*, and trajectories are attracted from certain directions and repelled in others. These three classifications cover the majority of the fixed points found in cosmological systems. We will also encounter *spirals* in two dimensions, which occur when the eigenvalues have a non-zero imaginary part. These can be both stable or unstable, depending on the eigenvalues real part. One can go on to classify a larger variety of critical points (see [8]-[9]), but only these will be relevant for this work.

Linear stability theory, as described above, is valid only when the fixed point is *hyperbolic* [10], i.e. when the non-linear terms of $\mathbf{f}(\mathbf{x})$ do not determine the stability of the critical point.

Definition 4. *Hyperbolic Point.* A fixed point $\mathbf{x}_*$ of the system $\dot{\mathbf{x}} = \mathbf{f}(\mathbf{x})$ is hyperbolic if all of the eigenvalues of its Jacobian matrix have non-zero real part. If not, the point is *non-hyperbolic*.

2.2.1 Example: 2D Linear stability theory

Let us work through a concrete example of applying linear stability theory in two dimensions. Consider the non-linear dynamical system given by

$$\dot{x} = xy^2 - y^2 - 2x + 2 \tag{2.9}$$

$$\dot{y} = yx + y \ . \tag{2.10}$$

The fixed points (x_*, y_*) are at $(1, 0)$, $(-1, \sqrt{2})$ and $(-1, -\sqrt{2})$. The Jacobian matrix is found to be

$$J = \begin{bmatrix} y^2 - 2, & 2xy - 2y \\ y, & x + 1 \end{bmatrix} \ , \tag{2.11}$$

which can be evaluated at each of the fixed points. The eigenvalues can then be found with the *characteristic equation* [8],

$$\det\big(J|_{\mathbf{x}_*} - \mathbb{1}\lambda\big) = 0 \ , \tag{2.12}$$

where λ is the eigenvalue and $\mathbb{1}$ is the identity matrix. Applying this for our Jacobian (2.11) at the first fixed point $(1, 0)$, we obtain the equation

$$(-2 - \lambda)(2 - \lambda) = 0 \ , \tag{2.13}$$

which has the solutions $\lambda = \pm 2$. We can therefore conclude that the fixed point $(1, 0)$ of the system (2.9) & (2.10) is a saddle node.

Now consider the point $(-1, \sqrt{2})$. Applying the same method one finds the eigenvalue equation is simply $\lambda^2 = 0$. This critical point is therefore non-hyperbolic, meaning linear stability theory fails. Most of the cosmological models we will investigate will have hyperbolic fixed points, but not all of them (for example the power-law model in Section 5.5). If we wish to determine the stability of those non-hyperbolic points, we must go beyond linear stability theory.

2.3 Lyapunov Method

In general, determining the stability of non-hyperbolic critical points is not straight forward. The Lyapunov method in relation to most other methods is relatively simple and can be very powerful. The process involves finding what is known as a *Lyapunov function*, which can be thought of as a generalised energy function for the system and will be defined shortly [12]. However, there is no known systematic way of finding such a function and the inability to find one does not reveal anything about the stability of the critical point.

Definition 5. *Lyapunov Function.* Consider the fixed point $\mathbf{x}_*$ of a smooth dynamical system $\dot{\mathbf{x}} = \mathbf{f}(\mathbf{x})$, where $\mathbf{x} \in X \subset \mathbb{R}^n$. Let $V : \mathbb{R}^n \to \mathbb{R}$ be a continuous function in a neighbourhood U of $\mathbf{x}_*$. The function V is a Lyapunov function if it satisfies [13]:

1. $V(\mathbf{x}) > V(\mathbf{x}_*)$
2. V has continuous first derivatives for $\{\mathbf{x} \in U \big| \mathbf{x} \neq \mathbf{x}_*\}$
3. $\dot{V} \leq 0$ for all $\{\mathbf{x} \in U \big| \mathbf{x} \neq \mathbf{x}_*\}$

We understand the third requirement to mean

$$\begin{aligned}\frac{dV(\mathbf{x})}{dt} &= \frac{\partial V}{\partial x_1}\dot{x}_1 + \ldots + \frac{\partial V}{\partial x_n}\dot{x}_n \\ &= \frac{\partial V}{\partial x_1}f_1 + \ldots + \frac{\partial V}{\partial x_n}f_n \\ &= \nabla \cdot \mathbf{f}(\mathbf{x}) \leq 0 \ . \end{aligned} \tag{2.14}$$

The existence of a Lyapunov function, as defined in Definition 5, guarantees the (lyapunov) stability of the associated fixed point $\mathbf{x}_*$. If condition three is replaced by a strict inequality, $\dot{V} < 0$ for all $\{\mathbf{x} \in U \big| \mathbf{x} \neq \mathbf{x}_*\}$, then the fixed point is asymptotically stable. Additionally, if the function $V(\mathbf{x})$ is radially unbounded, such that $V(\mathbf{x}) \to \infty$ as $|\mathbf{x}| \to \infty$, then the fixed point is *globally stable* (or *globally asymptotically stable*). As previously mentioned though, being unable to find a suitable Lyapunov function for a fixed point does not guarantee instability.

2.3.1 Example: Lyapunov method for a non-hyperbolic fixed point

Let us explicitly see how to treat a non-hyperbolic fixed point using the Lyapunov method. We shall consider the dynamical system from section 2.5.2 of [4] as an example, given by the set of autonomous equations

$$\dot{x} = x^2 y - \gamma(x-y)^3 \ , \quad \dot{y} = (x+y)^2 - y \ . \tag{2.15}$$

Consider the fixed point $(x, y) = (0, 0)$. The Jacobian evaluated at the fixed point,

$$J\big|_{(0,0)} = \begin{bmatrix} 2xy - 3\gamma(x-y)^2, & x^2 + 3\gamma(x-y)^2 \\ 2(x+y), & 2(x+y) - 1 \end{bmatrix}_{(0,0)} = \begin{bmatrix} 0, & 0 \\ 0, & -1 \end{bmatrix} \ , \tag{2.16}$$

implies the eigenvalue equation is given by

$$\lambda(1+\lambda) = 0 \ . \tag{2.17}$$

One can immediately see that this fixed point is non-hyperbolic, with one of the eigenvalues equal to negative one $\lambda = -1$ and the other equal to zero $\lambda = 0$.

The Lypapunov candidate function we will be using for the fixed point is [4]

$$V = \frac{1}{2}x^2 + \alpha y^4 \ , \tag{2.18}$$

where α is a positive constant to be determined. It is clear that the Lyapunov function already satisfies the first two requirements in Definition 5, and also that $V(x, y) \to \infty$ as $|(x, y)| \to \infty$. Let us check the third requirement, $\dot{V} \leq 0$ close to the critical point,

$$\dot{V} = x\dot{x} + 4\alpha y^3\dot{y} = x\big(x^2y - \gamma(x-y)^3\big) + 4\alpha y^3\big((x+y)^2 - y\big) \ . \tag{2.19}$$

Around the fixed point (the origin) the lowest order terms will dominate. To see more clearly if the requirement is satisfied, let us introduce polar coordinates $x = r\cos(\theta)$ and $y = r\sin(\theta)$. The derivative of the function, (2.19), then becomes

$$\dot{V} = \Big(-\alpha \sin^4\theta - \gamma\cos\theta(\cos\theta - \sin\theta)^3 + \sin\theta\cos^3\theta\Big)r^4 + \mathcal{O}(r^5) \ . \tag{2.20}$$

One can then verify that for $\gamma > 0$ and sufficiently large values of α, the derivative $\dot{V}$ will be negative [4].

The function given in (2.18) is therefore a suitable lyapunov function, satisfying the requirements in Definition 5 when $\gamma > 0$. In that case, the fixed point $(0, 0)$ is globally asymptotically stable. We have hence demonstrated the effectiveness of the Lyapunov method, along with seeing the usefulness of introducing polar coordinates; both of which we will use in section 5.5.

3 Modern Cosmology

In this section we will briefly review the foundations of modern cosmology (see [14] and [15] for the two main references for this section). We shall start with the key assumption that the *cosmological principle* holds: on sufficiently large scales the Universe is both homogeneous and isotropic. In other words, there are no special points for comoving observers[2] within the Universe [14]-[16]. The other cornerstone of modern cosmology is the overwhelming evidence for the accelerated expansion of the Universe (see Section 3.3). The mysterious source of this accelerated expansion is commonly called dark energy and many theories attempt to explain its nature. One such explanation is Einstein's famous *cosmological constant*, a constant term added to Einstein's field equations resulting in the cosmological model know as the Lambda-cold-dark-matter (ΛCDM) model.

In this section we will begin by introducing elements of Friedmann cosmology and derive the cosmological evolution equations in the presence of a single fluid. We will outline some of the key cosmological observations of the 21$^{\text{st}}$ century and the evidence for dark energy. The cosmological constant and the ΛCDM model will be studied, and we will conclude this section with a short discussion on the cosmological constant problem.

3.1 Friedmann Cosmology

The cosmological principle implies that the spacetime of our universe must be highly symmetric, specifically, that the spatial components (ds_3^3) be maximally symmetric. The most general type of metric describing this spacetime in four dimensions is given by the *Friedmann-Lemaître-Robertson-Walker* (FLRW) metric[3] $g_{\mu\nu}$. In pseudo-spherical, polar coordinates $x^\mu = (t, r, \theta, \phi)$ this can be written as

$$ds^2 = g_{\mu\nu}dx^\mu dx^\nu = -dt^2 + a(t)^2\left(\frac{dr^2}{1-kr^2} + r^2 d\theta^2 + r^2\sin^2\theta d\phi^2\right) \ , \tag{3.1}$$

where $a(t)$ is the scale factor and k is the spatial curvature.[4] The scale factor $a(t)$ gives the rate of expansion of the universe, which we require to be strictly positive. The curvature can take values $k = -1, 0, +1$, each corresponding to a universe with a different spatial

[2]We will usually refer to comoving observers simply as observers. Likewise, we will drop the 'comoving' when describing comoving coordinates. For more details on comoving coordinates see [16].

[3]This can be shown to be true in [17].

[4]Here t is a measure of *cosmological time* with respect to a (comoving) observer.

geometry. For $k = -1$ we say the universe is open (or hyperbolic), for $k = 0$ the universe is flat, and for $k = +1$ the universe is closed (or spherical). We shall be focussing on the case of a spatially flat universe ($k = 0$) for reasons we will soon justify. See [18] for an example of studying cosmological models with non-zero curvature.

To describe the relationship between the geometry of our spacetime and the matter content within the universe, we look to Einstein's field equations,

$$G_{\mu\nu} \equiv R_{\mu\nu} - \frac{1}{2}Rg_{\mu\nu} = \kappa^2 T_{\mu\nu} \quad , \tag{3.2}$$

where $G_{\mu\nu}$ is the Einstein tensor, $R_{\mu\nu}$ is the Ricci curvature tensor defined in (1.3), R is the Ricci scalar defined in (1.4) and $g_{\mu\nu}$ is the metric tensor. The constant κ is defined as $\kappa^2 = \frac{8\pi G}{c^4}$ and $T_{\mu\nu}$ is the *stress-energy-momentum tensor* (or just *energy-momentum tensor*). The energy-momentum tensor is sourced by the matter content within the universe, so again the cosmological principle makes life easier for us. With the assumption of homogeneity and isotropy we can model the matter content as a relativistic *perfect fluid*, being completely characterised by its energy density ρ and pressure p (meaning no off-diagonal terms in the energy-momentum tensor corresponding to shear stress). The energy-momentum tensor can then be written as

$$T^{\mu\nu} = (\rho + p)u^\mu u^\nu + pg^{\mu\nu} \quad , \tag{3.3}$$

where $g^{\mu\nu}$ is the inverse metric, such that $g^{\mu\eta}g_{\eta\nu} = \delta^\mu_\nu$, and u^μ is the four-velocity vector of the fluid flow. The four-velocity is timelike and normalised,

$$u^\mu u_\mu = g^{\mu\nu}u_\nu u_\mu = -1 \quad , \tag{3.4}$$

and has components $u^\mu = (1, 0, 0, 0)$. The relationship between the energy density ρ and pressure p of a perfect fluid is given by an *equation of state* (EoS) of the form $p = p(\rho)$. If the fluid is *barotropic* then the equation of state has the simple linear relation,

$$p = w\rho \quad , \tag{3.5}$$

where w is the *equation of state parameter*. For normal matter[5], w typically takes values in the range $[0, 1]$ - some key cosmological examples being $w = 0$ for matter (non-relativistic particles including baryons and cold dark matter) and $w = \frac{1}{3}$ for radiation (relativistic particles such as photons). The equation of state parameter associated with a cosmological constant, or vacuum energy, is $w = -1$, implying negative pressure.

[5]'Normal' here meaning what we understand to be permitted by macroscopic physics

3.1.1 Evolution equations

Using the Einstein equation (3.2) and the FLRW metric (3.1) one can find the *cosmological equations* relating the scale factor $a(t)$ with the density ρ and pressure p, namely the *Friedmann* and the *Acceleration* equations. This relatively simple calculation involves finding the Christoffel components (1.1) from the metric, plugging them into the Riemann tensor (1.2), and then taking the trace: once to obtain the Ricci tensor (1.3) and again for the Ricci scalar (1.4). The time-time component of Einstein's equation (3.2) give rise to the Friedmann equation,

$$H^2 = \frac{\kappa^2}{3}\rho - \frac{k}{a^2} \quad , \tag{3.6}$$

where H is the *Hubble rate*,

$$H = \frac{\dot{a}}{a} \quad , \tag{3.7}$$

and $\dot{a} \equiv \frac{da}{dt}$ is the derivative of a with respect to time t. Similarly, the acceleration equation is found by considering the spatial components of Einstein's equation (3.2),

$$2\dot{H} + 3H^2 = \frac{k}{a^2} - \kappa^2 p \quad , \tag{3.8}$$

which can be rewritten using the Friedmann equation (3.6) as

$$\frac{\ddot{a}}{a} = -\frac{\kappa^2}{6}(\rho + 3p) \quad , \tag{3.9}$$

also known as the *Raychaudhuri* equation.

Equation (3.9) is particularly useful as it shows whether the scale factor $a(t)$ is accelerating ($\ddot{a} > 0$) or decelerating ($\ddot{a} < 0$). In the first case ($\ddot{a} > 0$), assuming a positive Hubble rate $H > 0$, the universe is not only expanding but expanding at an accelerated rate. In the second case ($\ddot{a} < 0$), with $H > 0$, the universe is still expanding but the rate of expansion is slowing down. We can rewrite the condition for accelerated expansion using (3.9) as $\rho + 3p < 0$. This also implies that the equation of state parameter from (3.5) must be less than $w < -\frac{1}{3}$.

Examining the Friedmann equation (3.6), it is useful to define the *critical density* as the density required to produce a spatially flat universe (k=0),

$$\rho_c \equiv \frac{3H^2}{\kappa^2} \quad . \tag{3.10}$$

One can then define the dimensionless *density parameter* (or *relative energy density*) as the ratio of the density over the critical density,

$$\Omega \equiv \frac{\rho(t)}{\rho_c} \quad . \tag{3.11}$$

Using observational data [19], the density parameter today Ω_0 is calculated to be 1, corresponding to a spatially flat universe ($\Omega_{k,0} = 0$) to a 1σ accuracy of 0.25%. The density ρ should more accurately be labelled the *total* energy density, as it is made up of the contributions from all the different sources of energy density in the universe. At the very least, this includes matter ρ_m and radiation ρ_r. Other possibilities include a cosmological constant ρ_Λ or contributions from one or more scalar fields, known more generally as *quintessence*. We can therefore also split up the density parameter into its contributions from different sources, including the curvature density parameter previously mentioned, $\Omega = \Omega_m + \Omega_r + \Omega_k + ...$, and an additional subscript 0 would indicate the value today. This is especially useful when working with observational data. From here onwards we shall focus on the case of a spatially flat universe ($k = 0$), and of a single fluid contribution at each a given time. For the most part, this simplification is a good approximation of our Universe when it is dominated by a single fluid during its different epochs [15].

The last equation we wish to derive is the *fluid equation*, which tells us how the energy in the universe evolves. Therefore we wish to have an equation which includes the time derivative of the energy density ρ. Consider the conservation of the energy-momentum tensor (3.3), $\nabla_\mu T^{\mu\nu} = 0$, where ∇_μ denotes the covariant derivative. Because of the symmetry of $T_{\mu\nu}$, with no off-diagonal terms, this leads nicely to the fluid equation

$$\dot{\rho} + 3H(\rho + p) = 0 \quad . \tag{3.12}$$

With an equation of state relating the density and the pressure, we can find an equation for the density $\rho(t)$ just in terms of the scale factor $a(t)$ and the EoS parameter w. This can then be substituted back into the Friedmann equation (3.6) in order to determine how the scale factor evolves with time. Solving the fluid equation (3.12) with an equation of state of the form (3.5) leads to

$$\rho \propto a^{-3(1-w)} \quad , \tag{3.13}$$

which is valid for $w \neq -1$. Substituting the above into the Friedmann equation (3.6), remembering we are considering a spatially flat universe ($k = 0$), gives the general solution

$$a(t) \propto t^{\frac{2}{3(1+w)}} \quad . \tag{3.14}$$

For a universe dominated by non-relativistic matter ($\Omega_m = 1$), the EoS parameter $w = 0$ gives

$$a(t) \propto t^{\frac{2}{3}} \quad , \tag{3.15}$$

known as the Einstein de Sitter solution. A universe consisting of only matter would expand forever and the temperature would decrease monotonically, being inversely proportional to the scale factor [14]. This end-of-the-universe scenario is hence known as the 'Big Chill'. As we know, our Universe isn't made up of only matter, but it turns out to be a good approximation for when our Universe was roughly between $t = 4.7 \times 10^4$ and $t = 9.8 \times 10^9$ years old, also known as the *matter epoch* [15].

In the case of a radiation dominated universe ($\Omega_r = 1$) with $w = \frac{1}{3}$, the scale factor evolves as

$$a(t) \propto t^{\frac{1}{2}} \quad . \tag{3.16}$$

This turns out to be a good approximation between the start of the Big Bang (or the end of inflation) until the start of the matter epoch at $t = 4.7 \times 10^4$ years, neglecting the transitional phase where a two-fluid model is needed. The fate of a universe consisting of only radiation is the same as the matter example previously discussed. In both of these cases the scale factor evolves as a power-law function of time, and in both, the EoS parameter implies the expansion rate of the universe is decelerating.

3.2 Dark Energy and Observation

Observational evidence from the Cosmic Microwave Background (CMB) Radiation [19] and type Ia supernovae [20] both indicate that the Universe is currently undergoing accelerated expansion ($\ddot{a} > 0$). Since the cosmological equations for both a matter dominated and a radiation dominated universe do not lead to accelerated expansion, it is clear that something is missing from our picture of the Universe. Some unknown form of energy must be contributing to the overall energy density, aptly labelled *dark energy*. What's more, all current observational data points toward dark energy making up around 70% of the cosmic energy budget, with a further 26% coming from an equally mysterious form of non-relativistic matter ($w = 0$) known as cold dark matter (CDM) [19]. (See Table 1 for a list of density parameters from the most recent Planck 2018 CMB data with the inclusion of Baryon Acoustic Oscillation (BOA) data [19]). Observational data from Planck and type Ia supernovae constrain the equation of state of dark energy to $w = -1.006 \pm 0.045$. Another useful cosmological parameter from Planck is the Hubble constant (the Hubble rate today), with a value of $H_0 = 67.66 \pm 0.42 \text{kms}^{-1}\text{Mpc}^{-1}$ [19]. However, it is worth mentioning that this is in tension with the recent results obtained from the Hubble Space Telescope type Ia

$\Omega_{\Lambda,0} = 0.6889 \pm 0.0056$
$\Omega_{m,0} = 0.3111 \pm 0.0056$
$\Omega_{b,0}h^2 = 0.02242 \pm 0.00014$
$\Omega_{c,0}h^2 = 0.11933 \pm 0.00091$
$\Omega_{k,0}h^2 = 0.0007 \pm 0.0019$
$\Omega_{r,0} \sim 0.0001$

Table 1: Density parameters for today's values of dark energy Λ, matter m, baryon matter b, cold dark matter c, curvature k and radiation r respectively. The uncertainty in the Hubble parameter is represented in $h = 0.6766 \pm 0.0042$. The upper table values are taken from the Planck CMB temperature, polarisation and lensing power spectra with the inclusion of BOA data [19]. The lower table value is a naive estimate based on the same results.

supernovae, giving $H_0 = 73.24 \pm 1.74 \text{kms}^{-1}\text{Mpc}^{-1}$ [21].[6]

As well as evidence from the CMB and supernovae, observations related to large scale structure (LSS) also supports the claim that the Universe is now dominated by some form of dark energy [23]-[24]. Moreover, a model of the universe with a period of radiation domination followed by matter domination, leading into a dark energy dominated phase seems to best fit all the observational data (for an example, see the *benchmark model* introduced by Ryden in [15]).

Despite making up such a huge fraction of the Universe's energy density, the nature of dark energy is truly still a mystery. The two most promising explanations are Einstein's famous cosmological constant Λ and quintessence in the form of scalar fields[7]. We shall first talk about the cosmological constant and outline the ΛCDM model, and then address the issues with such a model.

3.3 Cosmological Constant

Einstein's field equations (3.2) have the important property that both sides of the equation are divergence free, satisfying $\nabla^\mu G_{\mu\nu} = \nabla^\mu T_{\mu\nu} = 0$. Adding a bare cosmological constant

[6]More recent results from the Hubble Space Telescope and Gaia spacecraft in 2018 further add to the tension with the Planck result for H_0, with a Hubble constant of $H_0 = 73.52 \pm 1.62 \text{kms}^{-1}\text{Mpc}^{-1}$ [22].

[7]Other possible explanations include modifying gravity to get rid of the need for any dark energy component altogether (See [25] for a thorough review).

term $\Lambda g_{\mu\nu}$ to the left hand side of the equation does not spoil its covariance, giving us

$$G_{\mu\nu} + \Lambda g_{\mu\nu} \equiv R_{\mu\nu} - \frac{1}{2} R g_{\mu\nu} + \Lambda g_{\mu\nu} = \kappa^2 T_{\mu\nu} \quad . \tag{3.17}$$

The cosmological constant was originally added to Einstein's field equations as an attempt to obtain a static universe but is now the most popular explanation for dark energy, the model commonly referred to as the Lambda-cold-dark-matter (ΛCDM) model.

Physically, the cosmological constant represents the vacuum energy density of empty space, which is attributed to the zero-point energy of quantum fields [26]. The associated equation of state has negative pressure $\rho_\Lambda = -p_\Lambda$, thus the equation of state parameter is $w = -1$. A cosmological constant dominated universe will undergo accelerated expansion. The value of Λ can be calculated from observational parameters, which is found to be approximately

$$\Lambda \simeq 10^{-52} \mathrm{m}^{-2} \ . \tag{3.18}$$

For the evolution equations of (3.17), one follows the same procedure as before, arriving at the Friedmann (3.6) and acceleration (3.8) equations with an additional cosmological constant term:

$$H^2 = \frac{\kappa^2}{3} \rho + \frac{\Lambda}{3} \quad , \tag{3.19}$$

$$2\dot{H} + 3H^2 = -\kappa^2 p + \Lambda \quad , \tag{3.20}$$

where the curvature k has been set to zero. The fluid equation (3.12) clearly remains the same. If the cosmological constant contribution to the total energy density dominates then the solution to (3.12) becomes

$$a(t) \propto t^{Ht} \quad , \tag{3.21}$$

with $H = \sqrt{\frac{\Lambda}{3}}$ being constant. This is known as a de Sitter (dS) solution and the scale factor increases exponentially with increasing time. A universe of this type always undergoes accelerated expansion ($\ddot{a} > 0$).

Just like the previous other single-fluid dominated universes we have considered, a de Sitter universe cannot be an accurate model of our Universe for all times. This is because in such a universe no structures could have had the chance to form. However, we know that in the present day our Universe *is* accelerating and transitioning into a phase dominated by a cosmological constant-like term. Therefore the dS solution is a good approximation for our Universe after the period of matter domination. Moreover, the state of the Universe

is approaching a true de Sitter space in the asymptotic future, when the relative energy density of all other components goes to zero.

As previously mentioned, if the source of dark energy is a cosmological constant then the vacuum has some positive energy associated with it. In string theory, this can alternatively be realised as a scalar field sitting in the minima of its potential. One of the major current goals in string theory is to construct these potentials corresponding to stable de Sitter vacua (or positive cosmological constant). If one believes string theory, the inability to do so could make a strong case for the nature of dark energy not being tied to a cosmological constant. This approach shall be a key focus of this work in Sections 4 and 6.

3.3.1 The cosmological constant problem

Lastly, a discussion on the cosmological constant could not be complete without mentioning the infamous *cosmological constant problem*. We shall only briefly describe the issues that plague the cosmological constant and the ΛCDM model, but for a more complete description see the review by Carroll [27]. A naive calculation of Λ in quantum field theory (QFT), ignoring divergences and assuming a cut-off at the Planck scale $m_p = 1.2 \times 10^{19}\text{GeV}$, gives an energy density of $\rho_\Lambda \approx 10^{74}\text{GeV}^4$. If one instead works up to just the electroweak scale, the calculated energy density is around $\rho_\Lambda = 10^{8}\text{GeV}^4$. Compare these with the actual energy density of Λ according to observation, $\rho_\Lambda \approx 10^{-47}\text{GeV}^4$. This staggering 121 orders of magnitude difference up to the Planck scale, or 55 orders of magnitude difference up the electroweak scale, has long been a major cause for concern.

One may introduce counter terms, a bare cosmological constant $\rho_{\Lambda,B}$, in order to cancel the energy density to match that of observation. However, this requires one to *fine-tune* the value of $\rho_{\Lambda,B}$ to over 50 orders of magnitude, which does not seem like a natural solution. This problem of *fine-tuning* is what is popularly meant by the cosmological constant problem. As we are dealing with QFT, we are in the realm where renormalising theories and adding counter terms is commonplace. And one uses observation and experiment to fix the values of these counter terms in each theory. The deeper issue lies in the radiative instability of the cosmological constant, whereby this issue of fine-tuning reappears in each loop order of the perturbation theory. This is explained in much greater detail by Padilla [28].

A further problem is related to the ratio of today's dark energy density $\Omega_{\Lambda,0}$ and matter

density $\Omega_{m,0}$, although this problem is not exclusive to a cosmological constant. As shown previously in Table (1), the dark energy and matter densities are roughly of equal order, $\Omega_{\Lambda,0} \sim \Omega_{m,0} \sim \mathcal{O}(1)$. This means that today we are observing the Universe in the relatively brief transition between matter and dark energy domination, and any small change in the initial conditions would have caused the Universe to not be in such a coincidental state. This is known as the *cosmic coincidence problem* [29]. Any theory of dark energy would wish to address this problem, and the cosmological constant explanation seems to have no way of doing so.

For a possible solution to both of the problems mentioned, we look again to string theory and a concept known as the *string landscape*. We shall briefly summarise the idea here and refer the reader to two encompassing pieces of work on the topic by Susskind [30] and Linde [31]. In some string theory (or *inflationary multiverse*) models, the number of different predicted vacua states is enormous - up to around 10^{500} in some cases [32]. One can interpret this as the existence of a multitude of different universes, or *pocket universes*, each with a different vacuum state and value of the cosmological constant Λ. One of these universes corresponds to ours, with a cosmological constant matching the one we observe. Using anthropic reasoning it can be concluded that only universes that are able to support intelligent life (observers) will be observed. In other words, the fact we are observing this Universe with a value of Λ able to support intelligent life is anything but a coincidence. The nature of these string vacua will be explored in greater detail in Section 4, and we how this landscape arises.

This type of anthropic argument has also been applied generally to the cosmological constant in the absence of string theory (for example [33]-[34]). In this case it is disliked by many, either because it discourages further investigation for physical explanations or because it can be seen as a tautology: we can observe the Universe because it can be observed. Nonetheless, it does not mean that this unfavourable explanation is incorrect. The Universe may just appear to be fine-tuned with no further physical explanation. We wish instead to explore models which do not rely on such reasoning.

4 Scalar Fields in String Theory

The purpose of this section will be to introduce the unfamiliar reader to elements of string theory as well as to show its relation to the field of cosmology. Scalar fields appear naturally in string theory, which have direct applications in cosmology. The two main areas being inflationary regimes in the early Universe, and the late Universe with dark energy. We shall focus on the late-time applications, otherwise known as Quintessence models (see [35]-[36] for two motivating examples).

We will begin by simply stating some of the general properties of string theory and covering some of the terminology that will be used in later sections. We will then move on to a topic known as compactification, treating two well known examples: dimensional reduction in Kaluza-Klein theory and flux compactifications in Einstein-Maxwell theory. The aims of these examples will be to show how scalar field potentials are produced under compactifications. They will also familiarise the reader with the mathematical techniques used later in Section 6, when we look at the motivating string theory examples that will be relevant for cosmology.

4.1 Introductory to String Theory

String theory is an attempt to explain the physical world in a unified framework, motivated by the need to go beyond general relativity (GR) and quantum field theory (QFT).[8] Both GR and QFT are now thought to be only effective theories, whereby at some cut-off energy scale they break down.[9] In other words, they are not true descriptions of nature. String theory, on the other hand, appears to be a consistent theory of quantum gravity despite not yet being fully formulated. The subject area is expansive but the most popular variants of string theory can be classified into two main categories: ten-dimensional superstring theories, based on the principle of supersymmetry; and eleven-dimensional M-theory, which is thought to unify all the superstring models [40].

Let us briefly review some of the general properties of string theory, all of which are covered in much greater detail in [40]-[42]. In string theory, the fundamental point-like

[8] Originally, string theory arose in an attempt to understand the strong nuclear force in the late 1960's. It has since grown and become a potential candidate as a *Theory of Everything* [37]

[9] General relativity can in fact be quantised and treated as a well behaved QFT at ordinary energies [38], but admits ultraviolet (UV) divergence at higher energies [39]

particles of conventional physics are replaced by one-dimensional extended objects called strings. The length of these strings l_s gives the characteristic length scale, typically taken to be of order Planck length $\sim l_p = 1.6 \times 10^{-35}$m. The number of spacetime dimensions is predicted by the theory itself, usually ten or eleven. These dimensions we do not observe can be thought of as being too small to detect, *compactified* on some internal manifold. The details of the manifold gives rise to the different properties of the different string theories. We shall be particularly interested in the method of compactification as it determines the form of the four-dimensional effective theory.

As previously mentioned, supersymmetry is a key concept in string theory, with most realistic theories requiring it. The concept relates bosons to fermions, implying that each boson has a corresponding superersymmetric fermion partner and vice-versa. Models based on this principle are known as *superstring* theories. There are five distinct superstring theories, all in ten spacetime dimensions: type I, type IIA, type IIB, heterotic $E_8 \times E_8$ and heterotic $SO(32)$. The details of these different theories can be found in either of [40]-[41]. A number of dualities were found in recent years which relate some of the different superstring theories previously listed, for example, *T-duality* relates the two type II and two heterotic theories [40]. It turns out that all five of the superstring theories are related through a web of dualities and can be realised as different limits of a higher dimensional string theory, known as eleven-dimensional *M-theory*. M-theory is approximated in the low energy limit as eleven-dimensional *supergravity* ($11d$ SUGRA), which will be one of the key examples we will focus on.

Superstring cosmology is a new and growing field of research situated at the intersection between string theory and cosmology (see [43] for a short review or [44] for a more complete review). Predictions specific to string theory may be observable and testable in the regime of cosmology: the existence of scalar fields. The compactification of string theories from higher dimensions down to four spacetime dimensions produces one or more scalar fields, which could be candidates for the inflaton field driving inflation ([45]-[47]), the vacuum associated with a cosmological constant ([30],[48]), or the scalar field(s) involved in quintessence ([35]-[36]). Unfortunately though, obtaining these solutions through compactifications is not so straightforward. A great deal of work over the past few decades has gone into obtaining stable solutions; an attempt to circumvent the so-called *moduli stabilisation problem*, where the scalar field potential has no stable minimum (see [49] for a cosmological perspective). A

technique involving the addition of fluxes appears to be a way of stabilising the moduli, and also gives rise to a landscape of possible vacua [50]. This is known as the string landscape, which we mentioned briefly before.

As it so happens, the types of stabilised moduli which tend to arise in flux compactifications often correspond to anti-de Sitter spacetimes. Obtaining stable de Sitter solutions turns out to be more of a challenge. We will later be investigating a recent claim that all meta-stable[10] de Sitter solutions are not represented in the landscape of effective string theories. Instead it is proposed that they belong in the *swampland*[11] [5]. Despite originating in string theory, these ideas are undoubtedly linked to cosmology as it is the domain where observational evidence would likely come from. We will now explore how scalar fields arise from compactifications.

4.2 Introduction to Compactifications

4.2.1 Kaluza-Klein compactification

To get a taste for how compactification works, we shall start with the famous Kaluza-Klein (KK) dimensional reduction[12]. Kaluza [52] and Klein [53] were originally interested in unifying gravity and electromagnetism, but their method has since been generalised and is now employed in the compactification of 10-dimensional superstring theories and 11-dimensional M-Theory. The same techniques we employ here shall be later used in both of those areas, so our focus will be on the methodology.

Kaluza and Klein hypothesised that a fifth spacetime dimension exists; an extension of general relativity in an attempt to unify gravity and electromagnetism. Let us first explain the Kaluza-Klein idea qualitatively for a general $D = d + 1$ dimensional spacetime, where d is the number of spacetime dimensions we observe. The extra dimension we do not observe is known as the *compact dimension* which is curled up on a circle of radius L.

As an analogy, imagine an infinitely long two-dimensional cylinder of radius L, where

[10]'Meta-stable' means we that are not assuming the minima in question is a global one. Ruling out meta-stable solutions is a stronger claim than just stable solutions.

[11]The string swampland, in contrast to the string landscape, refers to the semi-classical effective field theories which appear consistent but are actually inconsistent. For more details see the original paper by Vafa [51].

[12]Dimensional reduction differs from compactification because in the former we take the size of the compact dimension to go to zero and consider only the massless modes, see equation (4.2).

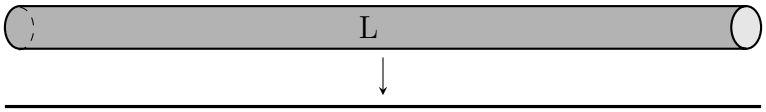

Figure 1: Kaluza-Klein cylinder of radius L (top). The length represents the non-compact spacetime dimensions and the width represents the compact dimension. From far away the cylinder appears as a one-dimensional line (bottom).

its length represents our d dimensional spacetime and its width represents the compact dimension, illustrated in Figure 1. At a distance far from the cylinder, its finite width would not be visible and it would appear to be a one dimensional line. This corresponds to our spacetime appearing to only have d dimensions, assuming the L is small enough. In Kaluza-Klein theory the length scale of the compact dimensions is taken to be of order Planck length l_p. Let us move on to show how we compactify these extra dimensions.

Starting with the gravitational part of the Einstein-Hilbert action in $D = d + 1$ dimensions, we have

$$S = \frac{1}{\kappa_D^2} \int d^D x \sqrt{-G} R_D \ , \tag{4.1}$$

where κ_D is the D-dimensional gravitational coupling constant, $G = \det[G_{MN}]$ is the determinant of the D-dimensional metric tensor and R_D is the Ricci scalar in D dimensions. The indices in the metric run over $N, M = 0, 1...d, D$. The next step is to compactify one of the dimensions onto an internal manifold, namely a circle S^1. In general, one can compactify any number of dimensions onto a variety of manifolds; the topology of the manifold being an important feature for string theory. Our choice of a circle means that we make one of the coordinates periodic. We shall introduce coordinates $x^M = (x^\mu, y)$, where y corresponds to the compact spatial dimension with periodicity defined by $y = y + 2\pi L$, Greek letters run over d dimensions and L is the radius of the compact dimension. Along this one-dimensional line, the circumference of S^1, we have identified any two points which differ by $2\pi L$.

Expanding the metric G_{MN} in terms of its Fourier series gives [25]

$$G_{MN}(x, y) = \sum_{n=0}^{\infty} G_{MN}^{(n)}(x) \exp\left(\frac{iny}{L}\right). \tag{4.2}$$

Each value of n corresponds to a different mode (or field or particle). The $n = 0$ mode is massless and the others have mass $M = \frac{|n|}{L}$. If L is very small then the masses of each $n \neq 0$ mode will be very large. For example, the Planck length l_P and associated Planck energy E_P are around 10^{-35}m and 10^{19}GeV respectively. The energies of these massive modes are

beyond what we could ever hope to resolve, so we are justified in focussing on the low-energy approximation by considering only the 0^{th} mode. The metric is then independent of y and we will be free to integrate out the compact dimension. The KK ansatz for the massless mode is given by the following line element [54],

$$ds_0^2 = G^{(0)}_{MN}(x)dx^M dx^N = g_{\mu\nu}(x)dx^\mu dx^\nu + \mathrm{e}^{2\Phi(x)}\Big(A_\mu(x)dx^\mu + dy\Big)^2 \,, \tag{4.3}$$

where $g_{\mu\nu}$ is the metric for the non-compact spacetime, Φ is the scalar dilaton field and A_μ is the electromagnetic gauge field. It is the dilaton Φ which parametrises the structure of the compact manifold [49].

Under the compactification, the full derivation given in Appendix A.1, the action (4.1) in $d = 4$ dimensions becomes [25] [54]

$$S^E_{(0)} = \frac{2\pi L}{\kappa_D^2}\int d^4x\sqrt{-\tilde{g}}\Big[\tilde{R}_d - \Big(\frac{1}{2}\Big)(\tilde{\nabla}\Phi)^2 - \frac{1}{4}\mathrm{e}^{-\sqrt{3}\Phi}\tilde{F}^2\Big] \quad . \tag{4.4}$$

Here we encounter a number of new terms (see Appendix A.1 for the full details). The last term $\tilde{F}^2 = \tilde{F}_{\mu\nu}\tilde{F}^{\mu\nu}$ represents the electromagnetic field strength squared. The tilde indicates that a *conformal transformation* (or *Weyl rescaling*) of the metric has been made, and those terms are now with respect to the new metric. The square of the derivative of Φ is the kinetic energy component of the field and the factor of $2\pi L$ comes from integrated circumference of the compact dimension.

Let us examine the action in more detail. The kinetic term is canonically normalised and the Ricci scalar is coupled only to the metric, which means the action in the Einstein-Hilbert form (or the *Einstein frame*). There is a non-trivial coupling between F^2 and the dilaton field, which converges in the limit $\Phi \to \infty$. To reduce the action to Einstein-Maxwell theory in four dimensions, the dilaton would have to be set to zero. However, when examining the field equations of (4.4) one finds that there are interactions between the fields which prohibit us from doing this [25]. Another way of saying this is that switching off the dilaton is not a consistent truncation of the higher dimensional theory [55]. If Φ cannot be set to zero, one could instead posit that Φ must remain constant and close to zero. Another reason for requiring Φ to be small is that the physical size of of the compact dimension is given by $2\pi L\mathrm{e}^{\Phi}$. A constant small Φ is required for the dimension to remain undetectable and stable from decompactification. However, this is also unachievable in the absence of a potential $V(\Phi)$.

This problem appears more generally in all KK-compactifications, where massless scalar fields, such as the dilaton, are not stabilised by a potential and their vacuum expectation values (VEVs) are unconstrained. This is what is known as the *moduli stabilisation problem*, which, until recently, was a major obstacle when constructing consistent 4-dimensional compactifications in string theory [40].

4.2.2 Flux compactifications

To resolve the moduli stabilisation problem, a method known as *flux compactification* was developed in the early twentieth century. We shall briefly explain what these flux compactifications are and how they work with a discussion of six-dimensional Einstein-Maxwell theory. For a more in-depth review than we shall be addressing see [56] or [57].

Following the example laid out by Douglas and Kachru in [57], let us begin by considering Einstein-Maxwell theory in six dimensions and compactifying down to four dimensions on a sphere S^2 with genus $g = 0$.[13] The Lagrangian takes the form

$$S = \int d^6x \sqrt{-G_g}\big(M_6^4 R_6 - M_6^2 |F_2^2|\big) \quad , \tag{4.5}$$

where G_6 is the metric determinant, R_6 is the Ricci scalar and F_2 represents the two-form *magnetic flux* or field strength. We will absorb the fundamental mass scale M_6 into the dimensions of the other terms for simplicity.

To compactify to four dimensions, let us use the metric ansatz

$$ds^2 = g_{\mu\nu} dx^\mu dx^\nu + L^2(x)\gamma_{mn}(y) dy^m dy^n \quad , \tag{4.6}$$

where m and n run over the two dimensions of the compact space and γ_{mn} is its corresponding metric. Similar to in our previous example, the modulus field $L(x)$ is a function of the non-compact coordinates x^μ and related to the size of the compact dimension. The physical volume of the compact dimension is given by $L^2(x)V_2$, where V_2 is the volume calculated from the compact metric γ_{mn} [42].

Without fluxes turned on (setting F_2 to zero) one goes through a similar calculation as before, reducing to four dimensions and performing a Weyl rescaling to the Einstein frame. The resulting $4d$ effective theory has a potential of the form

$$V(L) \sim -\frac{1}{L^4} \quad . \tag{4.7}$$

[13] For a more general S^2 with genus g, see [58]. It will however turn out that only genus $g = 0$ leads to a stabilised modulus.

This is clearly unstable as the field $L(x)$ will runaway to zero, the size of the compact sphere shrinking to zero.[14] The solution to this problem comes with the inclusion of a non-zero flux (4.5). Let us thread the two-sphere S^2 with N units of flux

$$\int_{S^2} F_2 = N \quad . \tag{4.8}$$

The contribution to the $4d$ theory from the flux term are as follows. By flux quantisation, the flux term goes as $F_2 \sim \frac{N}{L^2}$. So for F_2^2 we have an $\frac{N^2}{L^4}$ contribution. Integrating over the compact dimension gives an L^2 contribution, and the Weyl rescaling brings an additional factor of $\frac{1}{L^4}$. Therefore the flux potential goes like $\frac{N^2}{L^6}$ and the full potential has the form

$$V(L) \sim \frac{N^2}{L^6} - \frac{1}{L^4} \quad . \tag{4.9}$$

It can now be seen that with the addition of fluxes the moduli field $L(x)$ can been stabilised. The potential (4.9) exhibits stable minima which depend on the value of N. For $L > 0$ the minimum (or critical radius) is roughly at $L \sim N$.

An important feature of flux compactifications is that for each different value of N we have a different stabilised critical radius. Each of these radii is related to a vacuum energy, and hence, the landscape of all possible vacua is vast. For the potential in our example (4.9), the associated vacuum energy is negative and corresponds to an anti-de Sitter (AdS) spacetime. Many string theory models suffer the same problem, and an accompanying host of *no-go theorems* [59] [60] claimed to rule out consistent compactifications to de-Sitter spacetimes. In recent years, there have been positive developments which circumvent these theorems, the most notable being the KKLT constructions [48]. The basic idea is that methods such as compactification are used to stabilise the moduli in a supersymmetric anti-de Sitter (AdS) vacuum. And then with the inclusion of objects known as $\overline{D3}$ branes, the AdS vacuum can be uplifted to a meta-stable de Sitter ground state [45]. In Section 6 we will return to some of these topics and see how they are fundamentally important for cosmology.

[14] For genus $g \neq 0$ the potential is either: zero and L is a modulus ($g = 1$); or positive $\frac{1}{L^4}$ and L is also unstable ($g > 1$) [58].

5 Scalar Field Quintessence

In this section we will see how canonical scalar fields play a role in cosmology, specifically in late-time quintessence models. Using the right choice of variables it is possible to transform the cosmological equations into a closed set of autonomous equations, which can then be studied with the dynamical systems techniques introduced in Section 2. The observed cosmological parameters we looked at in Section 3.2 will be particularly useful here, giving us constraints by which to fit our models if we want them to be accurate representations of our Universe. As an added note, we will often refer to dark energy and scalar fields synonymously, especially in the context of observation.

The three types of scalar field models we will discuss in this section are the single exponential, the double exponential and the power-law potentials. There are a much wider class of models that can be explored (see [4]), but these three in particular display phenomenologically interesting properties. Using a mix of qualitative analysis and numerical simulations we will accurately be able to characterise not just the late-time but also the evolutionary behaviour of all three models.

5.1 Canonical Scalar Fields in Cosmology

Let us consider the cosmology of a canonical scalar field minimally coupled to matter in four spacetime dimensions. The action for such a system is given by [4]

$$S = \int d^4x\sqrt{-g}\left(\frac{R}{2\kappa^2} + \mathcal{L}_m + \mathcal{L}_\phi\right) \quad , \tag{5.1}$$

where R is the Ricci scalar, $\sqrt{-g}$ is the metric determinant and $\mathcal{L}_m$ is the Lagrangian for matter fields. The canonical scalar field Lagrangian $\mathcal{L}_\phi$ has the form

$$\mathcal{L}_\Phi = -\frac{1}{2}g^{\mu\nu}\partial_\mu\phi\partial_\nu\phi - V(\phi) \quad , \tag{5.2}$$

where $V(\phi)$ is the scalar field potential, which we require to be positive. Varying the action with respect to ϕ leads to the *Klein-Gordon equation*,

$$\Box\phi - V_{,\phi} = 0 \quad , \tag{5.3}$$

where $V_{,\phi} = \frac{\partial V}{\partial\phi}$ and $\Box\phi = \nabla_\mu\nabla^\nu\phi$. Variation with respect to the metric $g_{\mu\nu}$ yields the gravitational field equations,

$$R_{\mu\nu} - \frac{1}{2}g_{\mu\nu}R = \kappa^2(T_{\mu\nu} + T^\phi_{\mu\nu}) \quad , \tag{5.4}$$

where we define the energy-momentum tensor for a canonical scalar field as

$$T^{\phi}_{\mu\nu} = \partial_\mu\phi\partial_\nu\phi - \frac{1}{2}g_{\mu\nu}(\partial\phi)^2 - g_{\mu\nu}V(\phi) \quad , \tag{5.5}$$

and $(\partial\phi)^2 \equiv g_{ab}\partial^a\phi\partial^b\phi$.

Just like when deriving the cosmological evolution equations in section 3.2, it is useful to assume that the spacetime we are dealing with is accurately described by the FLRW metric (3.1) and that the matter content can be modelled as a single perfect fluid (3.3) with a barotropic equation of state $p = w\rho$. If we also assume that the spacetime is flat (k=0) then the FLRW metric, in Cartesian coordinates, is given by

$$ds^2 = -dt^2 + a^2(t)\big(dx^2 + dy^2 + dz^2\big) \ . \tag{5.6}$$

From the field equations (5.4) one can derive the Friedmann and acceleration equations, as shown in Appendix B.1,

$$3H^2 = \kappa^2\Big(\rho + \frac{1}{2}\dot{\phi} + V(\phi)\Big) \quad , \tag{5.7}$$

$$2\dot{H} + 3H^2 = -\kappa^2\Big(\omega\rho + \frac{1}{2}\dot{\phi}^2 - V(\phi)\Big) \quad . \tag{5.8}$$

The Klein Gordon equation (5.3) can also be rewritten in a simple form,

$$\ddot{\phi} + 3H\dot{\phi} + V_{,\phi} \quad . \tag{5.9}$$

The energy density and pressure for the scalar field ϕ can be defined as

$$\rho_\phi = \frac{1}{2}\dot{\phi}^2 + V(\phi) \quad , \tag{5.10}$$

$$p_\phi = \frac{1}{2}\dot{\phi}^2 - V(\phi) \quad . \tag{5.11}$$

Using these definitions, the equation of state is then given by

$$w_\phi = \frac{p_\phi}{\rho_\phi} = \frac{\frac{1}{2}\dot{\phi}^2 - V(\phi)}{\frac{1}{2}\dot{\phi}^2 + V(\phi)} \quad , \tag{5.12}$$

which can take values in the range $[-1, 1]$. It is important to remember that, unlike the EoS for matter, the scalar field EoS w_ϕ is a dynamically evolving parameter and can change over time. When the kinetic energy $\frac{1}{2}\dot{\phi}^2$ dominates over the potential energy $V(\phi)$ in (5.12), $w_\phi = 1$. Conversely, when the potential energy dominates we have $w_\phi = -1$. The latter case is the physically interesting one, where the scalar field can be the cause of the accelerated expansion of the universe. Models where the potential energy dominates are commonly

known as *slow-roll* models, where the scalar field ϕ is slowly rolling in its potential $V(\phi)$ such that $\dot{\phi}$ is small in comparison [61].[15] Hence, we can already see how a canonical scalar field could, in principle, be a candidate for dark energy. Unlike a cosmological constant, scalar fields are a dynamical explanation of dark energy, which leads to interesting new features that we shall soon explore.

5.2 Dynamical Systems Approach

If we are to take a dynamical systems approach, the next obvious step is to transform the cosmological equations (5.7), (5.8) and Klein-Gordon equation (5.9) into a set of autonomous differential equations. To do so, we introduce new variables defined as

$$x = \frac{\kappa\dot{\phi}}{\sqrt{6}H} \quad ; \quad y = \frac{\kappa\sqrt{V}}{\sqrt{3}H} \ , \tag{5.13}$$

first introduced by Copeland et al. in [62]. We will refer to these variables as *expansion normalised* (EN) variables. We will assume that the scalar potential V is positive, and therefore $y \geq 0$ for positive H.[16] This will indeed be the case for all the potentials we will be dealing with. See Appendix B.2 for the derivation of all key equations in EN variables.

Consider first the Friedmann constraint (5.7), which written in terms of the new EN variables is given by

$$1 = \Omega_m + x^2 + y^2 \ , \tag{5.14}$$

where the density parameter (or relative energy density) for matter is defined as

$$\Omega_m = \frac{\kappa^2\rho}{3H^2} \ . \tag{5.15}$$

Using the fact that we require $\Omega_m + \Omega_\phi = 1$, we can deduce that the total relative energy density of the scalar field is given by

$$0 \leq \Omega_\phi = x^2 + y^2 \ \leq 1 \ , \tag{5.16}$$

where x^2 and y^2 represent the kinetic energy density and potential energy density of the scalar field respectively. The upper bounds come from the fact that the energy density of matter cannot be negative, $\rho \geq 0$. The equation of state (5.12) can then be rewritten as

$$w_\phi = \frac{x^2 - y^2}{x^2 + y^2} \ . \tag{5.17}$$

[15] The same concept of slowly rolling scalar fields is also popular in inflationary models.

[16] If this is not the case one could define $y = \kappa\sqrt{|V|}/(\sqrt{3}H)$.

Now that we have the density parameters for both matter and the scalar field, we can define the *effective EoS parameter* of the universe as the ratio of the total pressure to the total energy density. Written in terms of x and y,

$$w_{eff} \equiv \frac{p_{tot}}{\rho_{tot}} = \frac{p + p_\phi}{\rho + \rho_\phi} = w\Omega_m + w_\phi \Omega_\phi \ . \tag{5.18}$$

$$= w(1 - x^2 - y^2) + x^2 - y^2 \ . \tag{5.19}$$

The effective EoS tells us the state of the universe, which can now be described solely in terms of x, y, and w. For example, a matter dominated universe with $w_{eff} = w$ has $x = 0$ and $y = 0$. In terms of the phase space (x, y) this is simply the origin. Accelerated expansion is given by the condition $w_{eff} < -1/3$, which will also correspond to certain regions of the phase space. Two more points of interest are at $(\pm 1, 0)$ and $(0, 1)$ in the phase space. The former corresponds to a universe completely dominated by the kinetic energy of the scalar field, with an effective equation of state $w_{eff} = 1$ (also known as a *stiff matter fluid*). The point $(0, 1)$ corresponds to a universe dominated by the potential energy of the scalar field. The effective equation of state is then $w_{eff} = -1$, which behaves like a cosmological constant dominated (or de Sitter) universe and is undergoing accelerated expansion.

The *physical phase space*, the phase space of physically acceptable solutions, is constrained by (5.16). This is simply a circle of radius one centred on the origin. If we include the condition that V not be negative ($y \geq 0$), the physical phase space is cut in half along the x-axis leaving us with a semicircle in the upper half plane.[17] This is the region in which we will be interested in. Orbits outside of the physical phase space, which we will simply refer to as the phase space from now on, will not be considered.

The acceleration equation (5.8) and Klein-Gordon equation (5.9) can be rewritten as a dynamical system by using the EN variables defined in (5.13), the derivation shown in Appendix B.2. The set of equations for the system are given by

$$\frac{dx}{dN} \equiv x' = -\frac{3}{2}\Big[2x + (w-1)x^3 + x(x+1)(y^2-1) - \frac{\sqrt{2}}{\sqrt{3}}\lambda y^2\Big] \ , \tag{5.20}$$

$$\frac{dy}{dN} \equiv y' = -\frac{3}{2}y\Big[(w-1)x^2 + (w+1)(y^2-1) + \frac{\sqrt{2}}{\sqrt{3}}\lambda x\Big] \ , \tag{5.21}$$

where $N \equiv \log a$ and we have defined

$$\lambda = -\frac{V_{,\phi}}{\kappa V} \ . \tag{5.22}$$

[17] Note that points along the x-axis (y=0) *are* included in the physical phase space.

In general, the set of equations (5.20), (5.21) and (5.22) do not represent a closed autonomous system because there is an explicit dependence on ϕ in the λ definition. It may already be obvious that for certain potentials λ will have no ϕ dependence[18], but to deal with the more general case where λ is a variable, let us consider its evolution by taking the derivative,

$$\frac{d\lambda}{dN} \equiv \lambda' = -\sqrt{6}\big(\Gamma - 1\big)\lambda^2 x \ , \tag{5.23}$$

where

$$\Gamma \equiv \frac{V V_{,,\phi}}{V_{,\phi}^2} \ , \tag{5.24}$$

and we understand $V_{,,\phi}$ to mean the second derivative with respect to ϕ [63]. If the function $\lambda(\phi)$ is invertible then it is possible to write Γ as a function of λ, thereby closing the dynamical system with the set of three autonomous equations (5.20), (5.21) and (5.23).

Consider the phase space of the dynamical system (5.20), (5.21) and (5.23). There exists an invariant submanifold at $y = 0$, about which trajectories cannot cross. This means that even had we not previously ruled out negative values of y, trajectories with positive or negative values of y would stay separate. Moreover, the system is invariant under the transformation $y \to -y$, so the qualitative dynamics for positive or negative values of y are the same. Let us move on to exploring concrete examples with potentials of different forms.

5.3 Single Exponential Potential

The first form of potential we shall be considering is that of a single exponential potential. Exponential potentials arise naturally in many areas of physics, particularly in relation to high-energy phenomenon such as string theory and inflation (for a review see [47] or for well known examples see [48]). In string theories and superstring theories, exponential potentials often emerge during the compactifications from higher dimensions down to four dimensions (see Section 4). We will see two more explicit examples of this in Section 6. As for the single exponential potential, it is the simplest type of quintessence model and also has interesting dynamical properties. It has been studied extensively, but somewhat less with a dynamical systems approach; the most notable example being credited to Copeland et al [62]. We will use the results of that work as a guide for this section.

[18] In fact, the EN variables were originally introduce in [62] to study the case of an exponential potential where λ is simply a constant parameter.

The single exponential potential is written as

$$V(\phi) = V_0 \exp^{-\kappa\lambda\phi} \ , \tag{5.25}$$

where $V_0 > 0$ is a positive constant and λ is a constant parameter, in line with (5.22). The dynamical system is now closed with just the x' and y' equations, (5.20) and (5.21), which represents a two dimensional autonomous system,

$$x' = -\frac{3}{2}\Big[2x + (w-1)x^3 + x(w+1)(y^2-1) - \frac{\sqrt{2}}{\sqrt{3}}\lambda y^2\Big] \ , \tag{5.26}$$

$$y' = -\frac{3}{2}y\Big[(w-1)x^2 + (w+1)(y^2-1) + \frac{\sqrt{2}}{\sqrt{3}}\lambda x\Big] \ . \tag{5.27}$$

The phase space for the above system is the upper half circle with radius one in the (x, y) plane. Also note the invariance under the simultaneous transformation $x \to -x$ and $\lambda \to -\lambda$, implying one only needs to consider positive values of λ to understand the full phase space dynamics (negative values corresponding to a reflection in the y-axis).

5.3.1 Critical points and stability

The critical points of the system (5.26)-(5.27) are given in Table 2. Also included are the key cosmological parameters defined in Section 5.2. The existence of the fixed point is determined by seeing under what conditions that point stays within the phase space, i.e. satisfying the Friedmann constraint $x^2 + y^2 \leq 1$. The last column of Table 2 is of significant importance as this describes how the universe is behaving. In Table 3 we outline the stability of each of the critical points along with listing their eigenvalues. Let us now discuss each critical point in greater detail.

Point O: The critical point at the origin of the phase space represents the matter dominated solution, the universe being completely characterised by the matter EoS parameter ($w_{eff} = w$). This point exists for all values of w and λ. The sign of the eigenvalues (Table 3) are always opposite for $w \in [0, 1)$, which is satisfied for all physically relevant equations of state (e.g. matter $w = 0$ and radiation $w = 1/3$).[19] This implies that the critical point

[19]The case when $w \to 1$, whilst not physical, is interesting in terms of the phase space dynamics. Point O becomes nonhyperbolic, however, its other eigenvalue is still positive and the point is therefore asymptotically unstable. As w approaches one, the strength of the attraction towards the saddle node along the x-axis decreases until it finally becomes an unstable point at $w = 1$. This is confirmed by the phase portraits.

Point	x	y	Existence	Ω_m	Ω_ϕ	w_ϕ	w_{eff}
O	0	0	Always	1	0	-	w
$A_\pm$	± 1	0	Always	0	1	1	1
B	$\frac{\sqrt{\frac{3}{2}(1+w)}}{\lambda}$	$\frac{\sqrt{\frac{3}{2}(1-w^2)}}{\lambda}$	$\lambda^2 \geq 3+3w$	$1-\frac{3+3w}{\lambda^2}$	$\frac{3+3w}{\lambda^2}$	w	w
C	$\frac{\lambda}{\sqrt{6}}$	$\sqrt{1-\frac{\lambda^2}{6}}$	$\lambda^2 < 6$	0	1	$\frac{\lambda^2}{3}-1$	$\frac{\lambda^2}{3}-1$

Table 2: Critical points and cosmological parameters for the system (5.26)-(5.27).

is a saddle node. Trajectories are attracted along the x-axis and repelled along the positive y-axis. The scalar field equation of state is undefined as both its kinetic energy and potential energy are zero here. There is no accelerated expansion ($w_{eff} > -1/3$), and the scalar field plays no important role at this point. Lastly, we note that any orbits coming through or from this point must be extremely fine-tuned, having exactly $y = 0$ as an initial condition.

Points $A_\pm$: The critical points at $(\pm 1, 0)$ represent the scalar field kinetic energy dominated solutions. The effective EoS $w_{eff} = w_\phi$ is always 1 and the universe behaves like a stiff matter fluid (no accelerated expansion). This point also exists for all values of w and λ. The eigenvalues for both points are either both positive (implying instability), or of opposite sign (implying a saddle). This is subject to the value of the parameter λ, the conditions stated in Table 3. From these conditions one can see that for certain values of λ it is possible to have both points unstable ($\lambda^2 \leq 6$) or one stable and the other a saddle ($\lambda^2 > 6$), but not both a saddle point at the same time. Being the only unstable points in the phase space, A_+ and/or A_- represent the past attractors (or repellers) for all trajectories that don't originate at a fixed point (i.e. orbits can be traced back to one of these points as $N \to -\infty$). However, a stiff matter fluid with $w_{eff} = 1$ does not represent an acceptable EoS in terms of macroscopic physics. These points are thought to correspond to the very early universe and so are often ignored in the context of dark energy applications.

Point B: This critical point, which moves around the phase space depending on the value of w and λ, is known as the *scaling solution* [64]. The scalar field equation of state matches that of the matter equation of state, $w_\phi = w$. Therefore, the universe always behaves as if dominated by matter $w_{eff} = w$, regardless of the values of the density parameters Ω_m

Point	Eigenvalues	Stability
O	$\left\{-\frac{3}{2}(1-w),\ \frac{3}{2}(1+w)\right\}$	Saddle node
A_+	$\left\{3-3w,\ 3-\sqrt{\frac{3}{2}}\lambda\right\}$	Unstable point for $\lambda \leq \sqrt{6}$ Saddle node for $\lambda > \sqrt{6}$
A_-	$\left\{3-3w,\ 3+\sqrt{\frac{3}{2}}\lambda\right\}$	Unstable point for $\lambda \geq -\sqrt{6}$ Saddle node for $\lambda < -\sqrt{6}$
B	$\left\{-\frac{3}{4}\left[(1-w) \pm \frac{\Delta}{\lambda^2}\right]\right\}$	Stable point for $3+3w \leq \lambda^2 \leq \frac{24(w+1)^2}{9w+7}$ Stable spiral for $\lambda^2 \geq \frac{24(w+1)^2}{9w+7}$
C	$\left\{\lambda^2-(3+3w),\ \frac{\lambda^2}{2}-3\right\}$	Stable point for $\lambda^2 < 3+3w$ Saddle node for $3+3w \leq \lambda^2 \leq 6$

Table 3: Eigenvalues and stability for the critical points of the system (5.26)-(5.27), where $\Delta = \sqrt{(w-1)\lambda^2(-24-48w-24w^2+7\lambda^2+9w\lambda^2)}$.

and Ω_ϕ. This solution is especially important as it could explain how a scalar field could be present in the Universe yet not disrupt structure formation, regardless of its relative energy density - meaning no need for fine-tuning of the scalar field energy density. It does not, however, represent a universe which is undergoing accelerated expansion. The fixed point exists for $\lambda > 3+3w$ and is always stable (see Table 3 for eigenvalues).[20]

Point C: This critical point's position in the phase space is dependant on the value of the parameter λ, and it represents a universe dominated by the scalar field potential energy. The effective EoS is then determined by the scalar field, $w_{eff} = w_\phi$, which depends directly on the value of λ and is given by $w_{eff} = \lambda^2 - 3$. Importantly, this means that it can take values between $(-1, 1)$. Accelerated expansion occurs when $w_{eff} < -1/3$ which translates to $\lambda^2 < 2$. In the limit that $\lambda \to 0$ the potential (5.25) becomes the constant V_0. This is simply a cosmological constant dominated universe that undergoes de Sitter accelerated expansion. The critical point C exists for $\lambda^2 < 6$ and is either a stable point for $\lambda^2 < 3+3w$

[20]In almost all cases when $w = 0$, point B is actually a stable spiral and trajectories tend to circle around the point before converging on it.

or a saddle node for $\lambda^2 \geq 3 + 3w$. Note that when point B exists in the phase space, point C must always be a saddle node; both cannot exhibit stable solutions at the same time.

5.3.2 Phase space analysis

Let us now examine the phase space and trajectories for the single exponential potential model by plotting the phase portraits with different values of the parameter λ. Restricting ourselves to the upper half unit circle, we find that the dynamics of the phase space can be encapsulated with just three different sets of values for λ, namely: $\lambda^2 < 3 + 3w$, $3 + 3w \leq \lambda^2 < 6$, and $\lambda^2 \geq 6$. This can be seen from the existence and stability conditions in Tables 2 and 3. Another important feature we would like to show in our phase portraits is the effective equation of state parameter w_{eff}, which is achieved through a simple contour plot. Obviously the value of the cosmological fluid equation of state w affects the phase space and the effective equation of state w_{eff}. However, with the focus being on late-time dynamics and dark energy applications, setting $w = 0$ is a sensible choice. The last point to note is that in these examples we will only consider positive values of λ; negative values are a reflection in the phase space about the y-axis and the qualitative behaviour is identical. Figures 2, 3 and 4 show the three distinct cases of phase portraits with $\lambda = 1$, 2 and 3 respectively. Also shown are the regions of accelerated expansion, heteroclinic orbits and the value of w_{eff} as a contour map.

Case 1 ($\lambda < \sqrt{3}$): The critical points that exist for these values of the parameter λ are $A_{\pm}$, O and C. The two unstable points $A_{\pm}$ are the past attractors for all trajectories in the phase space except the heteroclinic orbit $O \Rightarrow C$ (red line in Figure 2). The saddle point O attracts orbits close to the x-axis and repels them towards point C. Because point C is the only stable point and attracts all trajectories in the phase space, it must be globally stable. If $\lambda < \sqrt{2}$ then point C corresponds to accelerated expansion, represented by the region inside the blue dashed line in Figure 2. When $\lambda > \sqrt{2}$, the critical point C moves out of the accelerating region (as seen in Figure 3). It always lies on the unit semicircle, which is evident from its coordinates (Table 2) satisfying $x^2 + y^2 = 1$.

There are in fact two more possible heteroclinic orbits which aren't highlighted in Figure 2. They connect the past attractors $A_{\pm}$ with the origin O. We can therefore define the *heteroclinic sequence* [4] as the series of heteroclinic orbits that a trajectory can follow,

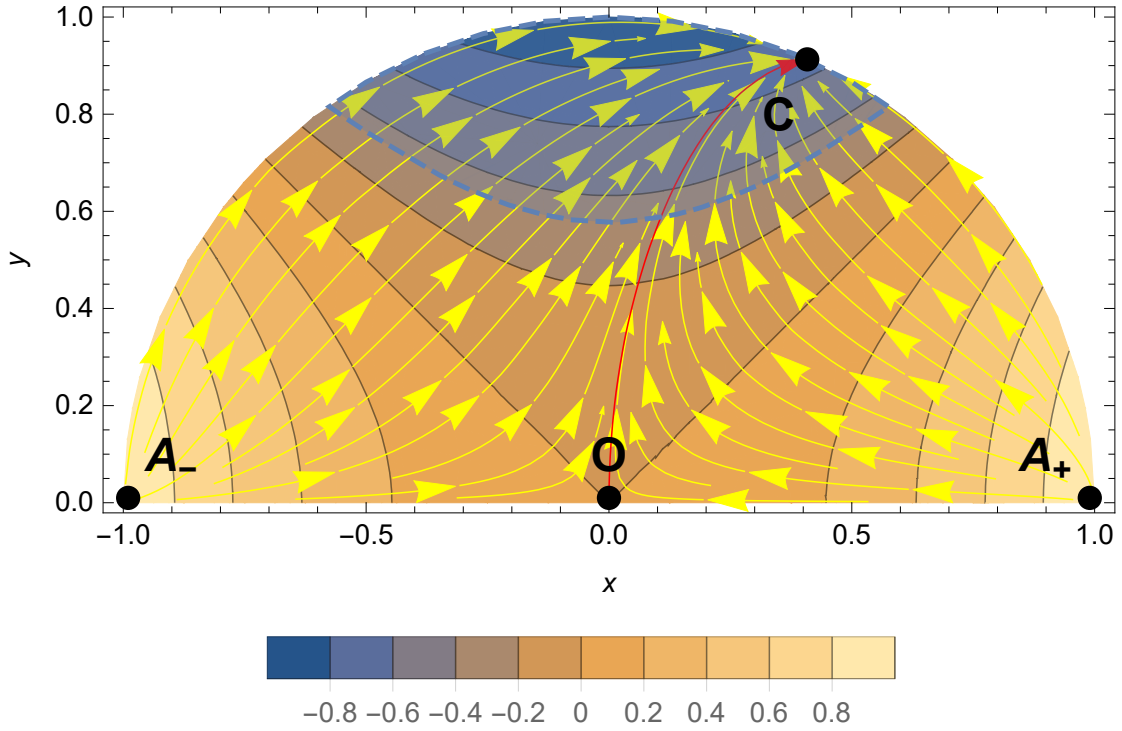

Figure 2: Phase portrait of (5.26)-(5.27) for $\lambda = 1$ and $w = 0$. The contour plot shows $w_{eff} \in [-1, 1]$. The red line is the heteroclinic orbit connecting points O and C. The blue dashed line represents the region with accelerated expansion ($w_{eff} < -1/3$). Point C is the only stable point of the phase space, situated in the accelerating region.

which connect some or all the fixed points. There are two such sequences: $A_- \Rightarrow O \Rightarrow C$ and $A_+ \Rightarrow O \Rightarrow C$. Trajectories that follow along, or close to, these orbits will correspond to a universe that initially begins in the stiff-fluid phase. It then enters a period of matter domination with an equation of state w, before heading off into a phase dominated by the potential energy of the scalar field (accelerating for $\lambda < \sqrt{2}$). The last two stages would provide a realistic cosmological model for the Universe, but a stiff-fluid equation of state for early times is unfavourable. This requires one to fine-tune the initial conditions around the origin for physically acceptable solutions; a general feature for the single exponential potential model.

Case 2 ($\sqrt{3} \leq \lambda < \sqrt{6}$): When λ is constrained between $\sqrt{3}$ and $\sqrt{6}$, all the critical points in Table 2 exist in the phase space (see Figure 3). Both the critical points $A_\pm$ are unstable and again represent the past attractors where all non-heteroclinic orbits can be traced back to. The saddle node O behaves the same as in Case 1, except now it repels

trajectories in the direction of the heteroclinic orbit $O \Rightarrow B$. The critical point C is now also a saddle node, attracting trajectories along the unit semicircle ($x^2+y^2=1$) and repelling them along a heteroclinic orbit towards point B. The global attractor of the phase space is the stable point B, which, along with point C, is not in the accelerating regime. The heteroclinic sequences can now either go like $A_\pm \Rightarrow O \Rightarrow B$ or $A_\pm \Rightarrow C \Rightarrow B$

As can be seen in Figure 3, neither of the heteroclinic sequences can really be used as a realistic model for late-time dark energy applications. This is because all of the critical points in the phase space lie outside of the accelerating regime ($\lambda < \sqrt{2}$). In particular, the global attractor B represents the matter scaling solution, where the scalar field mimics the matter equation of state $w_\phi = w$. Hence the effective equation of state is $w_{eff} = w$. In order to achieve a period of matter domination followed by accelerated expansion, one would need λ close to $\sqrt{3}$ and to follow an orbit from A_- above O into the blue dashed zone, before it is consequently attracted to the scaling solution B. Unfortunately, such an orbit either passes too quickly through the matter dominated phase for structure formation (somewhere across the diagonal contour line $w_{eff} = 0$), or does not enter the accelerating region.

Case 3 ($\lambda \geq \sqrt{6}$): In this case, there are again 4 critical points in the phase space, $A\pm$, O and B. This time however, only one of the $A_\pm$ points is unstable and the other is a saddle node. For $\lambda \geq \sqrt{6}$ the past attractor for the whole phase space is A_- and the saddle node is A_+.[21] The critical point B is a stable spiral and heteroclinic orbit $O \Rightarrow B$ follows this motion (see Figure 4). No solutions correspond to an accelerating universe and there are no viable cosmological trajectories. In the limit that $\lambda \to \infty$, the fixed point B merges with point O at the origin, which can be seen explicitly by considering the coordinates in Table 2. In this limit, the phase space is simply represented by trajectories following clockwise circular motion, originating from the negative x-axis and coming round to end at positive x-axis.[22] This corresponds to the potential $V(\phi) \to 0$.

From each of the three cases examined above, we can determine that the most viable single exponential potential model is when λ is constrained to $\lambda < \sqrt{2}$ and we follow the

[21] If we were to consider $\lambda \leq -\sqrt{6}$ the stability of these points would be swapped.

[22] This can be inferred by looking back at x' and y' equations (5.26)-(5.27) and taking the limit $\lambda \to \infty$. Then, $x' \propto y^2$ and $y' \propto -xy$. Considering the different points where x and y are negative or positive, the direction of motion can be deduced.

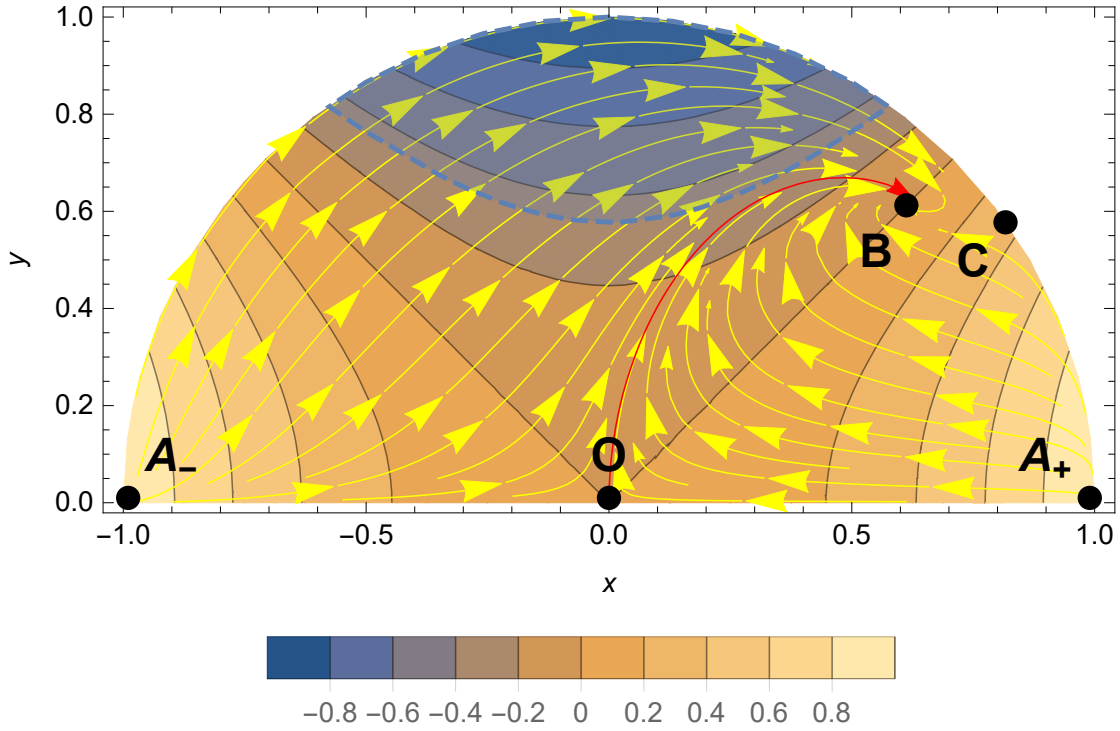

Figure 3: Phase portrait of (5.26)-(5.27) for $\lambda = 2$ and $w = 0$. The contour plot shows $w_{eff} \in [-1, 1]$. The red line is the heteroclinic orbit connecting points O and B. A heteroclinic orbit also exists between points C and B (not shown). The blue dashed line represents the region with accelerated expansion ($w_{eff} < -1/3$). Point B is the only stable point of the phase space and point C is a saddle point. Neither B nor C are in the accelerating region.

heteroclinic orbit from the saddle node O to the late-time attractor C (see Figure 2 as an example). The condition $\lambda < \sqrt{2}$ ensures that point C exists as a stable critical point and is within the accelerating region. A trajectory that passes close to point O ensures that at some point in the universes' past, it was dominated by matter with an effective equation of state equal to that of the matter equation of state w.

5.3.3 Evolution of cosmological parameters

To see exactly how long the period of matter domination lasts for, and the evolution of the other cosmological parameters, the solutions of the autonomous equations (5.26)-(5.27) for $N \equiv \log a$ have been plotted in Figure 5. Beginning at a point close to the origin $(x, y) \approx (0, 0)$ at $N = 0$, we solve for both increasing and decreasing N. Increasing N corresponds to the future trajectory from the origin, whilst decreasing N corresponds to the past trajectory. We have used the same values of $\lambda = 1$ and $w = 0$ as in first phase

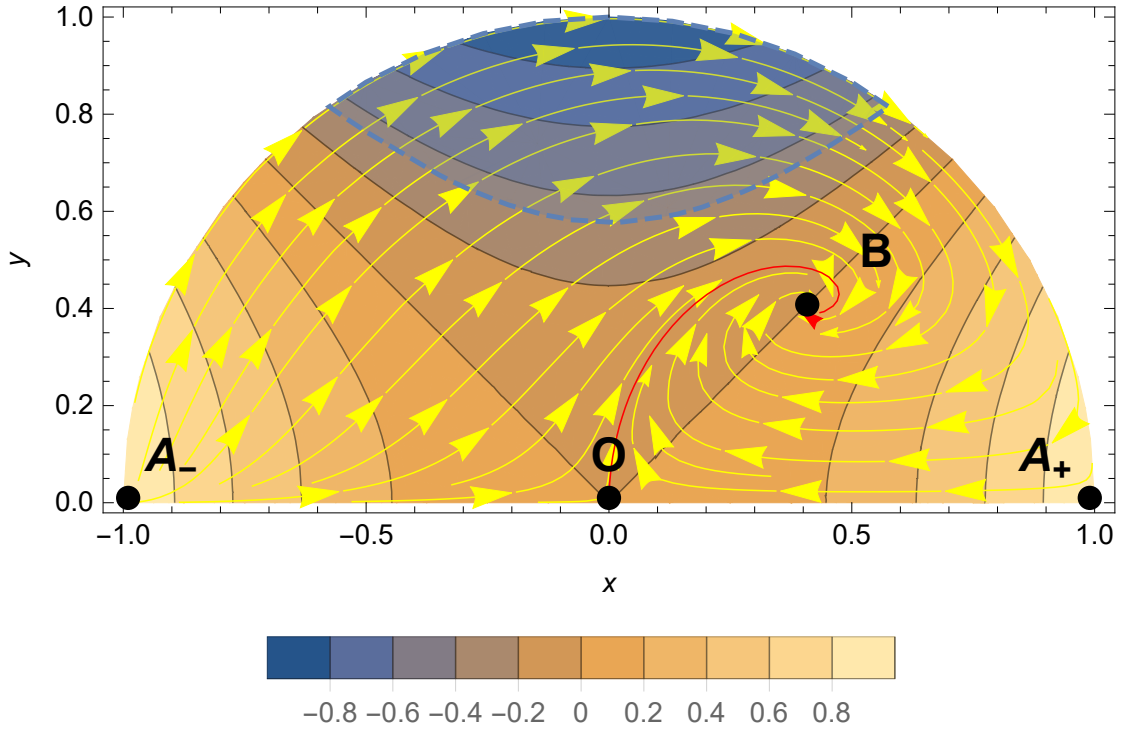

Figure 4: Phase portrait of (5.26)-(5.27) for $\lambda = 3$ and $w = 0$. The contour plot shows $w_{eff} \in [-1, 1]$. The red line is the heteroclinic orbit connecting points O and B. The blue dashed line represents the region with accelerated expansion ($w_{eff} < -1/3$). Point B is a stable spiral and the only stable point of the phase space. It is not within the accelerating region.

portrait (Figure 2). With these parameters we obtain a sufficiently long period of matter domination where the effective equation of state is at zero. At a later time, the scalar field potential energy comes to dominate, with the effective equation of state being well below $-1/3$ (the condition for accelerated expansion). We also notice that at very early times the scalar field kinetic energy dominates - the so called stiff-matter solution. As previously mentioned, we expect the early time solutions to be non-physical, with perhaps some other physics coming into play, e.g. effects from radiation, or inflation at very early times.

Using Figure 5 we can make some rough estimations for the times when different events occurred. The equations relating the independent variable N and the redshift z, which has been derived in Appendix B.3, is given by

$$z = \mathrm{e}^{N_0 - N} - 1 \ , \tag{5.28}$$

where we have used that both $N_0 = 5$ and $z = 0$ today. Using this equation we find that

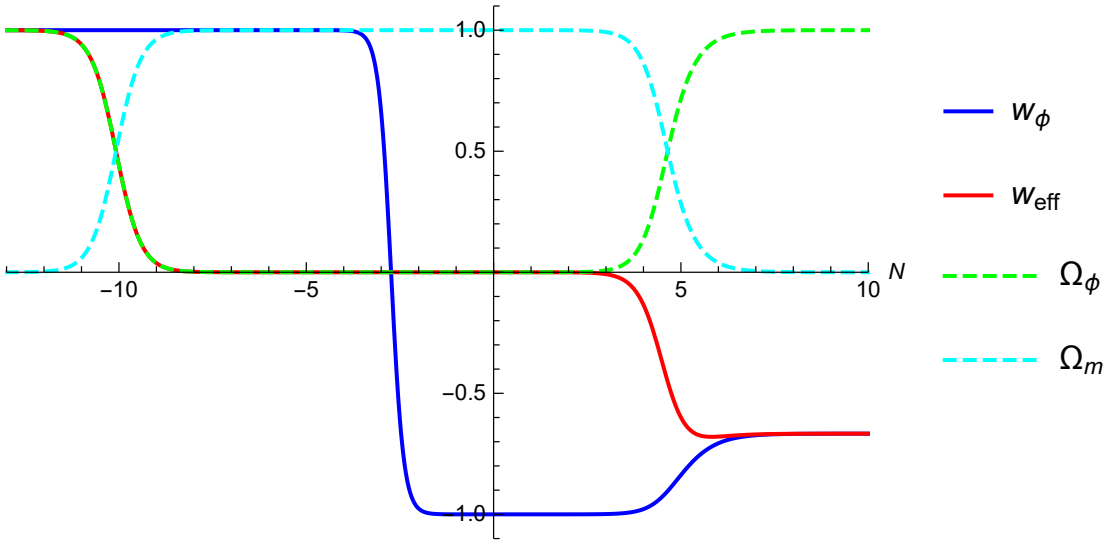

Figure 5: Evolution of cosmological parameters: effective equation of state w_{eff}, scalar field equation of state w_ϕ, matter density parameter Ω_m and scalar field density parameter Ω_ϕ. Solutions for $\lambda = 1$ and $w = 0$, and the initial conditions $x[N = 0] = 0$ and $y[N = 0] = 0.001$.

the matter-dark energy equality at roughly $N = 4.6$ corresponds to a redshift of $z = 0.49$. This prediction agrees reasonably with that found in literature [65]. One could also relate this redshift to time, using a model dependent equation. In Appendix B.3 we do this for a the cosmological model consisting of matter and dark energy. If we extrapolate further into the past to where the scalar field kinetic energy starts to dominate, $N \approx -10$, we obtain a redshift in the millions, $z \approx 3.3 \times 10^6$. This is clearly very early in the universes' evolution and we know not to trust these solutions.

What we can instead do, knowing that the matter-radiation equality occurred at a redshift of roughly $z = 3411$ (taken from the Planck 2018 results [19]), is use the start of the matter domination era as a cut-off point where our model should stop being trusted. The reason being is that we have included only a single matter fluid, and the solutions and phase space may not be accurate representations before this point.[23] This calculation, found in Appendix B.3, gives a value of $N \approx -3$. This is long after the effective equation of state w_{eff} has dropped down to zero in Figure 5. Thus we still retain all of the favourable late-time dynamics after this cut-off point.

[23] In fact, a model including a radiation-like fluid along with matter and a scalar field produces qualitatively different dynamics including the number of fixed points. See [66] as an example, also with a dynamical systems approach).

Another feature of Figure 5 that is immediately obvious is the apparently small crossover between the matter density parameter Ω_m and the scalar field density parameter Ω_ϕ. The fact that today we are in this transitioning period seems highly unlikely (i.e. the coincidence problem). However, if we plug in two conservative values of N for when both the matter and scalar field density parameters are significant (e.g. > 0.1), we find that the transition period is not as brief as it seems. For $N = 4.5$, such that the effective equation of state is still less than $-1/3$, to $N = 5.5$, we have a period between the redshifts $z = 0.65$ and $z = -0.40$. In Appendix B.3 we calculate this to correspond to slightly less than the Hubble time, which is of the order of the age of the universe (approximately between $t \approx 7 \times 10^9$ year sand $t \approx 21 \times 10^9$ years). This means that for this model with these specific parameters, being in a transitioning state from matter to dark energy may not be so coincidental.

This apparent relaxation of the coincidence problem can be better understood by looking back at the phase portraits of Section 5.3.2. The parameters for the model considered in Figure 5 correspond to a universe with extremely-fine tuned initial conditions, as we required that the orbit pass through the point $(x, y) = (0, 0.001)$. Looking at the phase portrait in Figure 2, which has the same values of λ and w, we see that this orbit follows the heteroclinic one from point O to point C. Along this path the trajectories have the slowest speed[24] and therefore correspond to the slowest change in the cosmological parameters. If we instead think in terms of the energy densities, which is more familiar in cosmology, we have required the initial energy density of the scalar field to be sufficiently small that it evolves in such a way to produce the desired results. The problem has simply been repackaged as a problem of fine-tuning of initial conditions. It is now clear that the cosmic coincidence problem and the initial conditions problem are just two sides of the same coin.

To see the extent of this fine-tuning problem and whether the initial energy densities can be relaxed, let us consider orbits starting from elsewhere in the phase space. It turns out that one reproduces the same solutions as in Figure 5 as long as the y value is very close to zero (to four significant figures for $x \to \pm 1$). Remember that in EN variables, y is proportional to the scalar field potential energy (5.13), so we are requiring the potential $V(\phi) \approx 0$. This is also evident from the phase portraits. If one deviates just slightly from the y-axis (for $\lambda < \sqrt{3}$) the matter solution $w_{eff} = w$ is only temporarily obtained when passing through the line $y = |x|$ (which can be seen on the contour plots of Figures 2, 3 and

[24]By speed we mean the rate at which they move through the phase space with respect to N.

4).

For values of $\lambda > \sqrt{3}$, one always obtains scaling solutions at late times, but the attractor (point B) is never accelerating. In Figure 19 of Appendix C, further plots showing the evolution of the cosmological parameters for $\lambda = 1$ and $\lambda = 3$ with different initial conditions are displayed. Figure 19a is in agreement with the conclusions reached above about the strong dependence on initial conditions, whilst Figure 19b shows the scaling behaviour for $\lambda = 3$.

To summarise what we have found for the single exponential potential model, one is able to achieve phenomenologically interesting solutions for different values of the parameter λ. The late-time dark energy attractor and the late-time scaling solutions being of particular interest, though not mutually compatible. Given certain initial conditions, one can produce semi-realistic cosmological models which are consistent with observation, though they must be fine-tuned and suffer the same problems as the cosmological constant model. The early-time solutions are non-physical but we know the single fluid model to be unrealistic at those points [66] for a more recent treatment including both radiation and dark matter components).

5.4 Double Exponential Potential

In the single exponential case, we noted that one could not achieve both scaling solutions and stable accelerating solutions. However, it was discovered by Barreiro, Copeland and Nunes [67] that a double exponential potential quintessence model can in fact obtain both of these solutions simultaneously. The reasoning being that if a single exponential can produce both the solutions but for different values of λ, then two exponentials with different exponents, α and β, should be able to produce both solutions at the same time. If α is large and β is small, then in the early universe the α contribution will be relevant and for later times the β term will be relevant.

Consider the potential

$$V(\phi) = V_1 \mathrm{e}^{-\kappa\alpha\phi} + V_2 \mathrm{e}^{-\kappa\beta\phi} \,, \tag{5.29}$$

where α, β, V_1 and V_2 are constants.[25] For the potential above, the definition of λ (5.22) is not a constant parameter and instead a function of ϕ. Therefore to close the set of dynamical

[25] We stress here that realistic values of V_1 and V_2 must be chosen to be order $\rho_\Lambda \approx 10^{-47}\mathrm{GeV}^4$ so as to match the observed value of Λ today [67]. There still exist this seemingly unnatural fine-tuning.

equations, (5.20)-(5.21), we would need to include its evolution, the λ' equation (5.23). One can see that $\lambda(\phi)$ is indeed invertible and the function $\Gamma(\lambda)$ (5.24) can be obtained. However, an alternative route is to use a different set of variables, a simple extension of the EN variables previously considered, which transforms the cosmological equations (5.7), (5.8) and (5.9) into a closed autonomous system. The advantage of this approach is that the system is already compact. The derivation of the equations used in this section under the change of variables is given in Appendix B.2.2.

The choice of variables, as employed by Li et al. [68], are given by

$$x = \frac{\kappa\dot{\phi}}{\sqrt{6}H} \quad , \quad y = \sqrt{\frac{\kappa^2 V_1 \mathrm{e}^{-\kappa\alpha\phi}}{3H^2}} \quad , \quad z = \sqrt{\frac{\kappa^2 V_2 \mathrm{e}^{-\kappa\beta\phi}}{3H^2}} \ . \tag{5.30}$$

Following the same procedure as in Section 5.2, one arrives at the Friedmann constraint,

$$1 = \Omega_m + x^2 + y^2 + z^2 \ , \tag{5.31}$$

where $\Omega_m = \kappa^2\rho/(3H^2)$ is defined as before. The scalar field density parameter, along with the constraints for x, y and z, is given by

$$0 \leq \Omega_\phi = x^2 + y^2 + z^2 \leq 1 \ . \tag{5.32}$$

The kinetic energy density of the scalar field is again represented by x^2, and the potential energy density is represented by the combination of $y^2 + z^2$.

The equation of state for the scalar field, defined in (5.12), can be written in terms of the new variables as

$$w_\phi = \frac{x^2 - y^2 - z^2}{x^2 + y^2 + z^2} \ . \tag{5.33}$$

The effective equation of state can then be written as

$$\begin{aligned} w_{eff} &= w\Omega_m + w_\phi\Omega_\phi \\ &= w(1 - x^2 - y^2 - z^2) + \Big(\frac{x^2 - y^2 - z^2}{x^2 + y^2 + z^2}\Big)(x^2 + y^2 + z^2) \\ &= w(1 - x^2 - y^2 - z^2) + x^2 - y^2 - z^2 \ . \end{aligned} \tag{5.34}$$

The scalar field equation of state w_ϕ can take values in the range $[-1, 1]$, which is the same as in the singe exponential case. The physical phase space is constrained by equation (5.32), which is a sphere of unit radius centred on the origin. However, arguments can be made for considering only positive values of y and z, which we shall see explicitly in the dynamical

Point	x	y	z	Existence	Ω_ϕ	w_ϕ	w_{eff}
(i)	0	0	0	Always	0	-	w
$(\text{ii})_\pm$	± 1	0	0	Always	1	1	1
(iii)	$\sqrt{\frac{3}{2}}\frac{(1+w)}{\alpha}$	$\sqrt{\frac{3(1-w^2)}{2\alpha^2}}$	0	$\alpha^2 \geq 3(1+w)$	$\frac{3(1+w)}{\alpha^2}$	w	w
(iv)	$\sqrt{\frac{3}{2}}\frac{(1+w)}{\beta}$	0	$\sqrt{\frac{3(1-w^2)}{2\beta^2}}$	$\beta^2 \geq 3(1+w)$	$\frac{3(1+w)}{\beta^2}$	w	w
(v)	$\frac{\alpha}{\sqrt{6}}$	$\sqrt{1-\frac{\alpha^2}{6}}$	0	$\alpha^2 \leq 6$	1	$\frac{\alpha^2}{3}-1$	$\frac{\alpha^2}{3}-1$
(vi)	$\frac{\beta}{\sqrt{6}}$	0	$\sqrt{1-\frac{\beta^2}{6}}$	$\beta^2 \leq 6$	1	$\frac{\beta^2}{3}-1$	$\frac{\beta^2}{3}-1$
(vii)	0	$\frac{\sqrt{b}}{\sqrt{b-a}}$,	$\frac{\sqrt{a}}{\sqrt{a-b}}$	$\alpha\beta < 0$	1	-1	-1

Table 4: Critical points and cosmological parameters for the system (5.35)-(5.37).

equations. Therefore we can safely consider the variables in the range $x \in [-1, 1]$ and $y, z \in [0, 1]$.

Employing the variables defined in (5.30), and shown clearly in Appendix B.2.2, the acceleration equation (5.8) and Klein-Gordon equation (5.9) can be written as a three-dimensional dynamical system defined by the autonomous equations

$$x' = -\frac{3}{2}x\Big[(w+1)(x^2+y^2+z^2-1) - 2x^2 + 2\Big] + \frac{\sqrt{3}}{\sqrt{2}}\big(\alpha y^2 + \beta z^2\big)\ , \tag{5.35}$$

$$y' = -\frac{3}{2}y\Big[(w+1)(x^2+y^2+z^2-1) - 2x^2\Big] - \frac{\sqrt{3}}{\sqrt{2}}\alpha xy\ , \tag{5.36}$$

$$z' = -\frac{3}{2}z\Big[(w+1)(x^2+y^2+z^2-1) - 2x^2\Big] - \frac{\sqrt{3}}{\sqrt{2}}\beta xz\ , \tag{5.37}$$

where prime denotes the derivative with respect to $N = \log a$. These equations are the same as those given in [68]. As previously hinted at, both the y' and z' equations have invariant submanifolds for $y = 0$ and $z = 0$ respectively. Additionally, they are symmetric under the individual transformations $y \to -y$ and $z \to -z$. For this reason, we can consider just the positive values of y and z. The equations are also invariant under the simultaneous transformations that $x \to -x$ along with $\alpha \to -\alpha$ and $\beta \to -\beta$. However, we will still need to consider both positive and negative values of the exponents α and β because of their sign relative to each other.

Point	Eigenvalues	Stability
(i)	$\{-\frac{3}{2}(1-w),\ \frac{3}{2}(1+w),\ \frac{3}{2}(1+w)\}$	Saddle
$(ii)_+$	$\{3-3w,\ 3-\sqrt{\frac{3}{2}}\alpha,\ 3-\sqrt{\frac{3}{2}}\beta\}$	Unstable for $\alpha,\ \beta \leq \sqrt{6}$ Saddle for α or $\beta > \sqrt{6}$
$(ii)_-$	$\{3-3w,\ 3+\sqrt{\frac{3}{2}}\alpha,\ 3+\sqrt{\frac{3}{2}}\beta\}$	Unstable for $\alpha,\ \beta \geq -\sqrt{6}$ Saddle for α or $\beta < -\sqrt{6}$
(iii)	$\left\{-\frac{3}{4}\left[(1-w) \pm \frac{\Delta_\alpha}{\alpha^2}\right],\ \frac{3(w+1)(\alpha-\beta)}{2\alpha}\right\}$	Stable $\begin{cases} \beta < \alpha < -\sqrt{3w+3} \\ \sqrt{3w+3} < \alpha < \beta \end{cases}$
(iv)	$\left\{-\frac{3}{4}\left[(1-w) \pm \frac{\Delta_\beta}{\beta^2}\right],\ \frac{3(w+1)(\beta-\alpha)}{2\beta}\right\}$	Stable $\begin{cases} \alpha < \beta < -\sqrt{3w+3} \\ \sqrt{3w+3} < \beta < \alpha \end{cases}$
(v)	$\left\{\alpha^2-3w-3, \frac{1}{2}\left(\alpha^2-6\right), \frac{1}{2}\alpha(\alpha-\beta)\right\}$	Stable $\begin{cases} 0 < \alpha < \sqrt{3w+3} \ \text{ for } \alpha < \beta \\ -\sqrt{3w+3} < \alpha < 0 \ \text{ for } \alpha > \beta \end{cases}$
(vi)	$\left\{\beta^2-3w-3, \frac{1}{2}\left(\beta^2-6\right), \frac{1}{2}\beta(\beta-\alpha)\right\}$	Stable $\begin{cases} 0 < \beta < \sqrt{3w+3} \ \text{ for } \beta < \alpha \\ -\sqrt{3w+3} < \beta < 0 \ \text{ for } \beta > \alpha \end{cases}$
(vii)	$\left\{-3(w+1),\ \frac{-3\pm\sqrt{12\alpha\beta+9}}{2}\right\}$	Stable

Table 5: Eigenvalues and stability for the critical points of the system (5.35-(5.36), where $\Delta_\alpha = \sqrt{(w-1)\alpha^2(-24-48w-24w^2+7\alpha^2+9w\alpha^2)}$ and $\Delta_\beta = \sqrt{(w-1)\beta^2(-24-48w-24w^2+7\beta^2+9w\beta^2)}$.

5.4.1 Critical points and stability

The critical points of the system (5.35)-(5.37) are shown in Table 4. The stability analysis of the critical points along with their eigenvalues is displayed in Table 5. The stability of all the critical points has been determined with linear stability theory (Section 2.2) and the results match those found by Li et al. [68]

We see that for the double exponential potential there are three more critical points than in the single exponential case, but only one of these points is distinctly new. Because most of the critical points in Table 4 share similarities with the critical points in the single exponential case, we shall focus mainly on the qualitatively new features. The stability of all the points has been determined with linear stability theory based on the calculated eigenvalues.

The critical point (i) is the origin of the phase space and corresponds directly to point O, sharing the same properties as its single exponential counterpart. It is the matter dominated solution whose existence is guaranteed, and it is always a saddle point. The two points $(\text{ii})_{\pm}$ at $(\pm 1, 0, 0)$ are the possible early time attractors and represent the scalar field kinetic energy dominated stiff-matter solutions. Their existence is also guaranteed and they can be either unstable or saddles. They are analogues to the points $A_{\pm}$, with the subtle difference that both $(\text{ii})_{+}$ and $(\text{ii})_{-}$ can be saddle points at the same time.

The two points (iii) and (iv) (see Table 4 for coordinates) are the scaling solutions, where the scalar field equation of state matches the matter equation of state $w_\phi = w$. They correspond to the scaling solution for the single exponential potential, point B, with the single exponent λ of point B replaced by either α for point (iii) or β for point (iv). Their stability conditions (Table 5) ensure that only one of the two points can exist as a stable point in the same phase space.

Likewise, points (v) and (vi) share the same properties with the late-time attractor point C, (see Table 4 for coordinates). They represent the scalar field potential energy dominated solutions and can both correspond to accelerated expansion. At the critical point (v), the universe undergoes accelerated expansion when $\alpha^2 < 2$. At the critical point (vi), accelerated expansion occurs for $\beta^2 < 2$. For a given value of α and β, only one of the critical points (v) and (vi) can be stable (see Table 5 for the exact conditions).

The last critical point (vii) shares no analogue with the single exponential case. Its existence is dependant on one of α or β being positive and the other being negative. The

scalar field potential (5.29) then exhibits a stable minimum for some positive value of ϕ. The scalar field equation of state w_ϕ is always equal to negative one here. This is then just a de Sitter solution (or positive cosmological constant), which was not realised as a critical point for the single exponential. We did see that in the special case when $\lambda = 0$, the fixed point C acted as a cosmological constant with $V = V_0$. However, this is strictly different from the situation presented here. In the previous case, the value of ϕ was unconstrained[26], whereas here it is sitting in the minimum of a potential well, determined by the coefficients α and β. Because of the existence condition, $\alpha\beta < 0$, the eigenvalues always have negative real part, with the last two also having an imaginary component for $\alpha\beta < -3/4$.

For the time being, let us restrict ourselves to positive values of α and β. We find that we can obtain both stable scaling solutions and stable accelerated expansion solutions in the same phase space, so long as α and β satisfy $\alpha > \sqrt{3(1+w)}$ and $\beta < \sqrt{2}$ (or the same conditions with α and β swapped over). The inability to obtain both of these solutions in the single exponential case is what led to its fine-tuning problems.

5.4.2 Phase space and evolution analysis

The phase space of the dynamical system (5.35)-(5.37) is three-dimensional and much more complicated than the previous $2d$ case (5.26)-(5.27). To represent all of the distinct cases of the different fixed points in Table 4, a large number of phase portraits must be drawn, and the dynamics of the trajectories are not so clear. For this reason, it is better to consider individual orbits, which we solve numerically.

In figure 6 we have plotted the solution for a specific set of initial conditions, with the parameters set to $\alpha = 3$, $\beta = 4$ and $w = 0$. Figure 6a shows the orbit for such a solution, with the yellow point indication the initial conditions and solving for increasing and decreasing N. One immediately sees that the critical point $(\text{ii})_-$ is the past attractor. The orbit then circles round and is attracted towards the saddle at the origin, point (i), before ending up at the late-time attractor point (iii). The solution then corresponds to the scaling solution at late times, with $w_{eff} = w$. This is confirmed in Figure 6b, where the evolution of the cosmological parameters has been plotted. In the past, at point $(\text{ii})_-$, the effective equation of state is equal to $+1$. The effective equation of state parameter w_{eff} then drops down to $w = 0$, where it stays for all later times.

[26]Reminiscent of the moduli stabilisation problem in string theory.

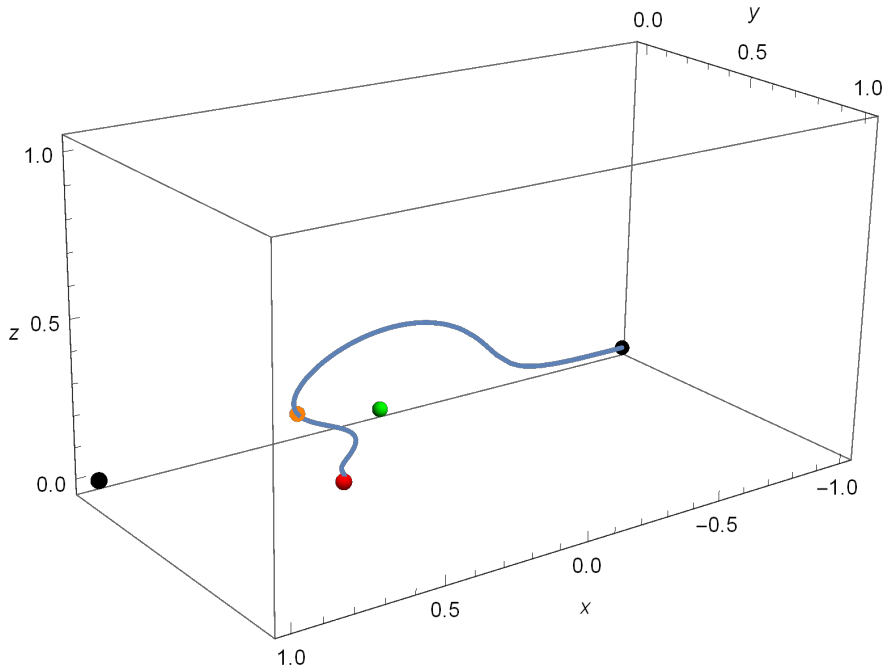

(a) Orbit of single trajectory through phase space. The yellow point represents the initial conditions at $(0.7, 0.1, 0)$ for $N = 0$. Point (i) is represented by the green ball, points $(\text{ii})_{\pm}$ are represented by the black balls and point (iii) is represented by the red ball. The future of the orbit is towards the stable point (iii). See Table 4 for coordinates.

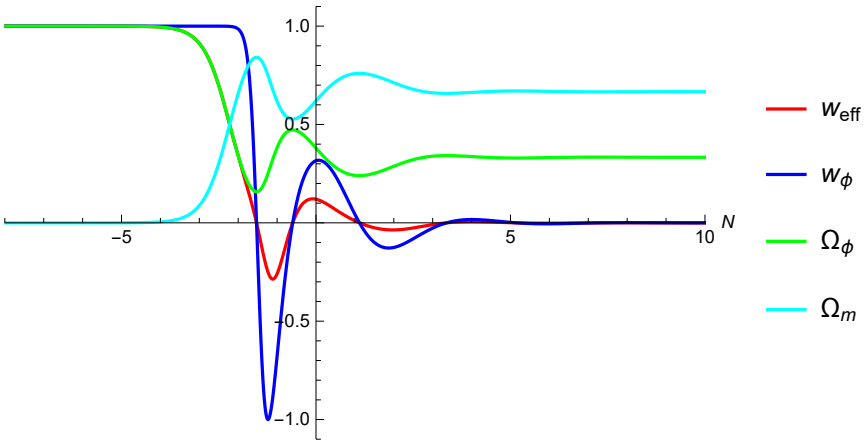

(b) Evolution of cosmological parameters.

Figure 6: Numerical solutions to the autonomous equations (5.35)-(5.37) for $\alpha = 3$, $\beta = 4$ and $w = 0$. Subfigure (a) shows one individual orbit, whilst Subfigure (b) shows the corresponding evolution of the cosmological parameters. The yellow point in Subfigure (a) corresponds to $N = 0$ in Subfigure (b).

With the values $\alpha = 10$, $\beta = 1$ and $w = 0$, let us consider a different trajectory. In Figure 7 we see the scalar field potential energy dominated fixed point acting as the late-time attractor. The orbit in Figure 7a again begins at the past attractor, point $(\text{ii})_-$, before circling round and coming up (in the z-direction) to point (vi). The evolution of the cosmological parameters (Figure 7b) confirms that the scalar field dominates at this point, and the effective equation of state is given by $\frac{\beta^2}{3} - 1$. For our value of $\beta = 1$, this corresponds to an accelerating expansion region.

In Figure 8 we have plotted the solutions for $\alpha = 10$, $\beta = 1$, $w = 0$, and a range of different initial conditions. In figure 8a the heteroclinic orbits have also been plotted as dashed lines: point $(\text{ii})_- \rightarrow$ (vi) (purple), point $(\text{ii})_+ \rightarrow$ (vi) (pink), and point (iii) $\rightarrow$ (vi) (black). The yellow orbit ends up at the saddle point (iii) because its initial condition was in the x-y plane with $z = 0$. The evolution of the cosmological parameter for specific orbits has also been plotted in Figure 8b. One can see that the red and green orbits, although having very different trajectories in the phase space, could both translate to viable models of the Universe. We are also assuming that the unrealistic early time predictions not be considered for the same reason as in the singe exponential case. Specifically, that we have neglected the presence of radiation.

The last solution we have plotted is for or $\alpha < 0$ and $\beta > 0$ in Figure 20 of Appendix C. In this case, the late-time attractor is always the the de-Sitter solution, critical point (vii). One can obtain significant periods of matter domination followed by accelerated expansion, with less of a dependence on initial conditions. For this reason, these solutions are phenomenologically favourable. However, the de Sitter solution will not be a viable consideration when we move on to our string theory motivated examples. This will become more clear in Section 6.

In summary, we note that the dynamical approach used in this section has revealed a lot about the late-time dynamics of the double exponential potential model. In Figure 8 we have seen how for a range of different initial conditions, corresponding to different initial relative energy densities for the scalar field (5.31), can be attracted towards the saddle scaling solution (iii), before being attracted to the late-time accelerating solution (vi). This means that even if the initial energy density of the quintessence field ρ_ϕ is greater than that of matter ρ, we can still obtain scaling solutions with the right conditions for matter formation. This was first noted by Barreiro et al. [67]. Lastly, we issue a reminder that

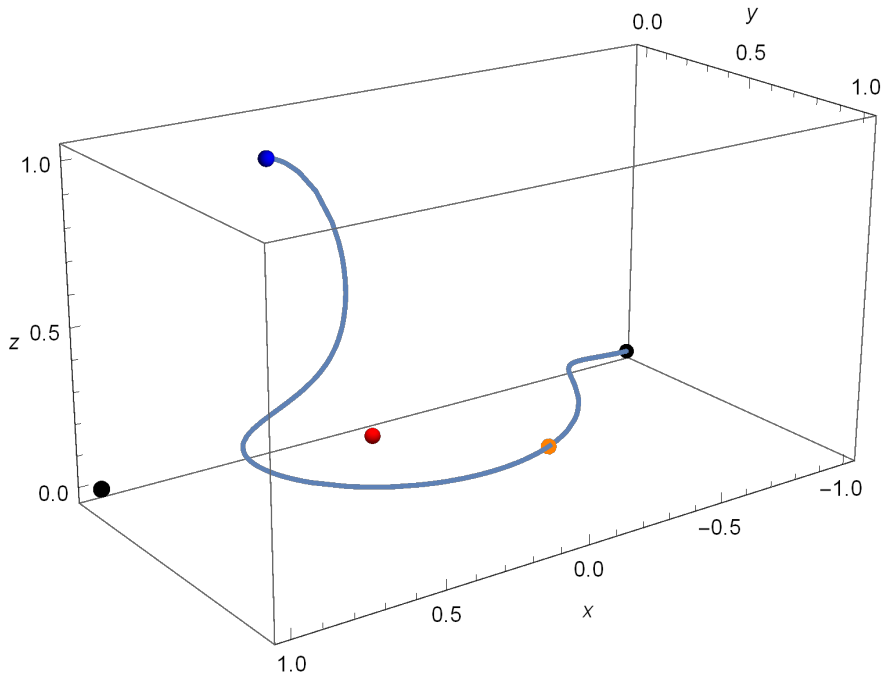

(a) Orbit of single trajectory through phase space. The yellow point represents the initial conditions at $(-0.2, 0.6, 0.05)$ for $N = 0$. Points $(\text{ii})_{\pm}$ are represented by the black balls, point (iii) is represented by the red ball and point (vi) is represented by the blue ball. The future of the orbit is towards the stable point (vi). See Table 4 for coordinates.

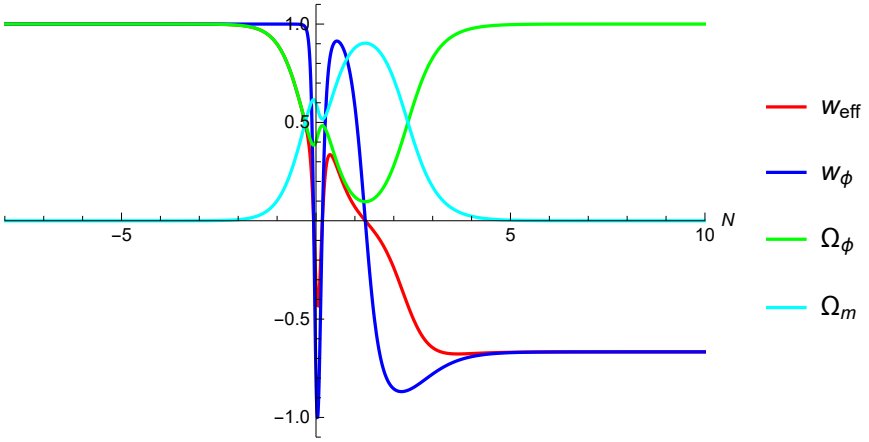

(b) Evolution of cosmological parameters.

Figure 7: Numerical solutions to the autonomous equations (5.35)-(5.37) for $\alpha = 10$, $\beta = 1$ and $w = 0$. Subfigure (a) shows one individual orbit, whilst Subfigure (b) shows the corresponding evolution of the cosmological parameters. The yellow point in Subfigure (a) corresponds to $N = 0$ in Subfigure (b).

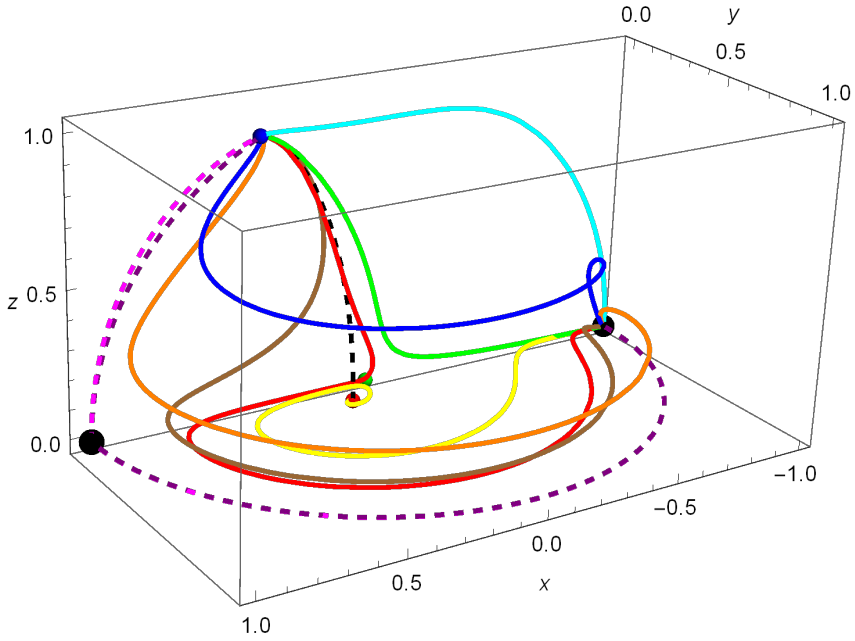

(a) Orbit of multiple trajectories through phase space. Point (i) is represented by the green ball, points $(ii)_{\pm}$ are represented by the black balls, point (iii) is represented by the red ball and point (vi) is represented by the blue ball. The future of the orbit is towards the stable point (vi). The dashed lines represent heteroclinic orbits.

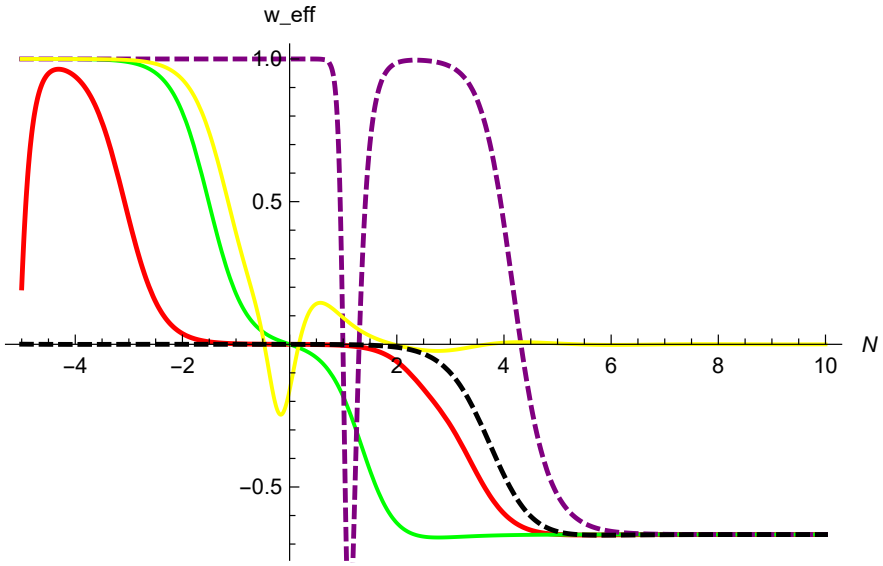

(b) Evolution of w_{eff} for some of the trajectories plotted above.

Figure 8: Numerical solutions to the autonomous equations (5.35)-(5.37) for $\alpha = 10$, $\beta = 1$ and $w = 0$. Subfigure (a) shows several orbits with different initial conditions, whilst Subfigure (b) shows the corresponding evolution of w_{eff} for those orbits

the dynamics models with more than barotropic fluid can be qualitatively different. For example, in [67], the presence of radiation allows one to choose a wider variety of initial conditions than we have considered here. One can also go on to include couplings between the matter and dark energy sectors [69].

5.5 Power-Law Potential

The last form of potential we shall consider is the inverse power-law potential, or the *Ratra-Peebles potential* [70]-[71], which can be well motivated from supersymmetry phenomenology and has notably interesting features.

Consider a potential of the form

$$V(\phi) = \frac{M^{\alpha+4}}{\phi^{\alpha}} \ , \tag{5.38}$$

where M and γ are both positive constants. One immediately sees that in order to have a closed set of autonomous equations, one must consider the evolution of λ, given in equation (5.23). This is because λ is now a variable which depends on ϕ,

$$\lambda = -\frac{V_{,\phi}}{\kappa V} = \frac{\alpha}{\kappa\phi} \ , \tag{5.39}$$

which can range from $\lambda = -\infty$ to $\lambda = +\infty$.

We find that the function Γ is given by

$$\Gamma = \frac{VV_{,,\phi}}{V_{,\phi}^2} = \frac{\alpha+1}{\alpha} \ , \tag{5.40}$$

which is constant and depends only on the parameter α. The set of autonomous equations governing the dynamics of a potential of the form (5.38) is then given by

$$x' = -\frac{3}{2}\Big[2x + (w-1)x^3 + x(x+1)(y^2-1) - \frac{\sqrt{2}}{\sqrt{3}}\lambda y^2\Big] \ , \tag{5.41}$$

$$y' = -\frac{3}{2}y\Big[(w-1)x^2 + (w+1)(y^2-1) + \frac{\sqrt{2}}{\sqrt{3}}\lambda x\Big] \ , \tag{5.42}$$

$$\lambda' = -\frac{\sqrt{6}}{\alpha}\lambda^2 x \ . \tag{5.43}$$

Note again the symmetry; under the simultaneous transformation $x \to -x$ and $\lambda \to -\lambda$, the system remains invariant. For this reason we can consider only the positive values of λ, which now ranges from $\lambda = 0$ to $\lambda = +\infty$. The symmetry in the y coordinate from the previous examples is also present, allowing us to ignore negative values of y.

As noted in [4], the phase space for the system is non-compact with λ stretching to positive infinity. To instead make it compact[27], we follow the work of Ng et al. [49] and introduce a new coordinate defined by

$$z = \frac{\lambda}{\lambda + 1} \ , \tag{5.44}$$

so that $\lambda = z/(1-z)$. With this new definition, the equations (5.41)-(5.43) can be rewritten as

$$x' = -\frac{3}{2}\Big[2x + (w-1)x^3 + x(w+1)(y^2-1) - \frac{\sqrt{2}}{\sqrt{3}}\frac{z}{1-z}y^2\Big] \ , \tag{5.45}$$

$$y' = -\frac{3}{2}y\Big[(w-1)x^2 + (w+1)(y^2-1) + \frac{\sqrt{2}}{\sqrt{3}}\frac{z}{1-z}x\Big] \ , \tag{5.46}$$

$$z' = -\frac{\sqrt{6}}{\alpha}z^2 x \ . \tag{5.47}$$

The phase space is then reduced to the positive y-half cylinder with z ranging from 0 to 1. The $z = 1$ points, however, are divergent, as can be seen in the last terms of the x' and y' equations. These points correspond to $\lambda \to \infty$. To remove these singularities we follow the procedure taken in [4] and multiple the right hand side of equations (5.45) to (5.47) by $(1-z)$. This allows us to study the phase space in the limit that $\lambda \to +\infty$ at $z = 1$. This slight trick does not change the qualitative features of the system, with all the symmetries discussed still intact.

The final set of equations forming the autonomous system that we shall be studying are given by following,

$$x' = -\frac{3}{2}(1-z)\Big[2x + (w-1)x^3 + x(w+1)(y^2-1)\Big] + \frac{\sqrt{3}}{\sqrt{2}}zy^2 \ , \tag{5.48}$$

$$y' = -\frac{3}{2}y(1-z)\Big[(w-1)x^2 + (w+1)(y^2-1)\Big] - \frac{\sqrt{3}}{\sqrt{2}}xyz \ , \tag{5.49}$$

$$z' = -\frac{\sqrt{6}}{\alpha}(1-z)z^2 x \ , \tag{5.50}$$

and the phase space bounded by $-1 \leq x \leq 1$, $0 \leq y \leq 1$ and $0 \leq z \leq 1$. The cosmological parameter are governed by the same x and y equations derived in Section 6.3.

[27] 'Compact' here being different to use of the word in previous sections regarding string theory.

Point	x	y	z	Existence	Ω_ϕ	w_ϕ	w_{eff}
O_z	0	0	Any	Always	0	-	w
$A_\pm$	± 1	0	0	Always	1	1	1
B_x	Any	0	1	Always	x^2	1	$x^2(1-w)+w$
C	0	1	0	Always	1	-1	-1

Table 6: Critical points and cosmological parameters for the system (5.35)-(5.37). The constant κ has been set to one.

5.5.1 Critical points and stability

The critical points obtained from equations (5.48)-(5.50) are displayed in Table 6, along with the cosmological parameters. The first significant difference about this phase space, compared to the exponential examples considered earlier, is that two of the critical points correspond to a *line of critical points* or *critical line*. Moreover, for the critical line B_x, where x can take any value, the cosmological parameters Ω_ϕ and w_{eff} depend on the position of the x coordinate. This will be explored in more detail when considering the phase portraits. All of the critical points in the phase space exist for all values of α and w.

The stability of each point, along with its eigenvalues, is given in Table 7. At least one of the eigenvalues for every critical point is equal to zero. This means all of the points are non-hyperbolic and must be treated carefully. The stability analysis of the points marked with a * in Table 7 are credited to the work done by Tamanini [72], where a combination of more advanced techniques such as centre manifold theory and computational methods have been used (see [4] for the review based on the same work, or [73] for an introduction on centre manifold theory). Let us move on to discussing each point.

Points O_z: The line of critical points on the z-axis from $z = 0$ to $z = 1$ are the matter dominated solutions and the scalar field plays no role. Just like for the single exponential potential, the scalar field equation of state is undefined and the effective equation of state is always $w_{eff} = w$. The stability of the critical line, though non-hyperbolic, can still be determined just by examining the eigenvalues in Table 7. Because $(w+1)$ is always positive, $(w-1)$ is always negative and $(z-1)$ is always positive, the two non-zero eigenvalues are always of opposite sign. Therefore the critical line is always a saddle.

Point	Eigenvalues	Stability
O_z	$\left\{0,\ -\frac{3}{2}(z-1)(w\pm 1)\right\}$	Saddle
A_+	$\left\{0,\ 3,\ 3-3w\right\}$	Unstable* for $\alpha<0$ Saddle* for $\alpha>0$
A_-	$\left\{0,\ 3,\ 3-3w\right\}$	Unstable* for $\alpha>0$ Saddle* for $\alpha<0$
B_x	$\left\{0,\ -\frac{\sqrt{3}}{\sqrt{2}}x,\ \frac{\sqrt{6}}{\alpha}x\right\}$	Saddle for $x>0$ and $\alpha>0$ Saddle for $x<0$ and $\alpha>0$ Stable* for $x>0$ and $\alpha<0$ Unstable* for $x<0$ and $\alpha<0$
C	$\left\{0,-3,-3-3w\right\}$	Stable* for $\alpha>0$ Saddle* for $\alpha<0$

Table 7: Eigenvalues and stability for the critical points of the system (5.48)-(5.50). Stabilities marked with a * indicate that non-hyperbolic methods must be applied.

Points $A_{\pm}$: The two critical points at $(\pm 1, 0, 0)$ are the stiff-matter solutions we've encountered in both the previous examples. The scalar field kinetic energy dominates at these points, with the effective equation of state always being $w_{eff} = 1$. As noted earlier, they are physically unfavourable and not relevant to the late-time dynamics. The critical points are non-hyperbolic with two of the eigenvalues being positive and the other being zero. As none of the eigenvalues are negative, we can infer that the points are at least asymptotically unstable. But to determine whether they are repellers or saddles, one must use more advanced techniques; in this case, centre manifold theory. This has been considered by Tamanini [72] and Bahamonde et al [4] leading to the stability conditions presented in Table 7.

Points B_x: Here we have another critical line, this time connecting the points $(-1, 0, 1)$ and $(1, 0, 1)$. The relationship between z and λ (5.44) implies that any point with $z = 1$ actually corresponds to the limit that $\lambda \to \infty$. The points B_x therefore characterise the asymptotic behaviour of orbits when $\lambda \to \infty$. The scalar field density parameter varies depending on the x coordinate, $\Omega_\phi = x^2$, and can take values in the range $0 \leq \Omega_\phi \leq 1$. The scalar field equation of state is always 1, as x^2 simply represents the kinetic energy. The effective equation of state therefore varies depending on the value of x, and is given by $w_{eff} = x^2(1 - w) + w$, which ranges between w and 1. The eigenvalues of B_x, displayed in Table 7, are non-hyperbolic. When $\alpha > 0$ the two non-zero eigenvalues are always of different sign, and so the critical line can be determined to be a saddle. In the case when $\alpha < 0$, the two non-zero eigenvalues have the same sign and non-hyperbolic methods must be considered. Tamanini [72] has shown through the use of centre manifold theory and numerical methods that the critical line is stable for $x > 0$ and $\alpha < 0$, and unstable for $x < 0$ and $\alpha < 0$.

Points C: The last critical point is the scalar field potential energy dominated solution, with an equation of state $w_{eff} = w_\phi = -1$. At the point, the universe undergoes accelerated expansion, satisfying $w_{eff} < -1/3$. Since the point is non-hyperbolic and both of the non-zero eigenvalues are negative, we shall make use of the Lyapunov method covered in Section 2.3. Beforehand, we note that numerical simulations [72] yield the stability results listed in Table 7. These results will also be confirmed from our phase space analysis.

5.5.2 Lyapunov method for the non-hyperbolic critical point C

For the fixed point C, let us consider the Lyapunov candidate function suggested in [4] and defined by

$$V = x^8 + (y-1)^6 + c_1 z^4 + c_2 x^2 z^4 \ , \tag{5.51}$$

where c_1 and c_2 are coefficients to be determined. The function satisfies the first two conditions of Definition 5: that $V(x,y,z) > V(1,0,1)$ and that V is differentiable. The third requirement is that $V' \leq 0$. The derivative of (5.51) is given by

$$V' = 8x^7 x' + 6(y-1)^5 y' + 4c_1 z^3 z' + 2xx' z^4 c_2 + 4z^3 z' c_2 x^2 \ . \tag{5.52}$$

Expanding the above equation with the definitions of x' (5.48), y' (5.49) and z' (5.50) yields the slightly longer expression

$$\begin{aligned} V' = 8x^7 \Bigg[-\frac{3}{2}(z-1)\Big[2x + (w-1)x^3 + x(w+1)(y^2-1)\Big] + \frac{\sqrt{3}}{\sqrt{2}} z y^2 \Bigg] + \\ 6(y-1)^5 \Bigg[-\frac{3}{2} y (z-1)\Big[(w-1)x^2 + (w+1)(y^2-1)\Big] - \frac{\sqrt{3}}{\sqrt{2}} xyz \Bigg] + \\ 4c_1 z^3 \Bigg[-\frac{\sqrt{6}}{\alpha}(1-z) z^2 x \Bigg] + \\ 2xz^4 c_2 \Bigg[-\frac{3}{2}(z-1)\Big[2x + (w-1)x^3 + x(w+1)(y^2-1)\Big] + \frac{\sqrt{3}}{\sqrt{2}} z y^2 \Bigg] + \\ 4z^3 c_2 x^2 \Bigg[-\frac{\sqrt{6}}{\alpha}(1-z) z^2 x \Bigg] \ . \end{aligned} \tag{5.53}$$

Examining the above function, it is difficult to tell whether the third requirement is satisfied. However, just like in the example in Section 2.3, it is useful to transform to polar coordinates $x = r\sin\theta\cos\phi$, $y = 1 + r\sin\theta\sin\phi$ and $z = r\cos\theta$. In polar coordinates, we have an expression with a large number terms from order r^6 to r^{11}. Collecting the lowest order terms gives

$$\begin{aligned} V' = r^6 \Bigg[\sqrt{6}\sin\theta\cos^5\theta\cos\phi\Big(c_2 - 4c_1\frac{1}{\alpha}\Big) - 6c_2\sin^2\theta\cos^4\theta\cos^2\phi \\ -18(w+1)\sin^6\theta\sin^6\phi \Bigg] + \mathcal{O}(r^7) \ . \end{aligned} \tag{5.54}$$

This matches the results shown in [4]. To deal with the above function, consider the powers of r and the trigonometric functions. Any even power is guaranteed to be positive. The

third term will then always be negative for suitable values of w, and the second term will be negative for $c_2 > 0$. To eliminate the first term, we can simply set $c2 = 4c_1/\alpha$. As we require c_2 to be positive, we place the restriction that $\alpha > 0$. Lastly, we can set $c_1 = 1$ for simplicity, leaving us with

$$V' = -r^6 \sin^2\theta \Big[\frac{24}{\alpha}\cos^4\theta\cos^2\phi + 18(w+1)\sin^4\theta\sin^6\phi\Big] + \mathcal{O}(r^7)\ . \tag{5.55}$$

We see that the function satisfies $V' < 0$ so long as $w > -1$ and $\alpha > 0$. Therefore point C is guaranteed to be stable for these conditions. The function can take a value of 0 when $\theta = 0$, meaning the point is not confirmed to be asymptotically stable. Lastly, we note that as $||(x, y, z)|| \to \infty$ the Lyapunov function also diverges $V \to \infty$, implying global stability.

5.5.3 Hypersurface phase space analysis

All of the points for the inverse power-law potential have turned out to be non-hyperbolic, so determining their stability has been less straight forward than the previous examples (see Table 7). One method that proves useful is consulting the phase portraits for the non-saddle cases. As expected, the three-dimensional dynamics of the system is also quite complex, so let us instead first focus on the two-dimensional hypersurfaces of constant x, y or z for simplicity. In these cases we will not have to result to using numerical methods. Our treatment shall not be too in-depth, so we direct the reader again to the work of Bahamonde et al. [4] for a more complete analysis of the inverse power-law phase space, specifically Chapter 4.4. Our focus here will be to show the characteristic behaviour of the critical line B_x for both positive and negative values of α. We will also use a matter equation of state parameter $w = 0$.

In Figure 9 we take a look at the hypersurface of constant $y = 0$, i.e. the x-z plane. The parameter α has been set to positive one. Coordinates will be given in the form $(x, -, z)$ here to avoid confusion. The coordinates of the critical points listed in Table 6 indicate that O_z, $A_\pm$ and B_x should all be present here, though we are seeing a simplified picture. In this plane, we see that points are repelled vertically downwards at $x = 1$, and attracted into the central line $x = 0$. From the other side, points are repelled vertically upwards at $x = -1$ and attracted towards the same central line $x = 0$, as well as to the horizontal line from $(-1, -, 1)$ to $(0, -, 1)$. The point A_- at $(-1, 0, 0)$ represents the past attractor, and the point A_+ at $(1, 0, 0)$ is a saddle. From table 7 we know that O_x is always a saddle point, represented by the central line at $x = 0$. We see from Figure 9 that all trajectories

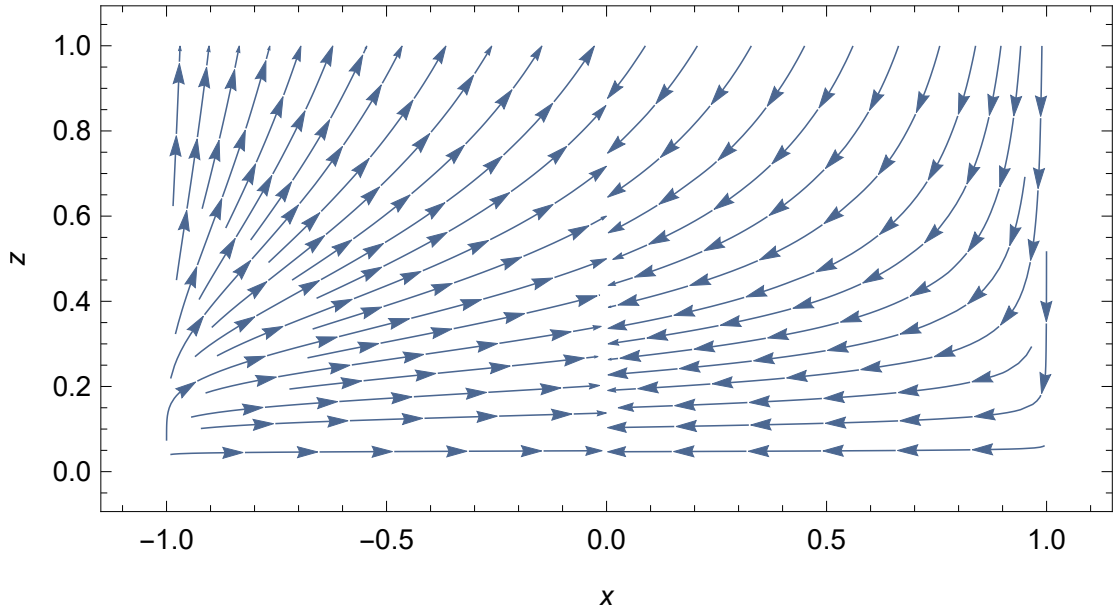

Figure 9: Phase space in the x-z plane for constant $y = 0$ and $\alpha = 1$.

in this plane are attracted towards the central line, therefore the saddle must repel them in the positive y direction (out of the paper). Lastly, consider the critical line B_x, the top of the phase portrait. For $\alpha > 0$ we concluded that the line is a saddle for all values of x (see Table 7). This means that for $x > 0$, trajectories must be going towards the B_x from the y direction. For $x < 0$, the converse must be happening, with trajectories being repelled in the y direction.

In Figure 10 we look again at the x-z plane for $y = 0$, but this time with $\alpha = -1$. The dynamics in comparison to the previous case are simple: the phase space is reflected about the z-axis. Point A_+ is now the past attractor and A_- is a saddle. The critical line of matter dominated solutions O_z is also still a saddle. The biggest qualitative change is that the critical line B_x is now stable for positive values of x, and unstable for negative ones. This makes sense as we concluded trajectories are incoming from the y direction for positive x, and outgoing for negative x. This is confirmed in the next phase diagram.

Looking now in the x-y plane for constant $z = 1$, the asymptotic behaviour as $\lambda \to \infty$, we note that the equations 5.48 and 5.50 are independent of α. In Figure 11 we see that trajectories always perform circular motion, beginning at the line from points $(-1, 0, -)$ to $(0, 0, -)$ and ending at the line from points $(0, 0, -)$ to $(1, 0, -)$. The critical point at $(0, 0, -)$ belongs to the critical line O_z and behaves as a centre. This is confirmed by the eigenvalues in Table 7, which all vanish for $x = 0$. The line corresponding to $x = 0$ is the

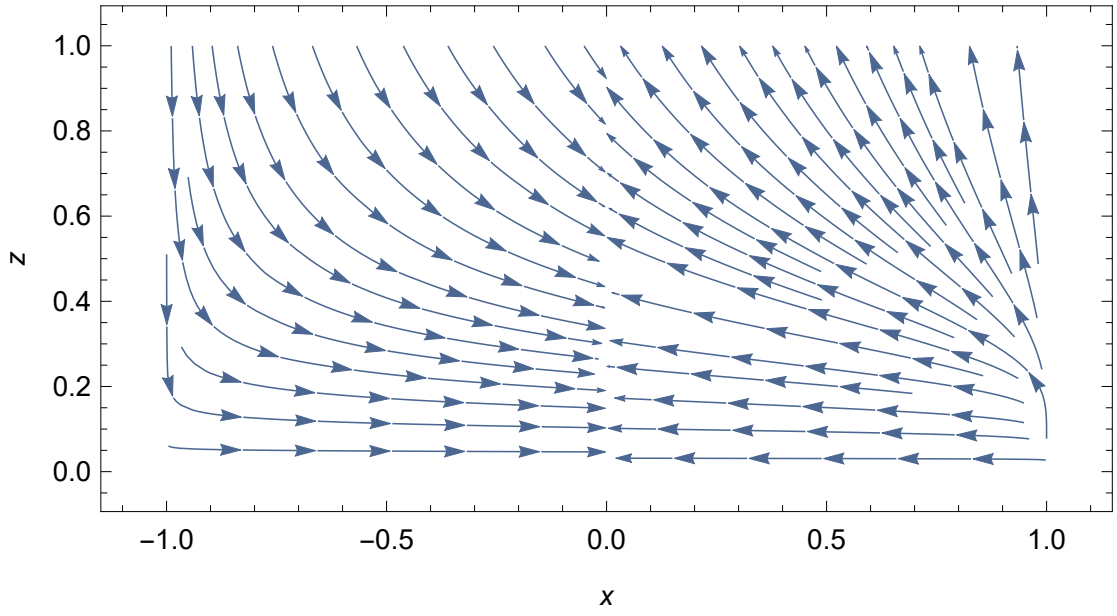

Figure 10: Phase space in the x-z plane for constant $y = 0$ and $\alpha = -1$.

critical line B_x. Our assumptions from the previous two figures that trajectories are repelled (in the y direction) for negative values of x and attracted (in the y direction) for positive values of x was indeed corrected. Hence, using these simplified hypersurfaces we have been able to accurately characterise the behaviour of critical line B_x.

In the final Figure, 12, we see the x-y plane for constant $z = 0$. The critical points in Table 6 that should be present here are O_z, $A_\pm$ and C. Again, the value of the parameter α does not change the phase space. The bottom corners are the critical points $A_\pm$, whilst the origin $(0, 0, 0)$ is a critical point belonging to the critical line O_z. All of the trajectories in this plane are attracted to the critical point C, which sits firmly in the accelerating region (blue shaded region). Along the $z = 0$ surface, point C appears to be stable. For $\alpha > 0$ at least, we have confirmed the point is globally stable with the Lyapunov method. However, the analysis performed by [72] shows that for $\alpha < 0$ the critical point C is in fact a saddle. In that case, it attracts trajectories in the x-y plane and repels them up through the three-dimensional phase space to the positive x values of the critical line B_x. One may also see the similarities between this phase portrait (Figure 12) and the single exponential potential ones (Figure 6-8). In fact, the x-y plane here corresponds exactly to the single exponential for $\lambda = 0$, which is the cosmological constant solution.

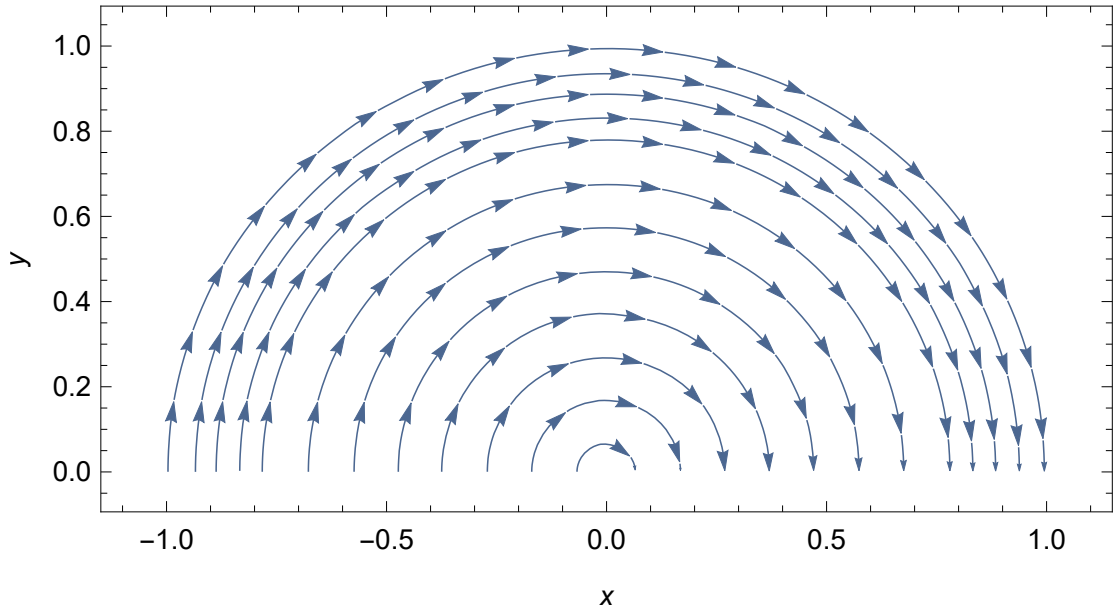

Figure 11: Phase space in the x-y plane for constant $z = 1$ ($\lambda \to \infty$).

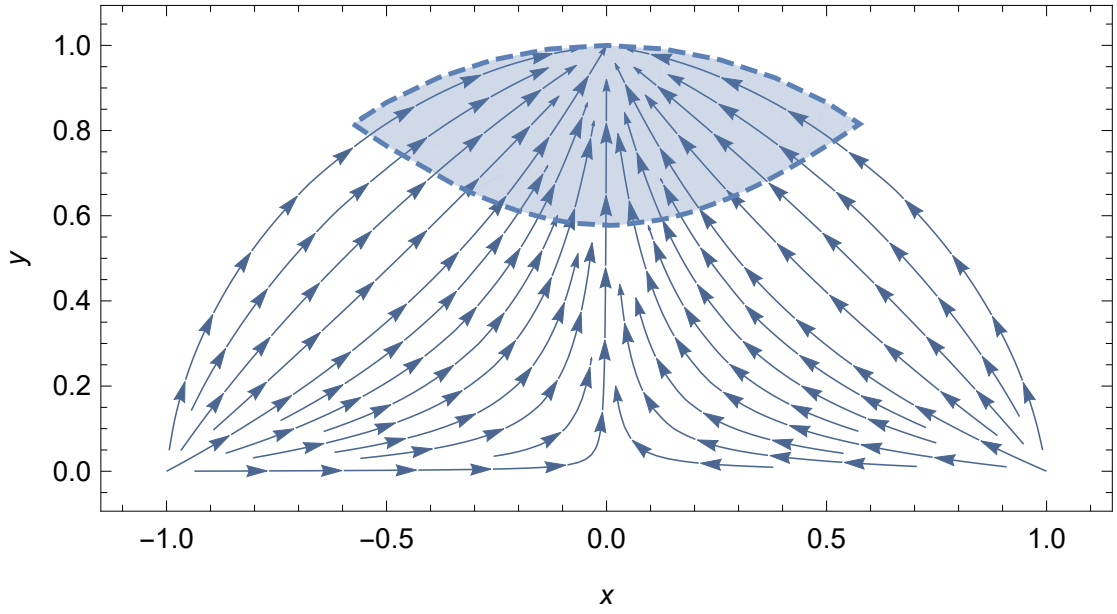

Figure 12: Phase space in the x-y plane for constant $z = 0$. The blue shaded region corresponds to accelerated expansion ($w_{eff} < -1/3$)

5.5.4 Inverse power-law tracking behaviour

One key property of the inverse power-law potential that what we have not yet investigated is known as the *tracking behaviour*. The two-dimensional phase portraits do not efficiently show this behaviour, so we shall once again plot specific trajectories within the full three-dimensional phase space using a numerical solver. Let us consider positive values of α ($\Gamma > 1$), which will lead to the phenomenologically interesting tracking solutions. In Figure 13a we plot trajectories in the phase space for the inverse power-law potential (5.48)-(5.50), with $\alpha = 10$ ($\Gamma = 1.1$) and $w = 0$. The critical point A_- is the past attractor and all trajectories originate from this point. In the $z = 1$ plane we see the circular behaviour depicted previously in Figure 11, where trajectories move from negative to positive values of x. This is the critical line B_x, which acts as a saddle for $\alpha > 0$. The trajectories then follow paths down through the phase space close to the saddle line O_z before being being attracted to late-time accelerating attractor, point C.

The way in which all of the trajectories converge on a similar path towards point C is of particular interest, hence the name *tracking solutions* [63]. To be clear, the word 'tracking' refers to the various trajectories with different initial conditions all converging on the same orbit. In figure 13b we plot a typical evolution for the effective equation of state along this tracking orbit. Ignoring the stiff-matter solution at early times, one sees that w_{eff} tracks along with the matter equation of state before entering a period of accelerated expansion with $w_{eff} = -1$ at point C.

To achieve this same type of behaviour in the single exponential case we had to fine-tune the initial conditions sufficiently close to the origin. We noted that this corresponded to forcing the initial energy density of the scalar field to be close to zero. With the tracking solutions obtained in Figure 13 however, we have alleviated the dependence on the initial conditions. We do though still require that trajectories eventually come to the $z = 1$ plane earlier in their history, which is the asymptotic limit of $\lambda \to \infty$. Two arguments laid out by Bahamonde et al. in [4] lead to the conclusion that this is indeed realised. The first is purely mathematical and related to the centre manifolds of the phase space, which we will not address here. In the second, they use the definition of λ, given in equation (5.39), to relate the amplitude of the field ϕ and the coordinate z,

$$z = \frac{1}{1 + \frac{\kappa\phi}{\alpha}} \ . \tag{5.56}$$

A small scalar field ϕ is favourable in the early Universe because it avoids the problems associated with large field excursions, which relates to the breakdown of the effective field theory description. If then we can assume that $\kappa\phi \ll \alpha$ at early times, we know that the trajectories will follow a path close to the z plane and then converge on the tracking solution.

Lastly, although we did not cover it here, we mention some of the key behaviour of the direct power-law potential. For $\alpha < 0$ ($\Gamma < 1$), one obtains what are is known as *thawing behaviour* [74]. In this scenario, the scalar field is frozen in the past, with an equation of state $w_\phi = -1$, and only recently does it begin to evolve, its equation of state becoming less negative. For more on thawing models with a dynamical systems approach see [75].

This concludes our study of scalar field models. We have now seen some of the key dynamical properties for the single exponential, the double exponential and the inverse power-law potentials. There are of course many more different forms of potentials than we have considered here, and whole classes of models that we haven't mentioned. For example, *phantom* models where the scalar field equation of state can take values lower than -1. These belong in a whole different class of models, where we are not limited to to just canonical scalar fields. For more on these other forms of potential, as well as the study of non-canonical scalar fields, we refer the reader to the works of Copeland et al. [76], [4].

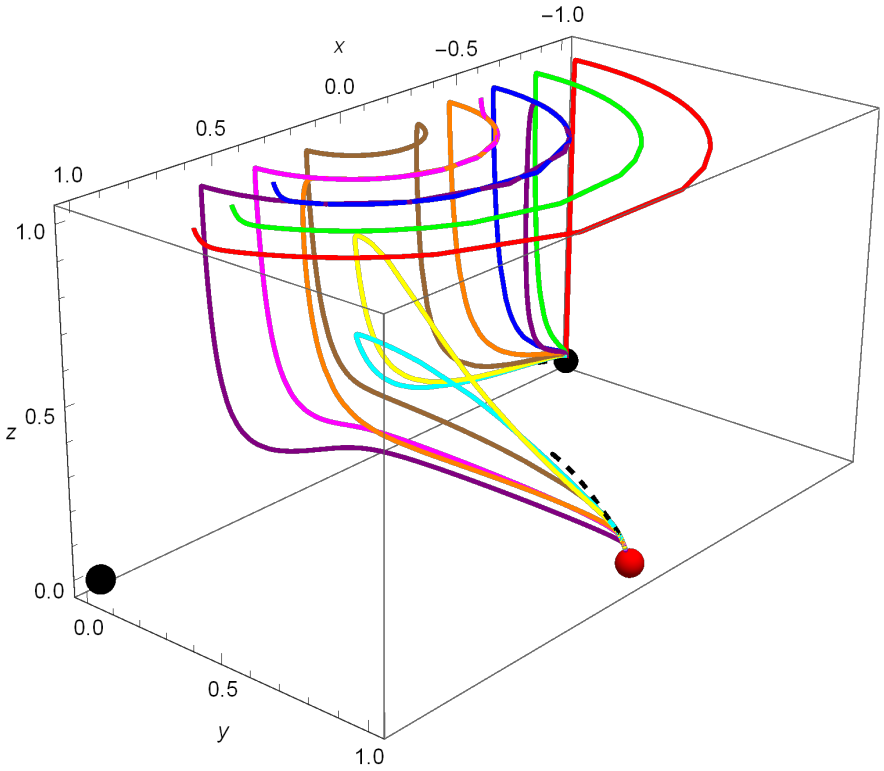

(a) Trajectories for the inverse power-law with $\alpha = 11$ ($\Gamma = 1.1$). The critical points $A_{\pm}$ are represented by the black points, with A_{-} being the past attractor of the phase space. The future attractor C is represented by the red point.

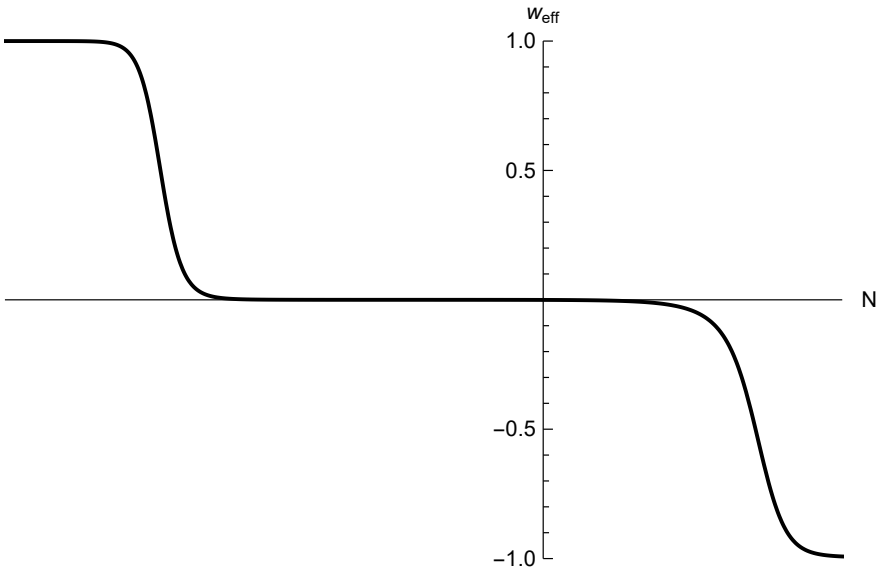

(b) Evolution of the effective equation of state for a typical trajectory. It tracks the matter equation of state for some time before coming to $w_{eff} = -1$ at the late time attractor.

Figure 13: Numerical solutions for the inverse power-law with $\Gamma = 1.1$.

6 Dynamical Systems Approach to the String Swampland Criterion

So far we have considered potentials motivated somewhat by high-energy physics phenomenology, but the focus has been on their dynamical properties. We have presented alternatives to the standard cosmological constant model and shown that certain scalar field quintessence models have the potential to alleviate some of the fine-tuning of initial conditions problems. This is achieved with either scaling solutions or tracking solutions, before leading to a phase of scalar-dominated accelerated expansion (see Sections 5.4 and 5.5). However, currently there is no real way of ruling out any of the classes of physically acceptable models.

Taking a different approach one may look to see if string theory has any say on the validity of different cosmological models. As introduced in Section 4, scalar fields appear naturally in string theory, so it seems fitting that one should include models phenomenologically motivated from that research area. Our focus shall be on the use of a dynamical systems approach on scalar field quintessence models, as covered in the previous section, but relating to a topical example at the forefront of string theory research.

In string theory, it has long been known that the construction of a meta-stable de-Sitter (dS) vacuum, corresponding to a universe with a positive cosmological constant, has been notoriously difficult to achieve (see [77] for a recent interpretation). We noted this in Section 4.1 and again at the end of our discussion on flux compactifications in Section 4.3. Recent work has further postulated that a meta-stable dS solution is forbidden in any consistent theory of quantum gravity [5]. Moreover, it places restrictions on the allowed scalar potentials in cosmology: a criterion in the form $|\nabla V| \geq c \cdot V$, where V is a scalar potential and c is a positive constant, known as the *swampland criterion*. (We shall make this more rigorous in section Section 6.1). Our intentions will not be on investigating the credibility of the claim — there have already been a number of serious objections on its validity from a string theory and cosmological perspective [78]-[80] — but instead to use the criterion as an example to test our dynamical systems approach to scalar field quintessence. We will however, show where this criterion originates from.

In this section we will begin by formally introducing the aforementioned swampland criterion. We will then go through two motivating examples: the compactification of 11-

dimensional supergravity and 10-dimensional heterotic string theory. The concepts and mathematical techniques along with the referenced material in Section 4 will prove as a useful prerequisite for these key examples. Once the criterion has been motivated and understood, we will go on to discuss the cosmological implications following the work in [6]. We will look at the scalar field models considered previously section and see which ones satisfy the criterion. More importantly, we will explore what bounds we can put on the value of the criterion constant c based on the physical constraints for our cosmological models.

6.1 The Swampland Criterion

In a recent set of papers by Obied et al. [5] and Agrawal et al. [6] it has been proposed that meta-stable de-Sitter solutions cannot arise in any consistent theory of quantum gravity. Despite attempts made in recent years at the construction of such a solution, there have been a number of issues raised at their validity. Instead the authors consider the possibility that the scalar potential of any low energy limit of a consistent theory of quantum gravity must satisfy the following bounds,

$$|\nabla V| \geq c \cdot V \ , \tag{6.1}$$

where c is a positive constant assumed to be of order $\mathcal{O}(1)$ in Planck units. We understand the norm of the gradient to be defined as $|\nabla V| = \sqrt{g^{ij}(\phi)\partial_{\phi_i} V \partial_{\phi_j}}$, where $g_{ij}(\phi)$ is the field space metric in the kinetic terms (see [6] for more details). The inequality (6.1) is known as the swampland criterion; one of two proposed criteria in [6]. If we restrict ourselves to positive scalar potentials $V \geq 0$, these being the phenomenologically important ones, we can write (6.1) as

$$\frac{|\nabla V(\phi)|}{V(\phi)} \geq c \ . \tag{6.2}$$

This criterion is in conflict with the cosmological constant model (as $|\nabla V| = 0$ and $V \neq 0$), but certain quintessence models where V is not at a minimum can satisfy the bounds.

The recent swampland criterion [5] along with a follow up paper on its cosmological implications [6] has already received the attention of many authors, to list a few: in fields of string theory [81]-[83], cosmology and inflation [84]-[87] and the overlap between the two [88]-[89]. It also received the attention from authors presenting evidence in conflict with the swampland criteria. In particular, Kachru and Trivedi recently released a paper on the

effective field theories of the low energy limits of string theories, their results being in stark contrast to the conjectures [80].

It is the cosmological implications that shall be our focus. In particular we wish to see how the late-time quintessence models studied in the previous section fair in relation to the criterion. Though a lower bound on c cannot be determined through cosmological observations, an upper bound may be acquired. If the criterion (6.1) turns out to be well founded, then these upper bounds may be important for cosmology and theories of quantum gravity.

6.2 M-Theory

The first example we shall consider to motivate the Swampland Criterion (6.2) is the compactification of the low-energy limit of M-Theory, which is 11-dimensional supergravity [40]. The bosonic part of the 11-dimensional supergravity action is

$$S = \frac{1}{2\kappa^2}\int d^{11}x\sqrt{-g^{(11)}}\Big[R_{11} - \frac{1}{2}|G_4|^2\Big] \quad , \tag{6.3}$$

where κ_{11} is the gravitational coupling constant (Newton's constant), $g^{(11)}$ is the metric determinant, R_{11} is the Ricci scalar and G_4 is the *G-flux* (or four-form field strength). Following the method in [5], we will compactify down to d dimensions on an arbitrary manifold of volume

$$V_{11-d} = \mathrm{e}^{(11-d)\hat{\rho}} \quad , \tag{6.4}$$

which we later shall set to unity. The metric ansatz we shall consider is of the form

$$ds^2 = dx_d^2 + \mathrm{e}^{2\hat{\rho}(x)}dy_{11-d}^2 = g_{\mu\nu}(x)dx^{\mu\nu} + \mathrm{e}^{2\hat{\rho}(x)}\gamma_{ab}(y)dx^a dx^b \quad , \tag{6.5}$$

where we have split up the metric corresponding to the d-dimensional space $g_{\mu\nu}$ and the metric corresponding to the compact space γ_{ab}. The overall modulus that we shall be considering, $\hat{\rho}$, is what determines the details of the compactification. We wish to follow the same procedure as in the Kaluza-Klein (Appendix A.1) and Flux compactification (Section 4.3)) examples, and end up with an effective potential to stabilise the modulus field. We will schematically describe how this is done, with calculations where appropriate, starting with the curvature term.

First we have the term from the metric determinant. Compactifaction with a metric of the form (6.5) means that $g^{(11)}$ transforms as,

$$\sqrt{-g^{(11)}} \to \sqrt{-g\mathrm{e}^{2\hat{\rho}(11-d)}} = \sqrt{-g}\mathrm{e}^{\hat{\rho}(11-d)} \quad , \tag{6.6}$$

where g denotes the d-dimensional metric. The ricci scalar transforms like

$$R_{11} \to R_d + \mathrm{e}^{-2\hat{\rho}}\tilde{R}_{11-d} \quad , \tag{6.7}$$

where R_d is the reduced Ricci scalar in d dimensions and $\tilde{R}_{11-d}$ is the average curvature of the compact dimension when the volume of the internal manifold (6.4) is set to 1. The last term contributing to the effective potential is from the Weyl rescaling, which we find in the same way as before. After compactification, the curvature part of the action is in the *string frame*, which we wish to rewrite in the Einstein frame:

$$\int d^d x\sqrt{-g}\mathrm{e}^{(11-d)\hat{\rho}}\Big[R_d + \mathrm{e}^{-2\hat{\rho}}\tilde{R}_{11-d}\Big] \to \int d^d x\sqrt{-\tilde{g}}\Big[\tilde{R}_d + ...\Big] \ , \tag{6.8}$$

where we've set V_{11-d} to 1. The conformal transformation for the metric given in (A.9) means the determinant and Ricci scalar transform like

$$\sqrt{-g} \to \sqrt{-\tilde{g}}\mathrm{e}^{d\omega} \quad , \quad R_d \to \mathrm{e}^{-2\omega}\tilde{R}_d + ... \ , \tag{6.9}$$

where we are only interested in the factors contributing to the effective potential from the Ricci scalar transformation. To satisfy (6.8), ω must satisfy

$$d\omega + (11-d)\hat{\rho} - 2\omega = 0 \ . \tag{6.10}$$

Substituting in $\omega = \frac{(d-11)\hat{\rho}}{d-2}$, the curvature part of the action is given by

$$\int d^d x\sqrt{-\tilde{g}}\mathrm{e}^{\frac{d(d-11)\hat{\rho}}{d-2}}\mathrm{e}^{(11-d)\hat{\rho}}\Big[\mathrm{e}^{\frac{-2(d-11)\hat{\rho}}{d-2}}\tilde{R}_d + \mathrm{e}^{-2\hat{\rho}}\tilde{R}_{11-d}\Big] \ . \tag{6.11}$$

The terms contributing to the effective potential can then be read off as

$$\mathrm{e}^{\frac{d(d-11)\hat{\rho}}{d-2}} \cdot \mathrm{e}^{(11-d)\hat{\rho}} \cdot \mathrm{e}^{-2\hat{\rho}}\tilde{R}_{11-d} = \mathrm{e}^{-18\frac{\hat{\rho}}{d-2}}\tilde{R}_{11-d} \quad , \tag{6.12}$$

the first term from the Weyl rescaling, the second from the metric determinant and the third from Ricci scalar.

Above we have considered the R_{11} part of the action (6.3). Next we consider the G-flux term. The weyl rescaling and metric determinant factors will be the same. The only new term will be from G-flux $|G_4|^2$, which is defined by the general formula [40],

$$|G_n|^2 = \frac{1}{n!}g^{M_1N_1}g^{M_2N_2}...g^{M_nN_n}G_{M_1M_2...M_n}G_{N_1N_2...N_n} \quad , \tag{6.13}$$

where g^{MN} denotes the inverse metric and G_{MN} is related to the flux. For our $|G_4|^2$ we will have four inverse metric factors, each with a $\hat{\rho}$ dependence of $\mathrm{e}^{-2\hat{\rho}}$. Therefore the total pre-factor for the G-flux term in our action will be proportional to

$$\mathrm{e}^{\frac{d(d-11)\hat{\rho}}{d-2}} \cdot \mathrm{e}^{(11-d)\hat{\rho}} \cdot \mathrm{e}^{-8\hat{\rho}} \propto \mathrm{e}^{-6\frac{d+1}{d-2}\hat{\rho}} \ . \tag{6.14}$$

In our calculations so far we have neglected any kinetic terms $(\nabla\hat{\rho})^2$. If they are included, one can then rewrite the action in a canonically normalised form, with a kinetic term $-\frac{1}{2}(\nabla\hat{\rho})^2$. The associated rescaling of the field is given by

$$\hat{\rho} \to \sqrt{\frac{d-2}{9(11-d)}}\hat{\rho} \quad , \tag{6.15}$$

which has been done in [5]. Under this rescaling, the effective potential given by the contribution of (6.12) and (6.14) can be written as

$$V = V_R \, \mathrm{e}^{-\lambda_1\hat{\rho}} + V_G \, \mathrm{e}^{-\lambda_2\hat{\rho}} \quad , \tag{6.16}$$

where $\lambda_1 = \frac{6}{\sqrt{(d-2)(11-d)}}$, $\lambda_2 = \frac{2(d+1)}{\sqrt{(d-2)(11-d)}}$, V_R is proportional to the average Ricci scalar curvature, and V_G is proportional to the average of the G-flux term in the action, which is always positive.

Now we have our effective potential (6.16), we can apply the criterion (6.2). First consider the case where the internal manifold has negative curvature $V_R > 0$. The lower bound on $\frac{|\nabla V|}{V}$ is the smaller of the exponents in (6.16), λ_1, whilst the upper bound is λ_2. This has been demonstrated clearly in Appendix B.4, along with more general bounds for a double exponential potential with arbitrary exponents. In the case of positive curvature $V_R < 0$, also shown in Appendix B.4, the lower bound is instead λ_2 and there is no upper bound. One can therefore summarise that the compactification of 11-dimensional supergravity implies that the effective scalar potential must satisfy the bound,

$$\frac{|\nabla V|}{V} \geq \frac{6}{\sqrt{(d-2)(11-d)}} \quad . \tag{6.17}$$

In four dimensions the lower bound is approximately ≈ 1.6. As noted by [5], this inequality is in fact a consequence of the supergravity action (6.3) satisfying the strong energy condition (SEC). In string theory, however, the SEC is often violated so we wish to also consider examples which do not satisfy it.

6.3 $O(16) \times O(16)$ Heterotic String Theory

The next example we will consider, onec again following the work in [5], is the compactification of the non-supersymmetric $O(16) \times O(16)$ heterotic string in ten dimensions, which has a positive cosmological constant [90]. Because of the positive cosmological constant in

ten dimensions, this theory does not satisfy the SEC. The effective action at weak coupling is given by

$$S = \int d^{10}x\sqrt{-g^{(10)}}\Big[\frac{1}{2\kappa^2}\mathrm{e}^{-2\phi}(R_{10} + 4(\partial\phi)^2) - \Lambda\Big] \quad , \tag{6.18}$$

where ϕ is the dilaton, Λ is the 10-dimensional cosmological constant and the other standard action terms we are familiar with from (6.3).

Let us once again run through the details of the compactification to d dimensions on an abitrary manifold with volume $\mathrm{e}^{(10-d)\hat{\rho}}$, most of which should now be familiar. The terms contributing to the effective potential will come from the Ricci scalar R_{10} and the cosmological constant Λ. After compactification, those terms appear in the action as

$$S = \int d^{d}x\sqrt{-g}\mathrm{e}^{(10-d)\hat{\rho}}\Big[\frac{1}{2\kappa^2}\mathrm{e}^{-2\phi}(R_d + \mathrm{e}^{-2\hat{\rho}}\tilde{R}_{10-d} + ...) - \Lambda\Big] \quad , \tag{6.19}$$

with ... indicating kinetic terms in ϕ, and $\tilde{R}_{10-d}$ being the Ricci scalar averaged over the internal manifold. After applying a Weyl rescaling,

$$g_{\mu\nu} \to \mathrm{e}^{2\frac{(d-10)\hat{\rho}+2\phi}{d-2}}\tilde{g}_{\mu\nu} \quad , \tag{6.20}$$

the terms contributing to the effective potential can simply be read off. For the averaged Ricci scalar $\tilde{R}_{10-d}$, the modulus field and dilaton field contributions are

$$\propto \mathrm{e}^{d\frac{(d-10)\hat{\rho}+2\phi}{d-2}} \cdot \mathrm{e}^{(10-d)\hat{\rho}} \cdot \mathrm{e}^{-2\phi} \cdot \mathrm{e}^{-2\hat{\rho}} \propto \mathrm{e}^{-\frac{4}{d-2}(4\hat{\rho}-\phi)} \quad . \tag{6.21}$$

The modulus and dilaton contributions for the cosmological constant term are

$$\propto \mathrm{e}^{d\frac{(d-10)\hat{\rho}+2\phi}{d-2}} \cdot \mathrm{e}^{(10-d)\hat{\rho}} \propto \mathrm{e}^{-\frac{2}{d-2}[(10-d)\hat{\rho}-d\hat{\phi}]} \quad . \tag{6.22}$$

Lastly we wish to define a canonical field $\hat{\tau} \equiv \frac{2}{\sqrt{d-2}}\big(\phi - \frac{10-d}{2}\hat{\rho}\big)$ and rescale the modulus field $\hat{\rho} \to \frac{\hat{\rho}}{\sqrt{10-d}}$, giving us the final effective potential

$$V = V_R\ \mathrm{e}^{-\frac{2}{\sqrt{10-d}}\hat{\rho}\ +\frac{2}{\sqrt{d-2}}\hat{\tau}} + V_\Lambda \mathrm{e}^{\sqrt{10-d}\hat{\rho}\ +\frac{d}{\sqrt{d-2}}\hat{\tau}} \quad . \tag{6.23}$$

The term V_R is again proportional to the average of the Ricci scalar curvature and V_Λ is proportional to the cosmological constant, which is always positive. Applying the criterion $\frac{|\nabla V|}{V}$ (6.2) is slightly more involved than the previous case because the potential is a function of two fields $(\hat{\rho}, \hat{\tau})$. In this case, we interpret $\nabla V = \sqrt{g^{ij}\partial_{\Phi_i}V\partial_{\Phi_j}V}$, where $g_{ij}(\Phi)$ is the field space metric [81]. The lower bound obtained in [5] for a negatively curved internal manifold $V_R > 0$, is given by

$$\frac{|\nabla V|}{V} \geq \frac{4\sqrt{2}}{\sqrt{(10-d)(d-2)}} \tag{6.24}$$

for $3 \leq d \leq 9$. In four dimensions the lower bound is ≈ 1.6.

In this example and the previous one, we have shown that for at least some string model compactifications there is a lower bound c of order $\sim \mathcal{O}(1)$. This, along with multiple other examples considered in [5] leading to similar bounds, is the reason for the proposed swampland criterion (6.2).

Before we move on to discussing its cosmological implications, let us quickly make a note of some of serious objections raised for the two examples studied here. In Section 4 we studied the Kaluza-Klein dimensional reduction and the flux compactification of six-dimensional Einstein-Maxwell theory. Our motivation for going from the former to the latter was the problem of moduli stabilisation. In the Einstein-Maxwell example, without the inclusion of fluxes, the effective potential was unstable and there was the problematic possibility of decompactification of the compact space. The two effective potentials in the M-Theory (6.16) and heterotic string (6.23) examples also face a similar problem. This has been noted by Akarmi et al. in a recent paper [78]. They also raise concerns about the conflicts with cosmological observations, which we will now explore.

6.4 Cosmological Implications of the String Swampland Criterion

Firstly, we mention again that any de Sitter solutions are firmly ruled out by the criterion 6.2. This applies to the de Sitter solution found for the double exponential potential corresponding to the critical point (vii) in Table 4. At that point, the potential was at a minimum and therefore $|\nabla V| = 0$. Any scalar field quintessence model which satisfies the criterion must have no extrema for all values of ϕ, with the exception being at $\phi = 0$.[28] A potential sitting in a stable minimum at $\phi = 0$ corresponds to a Minkowski universe, so this is equally unfavourable from a cosmological perspective.

The inverse power-law potential studied in Section 5.5 is also ruled out, along with the direct power-law potential. The class of functions which are not in direct conflict with the criterion are, of course, exponential functions. This includes more complicated exponential potentials than we have considered, such as $\exp(\alpha\exp(\beta\phi))$ [49]. We shall focus on the two simplest examples: the single and the double exponential potential.

Interestingly, as noted by Karthauser and Saffin [91], the scalar potentials found in the

[28] As a reminder, we are not considering potentials with $V < 0$. In this case, the criterion is trivially satisfied and we are dealing with an anti-de Sitter solution.

low energy effective actions of many models relating to unified gravity, gauigino condensation and instanton corrections are often exponential in nature. This may suggest a link between both inflationary physics and quintessence, and the dimensional reduction of string theories and M-theory. Moreover, Ng et al. in [49] suggest the use of a general exponential potential to dynamically stabilise the moduli in string theory, and Barreiro et al. use an exponential potential to stabilise the dilaton in superstring cosmology [92].

6.4.1 Single exponential potential and the swampland criterion

Here we shall follow the approach taken in [6] and consider the single exponential potential of Section 5.3, given by

$$V(\phi) = V_0 \mathrm{e}^{-\lambda\phi} \ , \tag{6.25}$$

where V_0 is a positive constant and λ a constant parameter. There is also an implicit factor of $1/M_p$ in the exponential, where M_p is the Planck mass. Applying the swampland criterion (6.2),

$$\frac{|\nabla V|}{V} = \lambda \geq c \sim \mathcal{O}(1), \tag{6.26}$$

we see that that λ is bounded from below by c, which we want to be of order one. The first thing we can take from our analysis in Section 5.3 is that for accelerated expansion λ must be less than $\sqrt{2}$. Hence we already have an upper bound on the value of c which is of order one.

If we want to use the single exponential case as a physically acceptable model, however, there are number of additional observational constraints which must be satisfied. Firstly, let us assess those proposed by Agrawala et al. in [6]:

1. $\Omega_\phi(z = 0) \approx 0.7$
2. $\Omega_\phi(z > 1) \ll 1$
3. $w_\phi(z < 1) \ll -1/3$
4. $w_\phi(z \approx 0.3 \text{ to } 0.4) < -0.95$

The first constraint is the density of dark energy today, as confirmed by the CMB data (see Section 3.2 on dark energy and observation). The second constraint requires that the scalar field have a negligible relative energy density at early times. This condition allows for LSS formation in the early universe. However, we have seen a number of regimes where the scalar

field equation of state mirrors the matter equation of state, which relinquishes the need for $\Omega_\phi \approx 0$. We have also seen that at early times the behaviour of the single-fluid exponential model is not to be trusted as contributions from radiation are not considered. For this reason, we shall treat this constraint with care.[29] The final two constraints are on the scalar field equation of state in recent times, based on observation from type IA supernovae [93]. It is constraint number 4 which is the most critical for tightening the bounds on c, being the most restrictive. Let us briefly describe where it comes from.

The observational bounds on $w_\phi(z)$ from type IA supernovae can be calculated by using the relation

$$w_\phi(z) = w_0 + \frac{w_a z}{1+z} \ , \tag{6.27}$$

where w_a and w_0 are observable quantities to be measured. In Figure 21 of [93] these measurements have been plotted. The results show that observations are in line with a non-dynamical explanation for dark energy, with $w_a \approx 0$ and $w_0 \approx -1$. This is also in agreement with the value of w_ϕ from the CMB. However, taking a 2σ range of acceptable values for the quantities w_a and w_0 (from Figure 21 of [93]), one can calculate constraints for $w_\phi(z)$ for recent redshifts. This is exactly what has been done in [6], Fig 1(a).

Using the single exponential autonomous equations (5.26)-(5.27) along with the equations for w_ϕ (5.17) and Ω_ϕ (5.16), we can represent the constraints 1-4 visually within the phase space. In Figure 14 we have drawn that phase portrait. The bound on the relative energy density of the scalar field for $z = 0$ is given by the green line. Hence any suitable orbit must be intercepting the green line today. The second constraint, $\Omega_\phi(z > 1) \ll 1$, can be interpreted as a trajectory having to originate from the dark blue shaded contour ($\Omega_\phi < 0.1$). The last two observational constraints are represented by the pink and red lines. Any physically acceptable orbit must be inside the red lines for a redshift around $z \approx 0.35$, i.e. the recent past.

Let us begin by considering the least constrained trajectories in the phase space, $\lambda < \sqrt{2}$. In Figure 15a we have plotted the results for $\lambda = 1.4$. The heteroclinic orbit (blue arrow) is of particular importance, as this is usually the optimum trajectory, or the one that is least in conflict with the constraints. This is because orbits which follow (close to) the heteroclinic orbit originate from a region of matter domination, and take the most central path towards

[29] A possible replacement of constraint 2 could be that $w_{eff} \approx w$ for a sufficiently long period in the distant past.

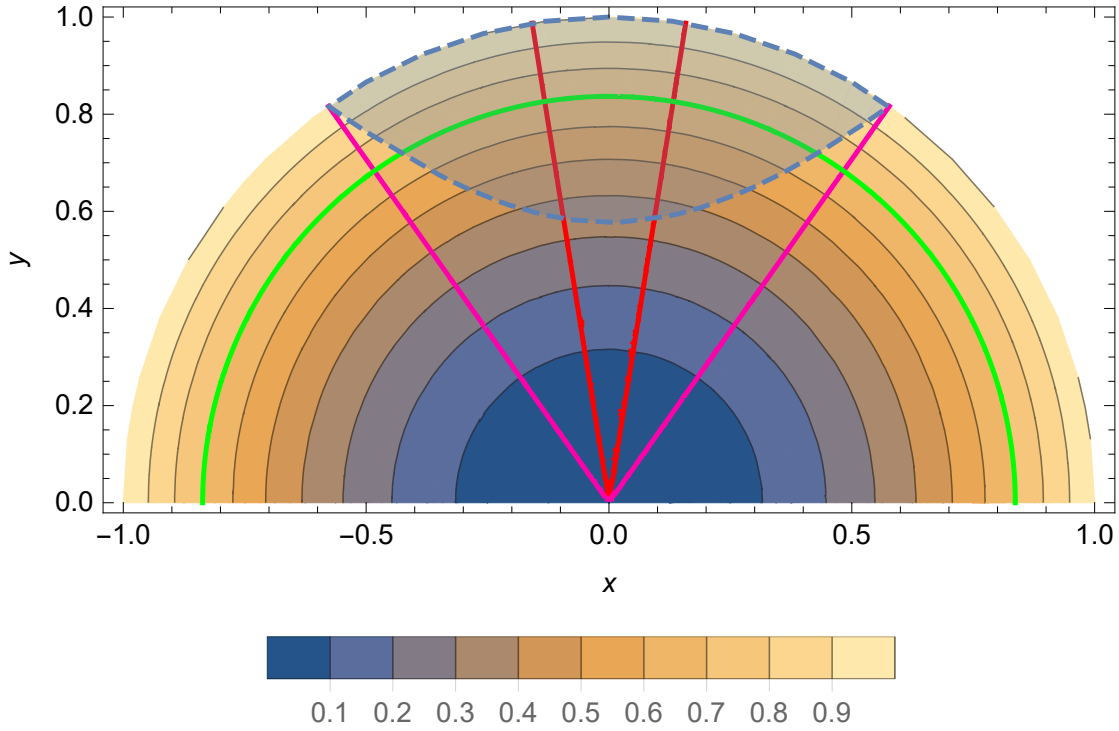

Figure 14: Phase portrait for the single exponential potential (5.26)-(5.27). The contour plot shows Ω_ϕ in the range $[0, 1]$. The dashed blue line represents the region for accelerated expansion. The circular green line is $\Omega_\phi = 0.7$ (constraint 1). The outer pink lines are $w_\phi = -1/3$ (constraint 3). The inner red lines are $w_\phi = -0.95$ (constraint 4).

the late-time attractor point C. Trajectories that intercept the green line (representing Ω_ϕ today) to the left of the heteroclinic orbit always originate from the past attractor A_-, whilst trajectories that intercept on the right of the heteroclinic orbit originate from A_+. Both of these would be in conflict with constraint 2. However, we already mentioned that the past attractors $A_\pm$ are non-physical so our analysis should be treated with care. Ignoring these other trajectories for now, we see that the heteroclinic orbit for $\lambda = 1.4$ does not reside in between the red lines at recent times. It is therefore in conflict with constraint 4. This is also evident from Figure 15b, where $N \approx 5.2$ roughly corresponds to today. The horizontal red dashed line is the constraint on $w(z \approx 0.35)$. Using the formula for the redshift in terms of N (5.28), we can calculate that $z = 0.35$ corresponds to $N \approx 4.9$. Examining the blue curve w_ϕ in Figure 15, we see that at this value of N the scalar field equation of state does not satisfy constraint 4 (being closer to $w_\phi(z \approx 0.35) \approx -0.75$).

We will now consider the value $\lambda = 0.6$, the proposed upper bound for λ in [6], which has been plotted in Figure 16. From the phase portrait in Figure 16a it becomes immediately

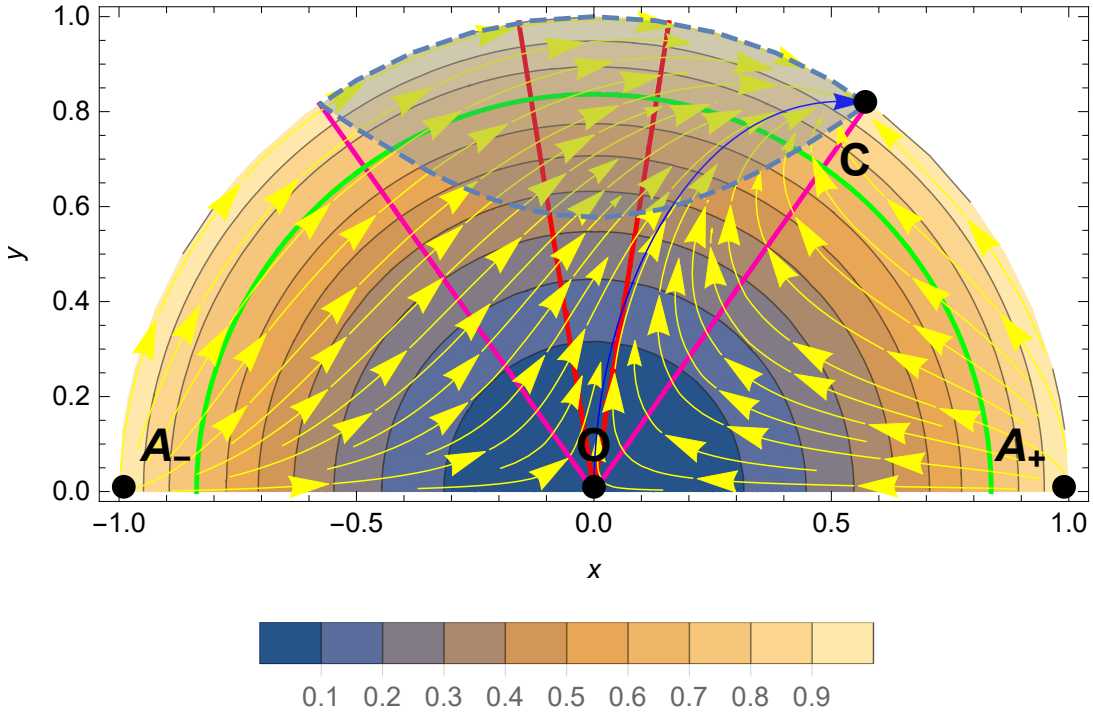

(a) Phase portrait for the single exponential potential (5.26)-(5.27) and a value of $\lambda = 1.4$. The contour plot shows Ω_ϕ, which ranges between 0 and 1 . The coloured lines, green, pink and red are the observational constraints 1, 3 and 4 respectively. The critical points $A_\pm$ and C are defined in Table 2, whilst the blue arrow represents the heteroclinic orbit $O \to C$.

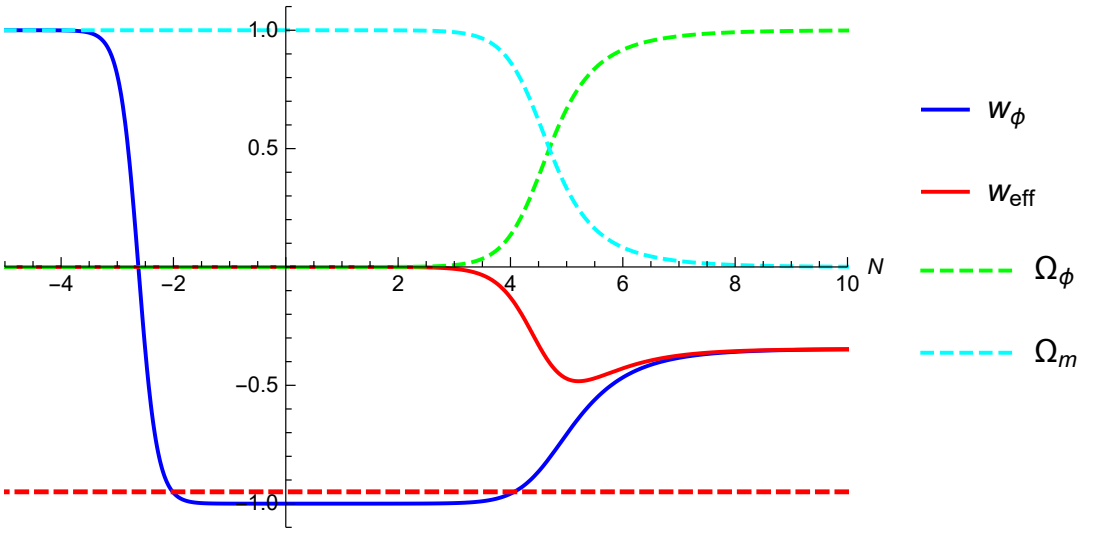

(b) Evolution of the cosmological parameters for the heteroclinic orbit in the Subfigure above and constraint 4 (red dashed line). Today we are at $N \approx 5.2$, when the density parameter is roughly $\Omega_\phi \approx 0.7$.

Figure 15: Single exponential potential for $\lambda = 1.4$.

obvious why this value of $\lambda = 0.6$ has been chosen. One can see that the heteroclinic orbit from the saddle point O to the late-time attractor C passes almost exactly through the point where the green and red lines intercept. In figure 16b we see the evolution of the cosmological parameters with N. Applying the same calculation as before with the a value of $N \approx 5$ today, one finds that a redshift of $z = 0.35$ corresponds to $N \approx 4.7$. This appears to coincide with where the red dashed line (constraint 4) and the blue curve w_ϕ intercept. It can therefore be concluded that for the single exponential potential model, the largest value of λ with a heteroclinic orbit $O \to C$ that satisfies all of the constraints 1-4 is around $\lambda = 0.6$. Any smaller value of λ will result in trajectories being even further within the two red lines of Figure 16 and so will automatically satisfy the constraints.

In Section 5.3, we discussed the issue of fine-tuning, noting that for the single exponential potential, one must have strict initial conditions in order to produce phenomenologically favourable behaviour. With the added constraint on w_ϕ (that it must be less than -0.95 at small redshifts), this problem of fine-tuning is exacerbated. Effectively, only trajectories passing extremely close to the origin O will follow an orbit which is not in conflict with the constraints listed previously (1-4). If we ignore condition 2, that at early times $\Omega_\phi \approx 0$, we are still faced with a problem where the initial condition of y must be almost zero. In Figures 21-23 of Appendix C we have plotted the solutions for the single exponential potential with $\lambda = 0.6$ and $w = 0$ for varying initial conditions close to the x-axis. We see that even with a y-coordinate close to zero, as we move further towards the past attractor A_-, the orbit becomes less viable and more in conflict with the constraints. This demonstrates the problem of fine-tuning. These problems are nothing new however. We already discovered that a single-exponential potential model displays interesting characteristics, but was not a realistic cosmological model.

Even in this simplistic model, we have seen how the use of a dynamical systems approach has been invaluable in assessing the cosmological constraints placed on the criterion constant c. Lastly we note that these values of c are distinctly below the lower bounds calculated in the M-Theory and heterotic stirng examples. This point has been raised in [78].

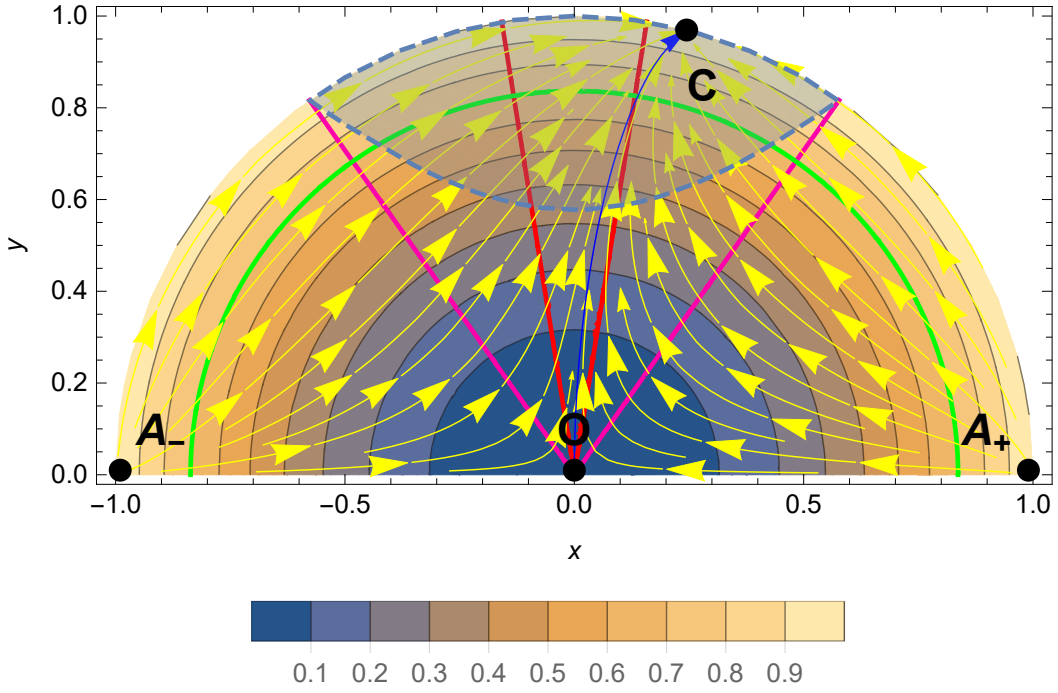

(a) Phase portrait for the single exponential potential (5.26)-(5.27) and a value of $\lambda = 0.6$. The contour plot shows Ω_ϕ, which ranges between 0 and 1 . The coloured lines, green, pink and red are the observational constraints 1, 3 and 4 respectively. The critical points $A_\pm$ and C are defined in Table 2. The heteroclinic orbit $O \to C$ (blue arrow) now stays between the red bounds (constraint 4) until just before it intercepts the green curve (constraint 1).

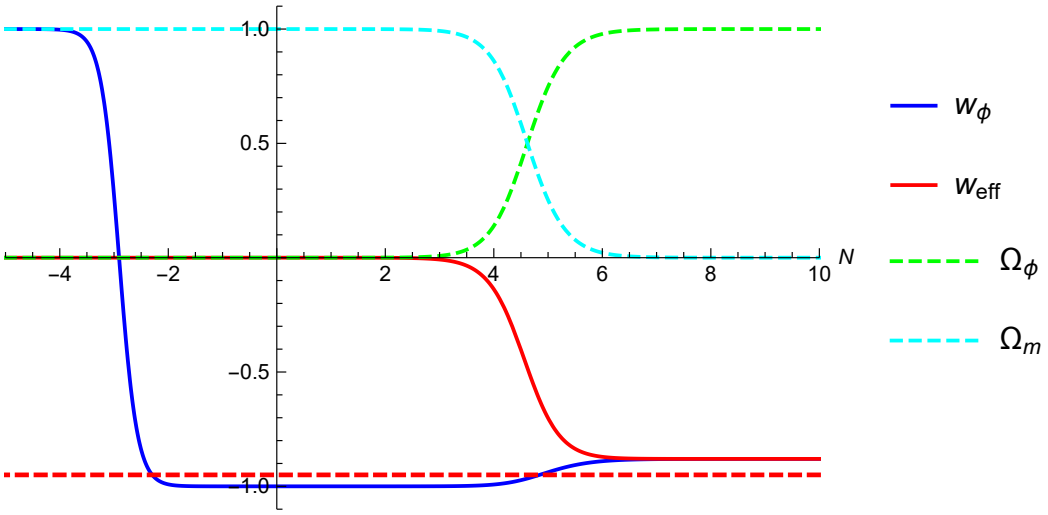

(b) Evolution of the cosmological parameters for the heteroclinic orbit in the Subfigure above and constraint 4 (red dashed line). Today we are at $N \approx 5.0$, when the density parameter is roughly $\Omega_\phi \approx 0.7$.

Figure 16: Single exponential potential for $\lambda = 0.6$.

6.4.2 Double exponential potential and the swampland criterion

To use a more realistic model, although unrealistic in the sense that we are ignoring radiation, let us consider the swampland criterion for the double exponential potential,

$$V(\phi) = V_1 \mathrm{e}^{-\alpha\phi/M_p} + V_2 \mathrm{e}^{-\beta\phi/M_p} \ , \tag{6.28}$$

where M_p is the Planck mass. This time when applying the swampland criterion (6.2) on the potential above it does not give us a constant. Instead the value of $\frac{|\nabla V|}{V}$ is given by a function which depends on the field ϕ. In Appendix B.4 we derived the lower bound for such a function, which is given by the smaller of α or β (assuming they share the same sign).

Constraints from Big Bang nucleosynthesis tell us that the scalar field density parameter must satisfy $\Omega_\phi(\mathrm{MeV}) < 0.045$ in the early universe [94]. Assuming α is the larger of the two exponents, this translates to a value of $\alpha > 9.4$ [95]. Consulting Tables 4 and 5 of Section 5, it is clear that in order to have a late-time attractor corresponding to accelerating expansion the other exponent must be bounded by $\beta < \sqrt{2}$. In [6] it is argued that the upper bound on β is the same as the upper bound on λ in the single exponential case, $c \approx 0.6$. To see this let us consider what the potential $V(\phi)$ is actually doing at early and late times. We know that it is the scaling behaviour and the larger of the exponents, α in this case, which will be important at early times. At late times it is the accelerating solution and the β exponent which will be important. It is therefore reasonable to assume that the late-time behaviour of the double exponential potential can be approximated by just the smaller of the exponents (the larger the difference between α and β, the better the approximation). With these assumptions one can more or less give an approximate upper bound of $\beta < 0.6$ (shown in Section 6.4.1), though without consulting a more detailed numerical analysis of a model with at least two barotropic fluids (matter and radiation) this should not be concluded for all models.

It is argued by Agrawal et al. [6] that these cosmological findings are in support of the swampland criterion, with a rolling quintessence field filling the place of the cosmological constant that is in conflict with (6.1). An alternative viewpoint is taken by Akrami et al. [78], who instead point out the inconsistencies between the lower bounds produced from the string compactification models ($c > 1.6$) for the two examples we considered here and the upper bounds from cosmological observation ($c < 0.6$). The same authors also study the cosmologies of scalar fields arising in string theory with a vast of range of potentials

[96]. There they explore the possibility that the scalar field ϕ plays a role in both late-time quintessence and early-time inflation, known as *quintessential inflation* (also see [97]).

An issue which we briefly touched on was the stability of these string compactification models. More generally in string theory, potentials which are exponential in nature tend to suffer from these moduli stabilisation problems. Not because they have no (local) minima but because the kinetic energy of the rolling field causes it to overshoot and escape that minima. In the context of superstring cosmology, it is found that the presence of a background density, such as radiation in the early universe, can help to slow down the dilaton field as it rolls down its potential [92]. These effects can be linked to the previously discussed scaling behaviour. When the field is then sitting in its minimum it will be characterised only by its potential energy $V(\phi)$, allowing for a negative equation of state w_ϕ. In [92] a dynamical systems approach has also been taken.

7 Summary

Through the use of a dynamical systems approach we have been able to map out the qualitative features of different scalar field quintessence models. By studying their critical point phenomenology as well as their corresponding phases spaces in Section 5, we have been able to assess which models display physically realistic behaviour. This has only been possible through the mathematical techniques developed in Section 2.

More specifically, we have seen how both types of exponential potential model can exhibit stable scaling solutions and stable late-time accelerating solutions. For the case of the accelerating solutions, the universe comes to be totally dominated by the potential energy of the scalar field. These solutions do indeed correspond to an accelerating universe with an effective equation of state $w_{eff} < -1/3$ for values of $\lambda < \sqrt{2}$ (for the double exponential case there are similar requirements on α or β, shown in Table 4). These late-time attractor solutions often represent the global asymptotic attractors of the phase space, making them favourable for physical models.

In the scaling case, the scalar field equation of state w_ϕ mimics the matter equation of state w and the universe evolves as if matter dominated. These solutions are important as they could help to explain how the Universe evolved in the presence of a scalar field without producing noticeable effects. For the single exponential potential, these points always represented stable solutions in the phase space and they were incompatible with a late-time stable accelerating solution. With the double exponential potential we were able to achieve both scaling solutions and late-time accelerating solutions, though without considering the added presence of radiation we could not remove the strong dependence on initial conditions.

For the inverse-power law potential we saw a new type of behaviour, the tracking regime. All solutions originating from near the $z = 1$ plane, which we noted was phenomenologically favourable, would end up converging on similar trajectories towards the late-time attractor. This behaviour helped solve some of the fine-tuning of initial conditions problems we had encountered previously. The study of this model was aided by the use of the Lyapunov method covered in Section 2, along with the numerical simulations.

We then moved on to treating a topical example in string theory, considering the single and double exponential potential models. With the consideration of observational constraints, which we were able to implement into our phase portraits, the cosmological conse-

quences of the swampland criterion became clear. In essence, this was the incompatibility of the bounds on the criterion constant c produced in the string theory compactifications (Sections 6.2 and 6.3) and the bounds needed to satisfy observational constraints for the exponential potential models.

The final point we would like to mention is the future prospects of the dynamical systems theory in relation to scalar fields in cosmology. Future observation may lead to notable deviations in w_ϕ from the standard ΛCDM model, indicating more of a need for quintessence models. If so, the power of the dynamical systems approach with regards to describing the qualitative behaviour of cosmological models will surely be a great asset. Here we have demonstrated how well these methods can capture the dynamical behaviour of different models, and more importantly, how we can constrain models based on observation and theory from different areas of physics.

A String Compactifications

Here we go through the more mathematical calculations accompanying the the work on string compactifications in Section 4.2. The calculations here should also prove useful for the understanding of the M-Theory and Heterotic string compactifications in Section 6.

A.1 Kaluza-Klein Compactification

In this derivation we shall loosely be following the work found in the lecture notes of [98]. This shall be used as the main reference to check the validity of our calculations, with the final result matching that found in more general literature such as [25].

Starting with the action defined in (4.1)

$$S = \frac{1}{\kappa_D^2}\int d^D x\sqrt{-G}R_D \ , \tag{A.1}$$

and the metric (4.3)

$$ds_0^2 = G^{(0)}_{MN}(x)dx^M dx^N = g_{\mu\nu}(x)dx^\mu dx^\nu + \mathrm{e}^{2\Phi(x)}\Big(A_\mu(x)dx^\mu + dy\Big)^2 \ , \tag{A.2}$$

let us compactify onto a circle of radius L.

The first step is to find the Ricci scalar by taking the trace of Ricci tensor $R = g^{ab}R_{ab}$. Likewise, one obtains the Ricci tensor $R_{\mu\nu}$ by tracing over the Riemann tensor, $R_{ab} = R_{acb}{}^c$, which can be calculated using only the metric (A.2) and is given by the following formula,

$$R_{abc}{}^d = -2\partial_{[a}\Gamma^d_{\ b]c} + 2\Gamma^\rho_{\ c[a}\Gamma^d_{\ b]\rho} \ , \tag{A.3}$$

where the Christoffel symbols are defined in (1.1). When one plugs in our metric, the Ricci curvature from equation (A.1) works out to be [98]

$$R_D = R_d - 2\mathrm{e}^{-\Phi}\nabla^2\mathrm{e}^{\Phi} - \frac{1}{4}\mathrm{e}^{2\Phi}F_{\mu\nu}F^{\mu\nu} \ , \tag{A.4}$$

where R_d now denotes the curvature in d dimensions, and $F_{\mu\nu} = \partial_\mu A_\nu - \partial_\nu A_\mu$ is the two-form representing the field strength in d dimensions. The covariant derivative squared is defined by

$$(\nabla\Phi)^2 = g^{\mu\nu}\nabla_\mu\Phi\nabla_\nu\Phi \ . \tag{A.5}$$

We will also be able to drop the second term term of (A.4), $-2\mathrm{e}^{-\Phi}\nabla^2\mathrm{e}^{\Phi}$, when we substitute (A.4) back into the action as it can be discarded as a total derivative [98],

$$-2\int d^d x\sqrt{-g}\nabla^2\mathrm{e}^{\Phi} = -2\int d^d x\ \partial_\mu(\sqrt{-g}\nabla^\mu)\mathrm{e}^{\phi} = 0 \ . \tag{A.6}$$

The other term left to treat in the action (A.1) is the metric determinant $\sqrt{-G}$. Using our metric (A.2), this is given by

$$\sqrt{-G} = \sqrt{-g\mathrm{e}^{2\Phi}} = \mathrm{e}^{\Phi}\sqrt{-g} \ , \tag{A.7}$$

with $g = \det[g_{\mu\nu}]$. Rewriting our action (A.1) with (A.4) and (A.7), integrating out the y coordinate and dropping the total derivative term gives the following compactified action,

$$S_{(0)} = \frac{2\pi L}{\kappa_D^2}\int d^d x\sqrt{-g}\mathrm{e}^{\Phi}\Big[R_d - \frac{1}{4}\mathrm{e}^{2\Phi}F_{\mu\nu}F^{\mu\nu}\Big] \ , \tag{A.8}$$

where the factor of $2\pi L$ comes from circumference of the compactified dimension.

It is convenient to rewrite the action in the standard Einstein-Hilbert form (known as the *Einsten frame*), where the scalar curvature is coupled only to the metric. The solution is to apply a *conformal rescaling*[30], or *Weyl rescaling*, of the metric given by

$$g_{\mu\nu} = \Omega^2\tilde{g}_{\mu\nu} \ , \tag{A.9}$$

where $\tilde{g}_{\mu\nu}$ is the new metric corresponding to the Einstein frame and Ω^2 is the conformal or Weyl scaling factor, which we are free to assign [40]. The metric determinant therefore becomes

$$\sqrt{-g} = \sqrt{-\tilde{g}}\Omega^d \ . \tag{A.10}$$

A similar conformal transformation must also be made to the Ricci curvature as it is dependent on the metric, which is given by

$$R_d = \Omega^{-2}\Big[\tilde{R}_d - 2(d-1)\tilde{\nabla}^2(\ln\,\Omega) - (d-2)(d-1)\tilde{g}^{\mu\nu}(\tilde{\nabla}_\mu \ln\,\Omega)(\tilde{\nabla}_\nu \ln\,\Omega)\Big] \ , \tag{A.11}$$

(the derivation can be found in Appendix D [99]). All the terms on the right hand side are with respect to the new metric, and the inverse is given by

$$g^{\mu\nu} = \Omega^{-2}\tilde{g}^{\mu\nu} \ . \tag{A.12}$$

Now that we know how R_d and $g_{\mu\nu}$ transform, we can compare with the action (A.8) to see how we should assign our conformal factor Ω. To make life we easier will also define $\Omega^2 = \mathrm{e}^{2\omega}$. Examining equations (A.8), (A.10) and (A.11), one sees ω must satisfy

$$\sqrt{-g}\cdot\mathrm{e}^{\Phi}\cdot R_d \to \sqrt{-\tilde{g}}\mathrm{e}^{d\omega}\cdot\mathrm{e}^{\Phi}\cdot\tilde{R}_d\mathrm{e}^{-2\omega} = \sqrt{-\tilde{g}}\tilde{R}_d \ , \tag{A.13}$$

[30]This isn't a coordinate transformation, simply a redefinition of the fields.

$$\Rightarrow \omega = \frac{\Phi}{2-d} \ , \tag{A.14}$$

where we have separated the first three terms for clarity. The ricci scalar and metric determinant then become

$$R_d = \mathrm{e}^{\frac{-2\Phi}{2-d}}\Big[\tilde{R}_d - \frac{2(d-1)}{2-d}\tilde{\nabla}^2\Phi - \frac{d-1}{d-2}\tilde{g}^{\mu\nu}\tilde{\nabla}_\mu\Phi\tilde{\nabla}_\nu\Phi\Big] \ ; \quad \sqrt{-g} = \sqrt{-\tilde{g}}\mathrm{e}^{\frac{d\Phi}{2-d}} \ . \tag{A.15}$$

The field strength terms $F_{\mu\nu}$ transform under the conformal rescaling in the action like

$$\sqrt{-g}g^{\mu\rho}g^{\nu\sigma}F_{\rho\sigma}F_{\rho\sigma} = \sqrt{-\tilde{g}}\mathrm{e}^{d\omega}\mathrm{e}^{-2\omega}\mathrm{e}^{-2\omega}\tilde{g}^{\mu\rho}\tilde{g}^{\nu\sigma}\tilde{F}_{\mu\nu}\tilde{F}_{\rho\sigma} = \sqrt{-\tilde{g}}\mathrm{e}^{\frac{\phi(d-4)}{2-d}}\tilde{g}^{\mu\rho}\tilde{g}^{\nu\sigma}\tilde{F}_{\mu\nu}\tilde{F}_{\rho\sigma} \ , \tag{A.16}$$

which we note is invariant in $d = 4$ dimensions.

Substituting our conformally scaled equations (A.10), (A.15) and (A.16) into the action (A.8), and dropping the total covariant derivative term in the Ricci scalar (A.15), we arrive at our equation for the d-dimensional action in the Einstein frame,

$$S^E_{(0)} = \frac{2\pi L}{\kappa_D^2}\int d^dx\sqrt{-\tilde{g}}\Big[\tilde{R}_d - \Big(\frac{d-1}{d-2}\Big)(\tilde{\nabla}\Phi)^2 - \frac{1}{4}\mathrm{e}^{\frac{\phi(4d-10)}{(d-2)}}\tilde{F}^2\Big] \ , \tag{A.17}$$

where $\tilde{F}^2 = \tilde{F}_{\mu\nu}\tilde{F}^{\mu\nu}$. Substituting $d = 4$, this then matches the end result in [98]. The final step is to rescale the field ϕ so the kinetic term is canonically normalised[31], $\phi \to -\sqrt{\frac{d-2}{2(d-1)}}\phi$, which leaves us with

$$S^E_{(0)} = \frac{2\pi L}{\kappa_D^2}\int d^dx\sqrt{-\tilde{g}}\Big[\tilde{R}_d - \frac{1}{2}(\tilde{\nabla}\Phi)^2 - \frac{1}{4}\mathrm{e}^{-\phi\Big(\frac{\sqrt{d-2}(4d-10)}{\sqrt{2(d-1)}(d-2)}\Big)}\tilde{F}^2\Big] \ , \tag{A.18}$$

which in four dimensions reduces to

$$S^E_{(0)} = \frac{2\pi L}{\kappa_D^2}\int d^4x\sqrt{-\tilde{g}}\Big[\tilde{R}_4 - \Big(\frac{1}{2}\Big)(\tilde{\nabla}\Phi)^2 - \frac{1}{4}\mathrm{e}^{-\sqrt{3}\Phi}\tilde{F}^2\Big] \ . \tag{A.19}$$

This result matches that found in more general literature, such as [25]. This is the result given in equation (4.4).

[31] We have also included a minus sign so that the field strength term F^2 vanishes for large positive values of Φ rather large negative ones.

B Detailed Calculations

B.1 Scalar Field Friedmann Equations

Starting from the gravitational field equations (5.4) and a metric of the form (5.6), with $T_{\mu\nu}$ and $T^{\phi}_{\mu\nu}$ defined as (3.3) and (5.5) respectively, let us derive the Friedmann (5.7) and acceleration (5.8) equations for a canonical scalar field ϕ. Consider the time-time components of (5.4),

$$R_{00} - \frac{1}{2}g_{00}R = \kappa^2\Big(T_{00} + T^{\phi}_{00}\Big) \quad . \tag{B.1}$$

The Ricci tensor (1.3) with the Christoffel symbols (1.1) then becomes

$$\begin{aligned} R_{00} &= \Gamma^a_{00,a} - \Gamma^a_{0a,0} + \Gamma^a_{ba}\Gamma^b_{00} - \Gamma^a_{b0}\Gamma^b_{0a} \\ &= -\Gamma^i_{0i,0} - \Gamma^i_{j0}\Gamma^j_{0i} \\ &= -\delta^i_i\frac{\partial}{\partial t}\left(\frac{\dot{a}}{a}\right) - \delta^i_j\delta^i_j\left(\frac{\dot{a}}{a}\right)^2 \\ &= -3\left(\frac{\ddot{a}}{a} - \frac{\dot{a}^2}{a^2}\right) - 3\left(\frac{\dot{a}^2}{a^2}\right) \\ &= -3\frac{\ddot{a}}{a} \ . \end{aligned} \tag{B.2}$$

Similarly, the Ricci scalar (1.4) is

$$\begin{aligned} R &= g_{00}R_{00} + g_{ij}R_{ij} \\ &= -R_{00} + \frac{1}{a^2}R_{ii} \\ &= 3\frac{\ddot{a}}{a} + \frac{1}{a^2}\left(\Gamma^a_{ij,a} - \Gamma^a_{ia,j} + \Gamma^a_{ba}\Gamma^b_{ij} - \Gamma^a_{bi}\Gamma^b_{ja}\right) \\ &= 3\frac{\ddot{a}}{a} + \frac{1}{a^2}\left(\Gamma^0_{ij,0} + \Gamma^l_{0l}\Gamma^0_{ij} - \Gamma^0_{li}\Gamma^l_{j0} - \Gamma^l_{0i}\Gamma^0_{lk}\right) \\ &= 3\frac{\ddot{a}}{a} + \frac{1}{a^2}\Big(\delta_{ij}\big[2\dot{a}^2 + a\ddot{a}\big]\Big) \\ &= 6\frac{\ddot{a}}{a} + 6\frac{\dot{a}^2}{a^2} \ . \end{aligned} \tag{B.3}$$

Combining (B.2) and (B.3), we find the RHS of (B.1) to be

$$R_{00} - \frac{1}{2}g_{00}R = 3\frac{\ddot{a}}{a} = 3H^2 \ . \tag{B.4}$$

For the LHS of (B.1), let us simply expand the definitions of the energy momentum tensors,

$$\begin{aligned} \kappa^2(T_{00} + T^{\phi}_{00}) &= \kappa^2\Big((\rho + p) - p + \dot{\phi}^2 - \frac{1}{2}\dot{\phi}^2 + V(\phi)\Big) \\ &= \kappa^2\Big(\rho + \frac{1}{2}\dot{\phi}^2 + V(\phi)\Big) \ . \end{aligned} \tag{B.5}$$

Putting together (B.4) and (B.5), we obtain our final result (5.7)

$$3H^2 = \kappa^2\big(\rho + \frac{1}{2}\dot{\phi}^2 + V(\phi)\big) \ . \tag{B.6}$$

Consider now the spatial components of the field equations (5.4),

$$R_{ij} - \frac{1}{2}g_{ij}R = \kappa^2\Big(T_{ij} + T^{\phi}_{ij}\Big) \ \ , \tag{B.7}$$

where the only non-trivial components are when $i = j$. The terms on the LHS are then

$$\begin{aligned} R_{ij} - \frac{1}{2}g_{ij}R = 2\dot{a}^2 + a\ddot{a} - \frac{1}{2}a^2\left(6\frac{\ddot{a}}{a} + 6\frac{\dot{a}^2}{a^2}\right) \\ = -\dot{a}^2 - 2a\ddot{a} \ . \end{aligned} \tag{B.8}$$

On the RHS, the spatial components of the matter energy-momentum reduce easily because the four-velocity is normalised,

$$T_{ij} = (\rho + p)u_i u_j + p g_{ij} = p a^2 \ . \tag{B.9}$$

The scalar field energy-momentum tensor is

$$\begin{aligned} T^{\phi}_{ij} = \partial_i\phi\partial_j\phi - \frac{1}{2}g_{ij}(\partial\phi)^2 - g_{ij}V(\phi) \\ = \partial_i\phi\partial_j\phi - \frac{1}{2}a^2\big(-\partial_0\phi\partial_0\phi + \frac{2}{a^2}\partial_i\phi\partial_j\phi\big) - a^2V(\phi) \\ = a^2\left(\frac{1}{2}\dot{\phi}^2 - V(\phi)\right) \ . \end{aligned} \tag{B.10}$$

Putting together (B.8), (B.9) and (B.10), we arrive at

$$\begin{aligned} -\dot{a}^2 - 2a\ddot{a} = \kappa^2\Big(pa^2 + a^2\big(\frac{1}{2}\dot{\phi}^2 - V(\phi)\big)\Big) \\ -\frac{\dot{a}^2}{a^2} - 2\frac{\ddot{a}}{a} = \kappa^2\Big(w\rho + \frac{1}{2}\dot{\phi}^2 - V(\phi)\Big) \\ 2\dot{H} + 3H^2 = -\kappa^2\big(w\rho + \frac{1}{2}\dot{\phi}^2 - V(\phi)\big) \ . \end{aligned} \tag{B.11}$$

This is the acceleration equation given in equation (5.8).

B.2 EN variables

B.2.1 Single exponential potential dynamical equations

The EN variables (5.13), written again for clarity, are

$$x = \frac{\kappa\dot{\phi}}{\sqrt{6}H} \quad ; \quad y = \frac{\kappa\sqrt{V}}{\sqrt{3}H} \ . \tag{B.12}$$

Squaring and rearranging for $\dot{\phi}$ and V gives

$$\dot{\phi}^2 = \frac{6x^2H^2}{\kappa^2} \quad , \quad V = \frac{3y^2H^2}{\kappa^2} \ , \tag{B.13}$$

which can be substituted directly into the Friedmann equation (5.7) to give

$$\begin{aligned} 3H^2 &= \kappa^2\rho + 3x^2H^2 + 3y^2H^2 \\ 1 &= \frac{\kappa^2\rho}{3H^2} + x^2 + y^2 \ . \end{aligned} \tag{B.14}$$

Then we simply define the first term on the RHS as matter density parameter (5.15)

$$\Omega_m = \frac{\kappa^2\rho}{3H^2} \ . \tag{B.15}$$

Equation (B.14) is the Friedmann constraint (5.14). The scalar field equation of state (5.12) can be written down simply using (B.13), giving (5.17)

Let us derive the x' and y' dynamical system equations (5.20) and (5.21) from the acceleration equation (5.8) and Klein-Gordon equation (5.9). Starting with the acceleration equation and substituting in (B.13) and (B.15):

$$\begin{aligned} 2\dot{H} + 3H^2 &= -\kappa^2\big(w\rho + \frac{1}{2}\dot{\phi}^2 - V(\phi)\big) \\ 3\frac{2\dot{H}}{3H^2} + 1 &= -\frac{\kappa^2}{3H^2}\Big(\frac{w\Omega_m 3H^2}{\kappa^2} + \frac{3H^2x^2}{\kappa^2} - \frac{3H^2y^2}{\kappa^2}\Big) \\ \frac{\dot{H}}{H^2} &= -\frac{3}{2}\Big(w(1-x^2-y^2) + x^2 - y^2 + 1\Big) \\ \frac{\dot{H}}{H^2} &= \frac{3}{2}\Big(x^2(w-1) + (w+1)(y^2-1)\Big) \ , \end{aligned} \tag{B.16}$$

where in the third line we have made use of the Friedmann constraint $\Omega_m = 1 - x^2 - y^2$.

Now let us consider the derivative of $x = \kappa\dot{\phi}/(\sqrt{6}H)$ with respect to $N = \log a$,

$$\begin{aligned} x' \equiv \frac{dx}{dN} &= \frac{1}{H}\frac{dx}{dt} = \frac{1}{H}\frac{d}{dt}\Big(\frac{\kappa\dot{\phi}}{\sqrt{6}H}\Big) \\ &= \frac{1}{H}\Big(\frac{\kappa\ddot{\phi}}{\sqrt{6}H} - \frac{\kappa\dot{\phi}\dot{H}}{\sqrt{6}H^2}\Big) \\ &= \frac{\kappa\dot{\phi}}{\sqrt{6}H}\Big(\frac{\ddot{\phi}}{\dot{\phi}H} - \frac{\dot{H}}{H^2}\Big) \ . \end{aligned} \tag{B.17}$$

The term outside the bracket is just the definition of x and the last term is the acceleration equation we already derived (B.16). The $\ddot{\phi}$ term can be rewritten using the Klein-Gordon equation (5.9),

$$\begin{aligned}\frac{\ddot{\phi}}{\dot{\phi}H} &= -3 - \frac{V_{,\phi}}{\dot{\phi}H} \\ &= -3 - \frac{V_{,\phi}\kappa}{x\sqrt{6}H^2} \\ &= -3 - \frac{V_{,\phi}\sqrt{6}y^2}{2x\kappa V}\end{aligned} \tag{B.18}$$

Substituting this into equation (B.17) leaves us with

$$\begin{aligned}x' &= x\left[-3 - \frac{V_{,\phi}\sqrt{6}y^2}{2x\kappa V} - \frac{3}{2}\Big(x^2(w-1) + (w+1)(y^2-1)\Big)\right] \\ x' &= -\frac{3}{2}\left[2x + (w-1)x^3 + x(w+1)(y^2-1) + y^2\frac{\sqrt{2}}{\sqrt{3}}\frac{V_{,\phi}}{\kappa V}\right] .\end{aligned} \tag{B.19}$$

Lastly, defining

$$\lambda = -\frac{V_{,\phi}}{\kappa V} , \tag{B.20}$$

brings us to the x' equation given in equation (5.26).

Let us do the same for the y, taking the derivative

$$\begin{aligned}y' \equiv \frac{dy}{dN} &= \frac{1}{H}\frac{dy}{dy} = \frac{1}{H}\frac{d}{dt}\Big(\frac{\kappa V^{1/2}}{\sqrt{3}H}\Big) \\ &= \frac{\kappa}{\sqrt{3}H}\Big[\frac{1}{2}\frac{\dot{V}V^{-1/2}}{H} - \frac{\dot{H}V^{1/2}}{H}\Big] .\end{aligned} \tag{B.21}$$

Let us examine the $\dot{V}$ term. Using the chain rule,

$$\dot{V} \equiv \frac{dV}{dt} = \frac{dV}{d\phi}\frac{d\phi}{dt} = V_{,\phi}\frac{x\sqrt{6}H}{\kappa} , \tag{B.22}$$

where in the last step we have just used the definition of x. Substituting this back into (B.21),

$$\begin{aligned}y' &= \frac{\kappa}{\sqrt{3}H}\Big[\frac{1}{2}\frac{V_{,\phi}}{V^{1/2}}\frac{x\sqrt{6}}{\kappa} - V^{1/2}\frac{\dot{H}}{H}\Big] \\ &= \frac{\sqrt{6}}{2}\frac{V_{,\phi}}{\kappa V}xy - y\frac{\dot{H}}{H} .\end{aligned} \tag{B.23}$$

Now let us substitute in (B.16) for the last term and the definition of λ in the first term,

$$\begin{aligned}y' &= -\frac{\sqrt{6}}{2}\lambda xy - y\frac{3}{2}\Big(x^2(w-1) + (w+1)(y^2-1)\Big) \\ y' &= -\frac{3}{2}y\Big[(w-1)x^2 + (w+1)(y^2-1) - \frac{\sqrt{2}}{\sqrt{3}}\lambda x\Big] .\end{aligned} \tag{B.24}$$

This is the y' equation of (5.21)

B.2.2 Double exponential potential dynamical equations

Here we shall derive the three autonomous equations x', y' and z' for the double exponential potential $V = V_1 \mathrm{e}^{-\kappa\alpha\phi} + V_2 \mathrm{e}^{-\kappa\beta\phi}$ using the variables defined by

$$x = \frac{\kappa\dot{\phi}}{\sqrt{6}H} \quad , \quad y = \sqrt{\frac{\kappa^2 V_1 \mathrm{e}^{-\kappa\alpha\phi}}{3H^2}} \quad , \quad z = \sqrt{\frac{\kappa^2 V_2 \mathrm{e}^{-\kappa\beta\phi}}{3H^2}} \, , \tag{B.25}$$

which can be rewritten as

$$\dot{\phi}^2 = \frac{6x^2H^2}{\kappa^2} \quad , \quad V = \frac{3y^2H^2}{\kappa^2} + \frac{3z^2H^2}{\kappa^2} \, . \tag{B.26}$$

Firstly, using the Friedmann equation (5.7), we obtain both the Friedmann constraint and the equation for the matter density parameter,

$$\begin{aligned} 3H^2 &= \kappa^2(\rho + 3x^2H^2 + 3y^2H^2 + 3z^2H^2) \\ 1 &= \frac{\kappa^2\rho}{3H^2} + x^2 + y^2 + z^2 \, . \end{aligned} \tag{B.27}$$

and we define $\Omega_m = \frac{\kappa^2\rho}{3H^2}$ as the matter critical density parameter. The above equation is then subject to the bounds $1 \leq x^2 + y^2 + z^2 \leq 0$. Let us now treat the acceleration equation (5.8),

$$\begin{aligned} 2\dot{H} + 3H^2 &= -\kappa^2\Big(w\rho + \frac{1}{2}\dot{\phi}^2 - V(\phi)\Big) \\ \frac{2\dot{H}}{3H^2} + 1 &= -\frac{\kappa^2}{3H^2}\Big(\frac{w\Omega_m 3H^2}{\kappa^2} + \frac{3H^2x^2}{\kappa^2} - \frac{3H^2y^2}{\kappa^2} - \frac{3H^2z^2}{\kappa^2}\Big) \\ \frac{\dot{H}}{H^2} &= -\frac{3}{2}\Big(w(1 - x^2 - y^2 - z^2) + x^2 - y^2 - z^2 + 1\Big) \, . \end{aligned} \tag{B.28}$$

Lastly let us consider the Klein-Gordon equation (5.9),

$$\begin{aligned} \ddot{\phi} &= -3H\dot{\phi} - \frac{\partial V}{\partial \phi} \\ &= -3H\dot{\phi} - \Big(- \kappa\alpha V_1 \mathrm{e}^{-\kappa\alpha\phi} - \kappa\beta V_2 \mathrm{e}^{-\kappa\beta\alpha} \\ &= -3H\dot{\phi} + \Big(\frac{3H^2\alpha y^2}{\kappa} + \frac{3H^2\beta z^2}{\kappa}\Big) \, . \end{aligned} \tag{B.29}$$

Now let us consider the derivative of x with respect to $N = \log a$,

$$\begin{aligned} x' \equiv \frac{dx}{dN} &= \frac{1}{H}\frac{dx}{dt} = \frac{1}{H}\frac{d}{dt}\Big(\frac{\kappa\dot{\phi}}{\sqrt{6}H}\Big) \\ &= \frac{\kappa\dot{\phi}}{\sqrt{6}H}\Big(\frac{\ddot{\phi}}{\dot{\phi}H} - \frac{\dot{H}}{H^2}\Big) \\ &= \frac{\kappa\dot{\phi}}{\sqrt{6}H}\left[- 3 + \frac{3H\alpha y^2}{\kappa\dot{\phi}} + \frac{3H\beta z^2}{\kappa\dot{\phi}} - \frac{\dot{H}}{H^2}\right] . \end{aligned} \tag{B.30}$$

Now we simply substitute in the acceleration equation (B.28) and tidy up term,

$$\begin{aligned} x' &= -3x + \sqrt{\frac{3}{2}}\alpha y^2 + \sqrt{\frac{3}{2}}\beta z^2 + \frac{3}{2}x\Big(w(1-x^2-y^2-z^2) + x^2 - y^2 - z^2 + 1\Big) \\ x' &= -\frac{3}{2}x\Big[(w+1)(x^2+y^2+z^2-1) - 2x^2 + 2\Big] + \frac{\sqrt{3}}{\sqrt{2}}(\alpha y^2 + \beta z^2) \ . \end{aligned} \tag{B.31}$$

Doing the same for y and taking the derivative,

$$\begin{aligned} y' \equiv \frac{dy}{dN} &= \frac{1}{H}\frac{dy}{dt} = \frac{1}{H}\frac{d}{dt}\Big(\frac{\kappa V_1^{1/2}\mathrm{e}^{-\kappa\alpha\phi/2}}{\sqrt{3}H}\Big) \\ &= \frac{\kappa V^{1/2}}{\sqrt{3}H}\left(-\frac{\kappa\alpha\dot{\phi}\mathrm{e}^{-\kappa\alpha\phi/2}}{2H} - \frac{\dot{H}\mathrm{e}^{-\kappa\alpha\phi/2}}{H^2}\right) \\ &= -\frac{\kappa\alpha y\dot{\phi}}{2H} - y\frac{\dot{H}}{H^2} \\ &= -\frac{\sqrt{6}\alpha xy}{2} - y\frac{\dot{H}}{H^2} \ . \end{aligned} \tag{B.32}$$

Now we again substitute in the acceleration equation (B.28) and tidy up the remaining terms,

$$\begin{aligned} y' &= y\frac{3}{2}\Big(w(1-x^2-y^2-z^2) + x^2 - y^2 - z^2 + 1\Big) - \frac{\sqrt{3}}{\sqrt{2}}\alpha xy \\ &= -\frac{3}{2}y\Big[(w+1)(x^2+y^2+z^2-1) - 2x^2\Big] - \frac{\sqrt{2}}{\sqrt{2}}\alpha xy \ . \end{aligned} \tag{B.33}$$

The calculation for z' almost identical to y' and can be followed from the above derivation.

B.3 Cosmological Time and Redshift

Here we shall derive the equation 5.28 and also make a naive calculation relating our parameter N to time t in a universe dominated by both matter and dark energy.

Starting with the definition,

$$N \equiv \log a(t) \ , \tag{B.34}$$

where log refers to the natural logarithm, let us plug in today's values of $N_0 = 5$ and $a_0 = 1$ (inferred from Figure 5),

$$\begin{aligned} N - N_0 &= \log a(t) - \log a_0 = \log \frac{a}{a_0} \\ \mathrm{e}^{N-N_0} &= \frac{a(t)}{a_0} \\ \mathrm{e}^{N-5} &= a(t) \ . \end{aligned} \tag{B.35}$$

Next we use the relation between the scale factor and redshift, making a a function of z instead of t,

$$a(z) = \frac{1}{1+z} \ , \tag{B.36}$$

such that

$$\begin{aligned} a(z) &= \mathrm{e}^{N-5} \\ \frac{1}{1+z} &= \mathrm{e}^{N-5} \\ z &= \mathrm{e}^{5-N} - 1 \ . \end{aligned} \tag{B.37}$$

For $N = 5$ we correctly obtain a redshift of $z = 0$, and for smaller N we obtain larger redshifts.

Next we can use the solution for $a(t)$ in a universe comprised of both matter and dark energy (with zero curvature) [100],

$$a(t) = a_0 \Big(\frac{\Omega_{m0}}{\Omega_{\Lambda 0}} \Big)^{\frac{1}{3}} \Big(\sinh \big(\frac{3}{2} H_0 \Omega_{\Lambda 0}^{\frac{1}{2}} t \big) \Big)^{\frac{3}{2}} \ , \tag{B.38}$$

where Ω_{m0} and $\Omega_{\Lambda 0}$ denote the values of the density parameters for matter and radiation today. Using equation (B.35) we can then relate time t and the parameter N.

$$t = \frac{1}{H_0} \frac{2}{3\sqrt{0.7}} \sinh^{-1} \left[\left(\frac{\mathrm{e}^{N-N_0}}{0.754} \right)^{3/2} \right] \ , \tag{B.39}$$

$$N = \log \left[0.754 \Big(\sinh \big(\frac{3}{2} \sqrt{0.7} H_0 t \big) \Big)^{\frac{3}{2}} \right] + N_0 \tag{B.40}$$

For the initial value $N_i \approx 4.5$ and final value $N_f \approx 5.5$ we can simply calculate $\Delta t = t_f - t_i$ using equation (B.39). This calculation yields

$$\Delta t = \frac{1}{H_0}(1.506 - 0.534) = \frac{1}{H_0}(0.972) \ , \tag{B.41}$$

which is comparable to the age of the universe. For reference, the age of the universe using $N = N_0$ is calculated to be $0.961/H_0$. With a value of $H_0 = 70\text{kms}^{-1}\text{Mpc}^{-1}$ this is simply

$$0.961 \times 1.40 \times 10^8\text{yr} = 13.4\text{Gyr} \tag{B.42}$$

B.4 Swampland Criterion Analysis of the Double Exponential Potential

Given a general double exponential potential of the form

$$V(x) = V_1 \mathrm{e}^{\lambda_1 x} + V_2 \mathrm{e}^{\lambda_2 x} \quad , \tag{B.43}$$

let us apply the LHS of the swampland criterion $\frac{|\nabla V|}{V}$ (6.2). Assuming we can take the derivative to mean $\nabla = \partial_x$, this gives us

$$\frac{|\nabla V|}{V} = \frac{|\lambda_1 V_1 \mathrm{e}^{\lambda_1 x} + \lambda_2 V_2 \mathrm{e}^{\lambda_2 x}|}{V_1 \mathrm{e}^{\lambda_1 x} + V_2 \mathrm{e}^{\lambda_2 x}} \quad . \tag{B.44}$$

To investigate the general properties of the above function, as well its range[32], consider the cases of the λ's possessing different signs. To start with, we will also assume that V_1 and V_2 are both positive; their absolute values are not relevant. The analysis is straight forward and as follows:

$\lambda_1, \lambda_2 > 0$: When both exponents are positive the lower bound is given by the smaller of the two (λ_1 or λ_2 as $x \to -\infty$). The upper bound is given by the bigger of the two (λ_1 or λ_2, as $x \to +\infty$). If $\lambda_1 = \lambda_2$ it is simply a straight line (single exponential case). See Figure 17 (left).

$\lambda_1, \lambda_2 < 0$: When both the exponents are negative we have a similar case as above, just with a flip in the y-axis. Again, the lower bound is the smaller of the exponents (λ_1 or λ_2 but as $x \to +\infty$), the upper bound is the bigger of the exponents (λ_1 or λ_2, as $x \to -\infty$), and for $\lambda_1 = \lambda_2$ we have a constant. See Figure 17 (middle).

$\lambda_1 > 0, \lambda_2 < 0$: If one exponent is negative and the other is positive then the functions minimum is always zero. The function asymptomatically approaches the positive exponent as $x \to \infty$ and the negative exponent as $x \to -\infty$, and touches zero in between (Figure 17) (right).

Note that for the case of V_1 or $V_2 < 0$ we must only consider the range where the potential is positive, $V > 0$. This is because if $V < 0$ then the swampland criterion, in its original form $|\nabla V| \geq V \cdot c$, is trivially satisfied.

[32] In most cases the function asymptotically approaches some constant value as $x \to \pm\infty$. We shall take that value as the appropriate bound.

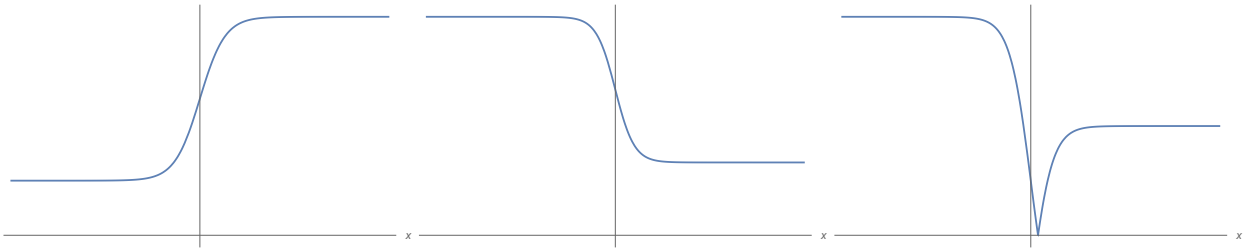

Figure 17: Shape of $\frac{|\nabla V|}{V}$ for: $\lambda_1, \lambda_2 > 0$ (left), $\lambda_1, \lambda_2 < 0$ (middle) and $\frac{|\nabla V|}{V}$ for $\lambda_1 < 0 < \lambda_2$ (right).

For the specific case of the M-theory compactification example (Section 6.2), we have $\lambda_1 > \lambda_2$ and V_2 is always positive. The case when V_1 is positive is described above. Let us examine when V_1 is negative. Excluding the region where $V < 0$, the function (B.44) is bounded only from below by λ_2. Figure 18 includes both the potential (B.43) and the function (B.44). Note that in the region where $V > 0$ our function is always positive.

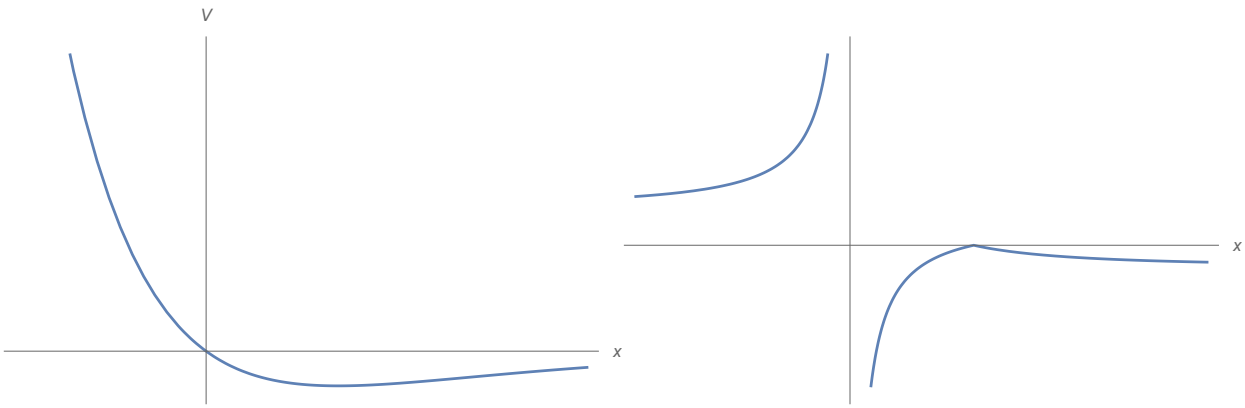

Figure 18: The potential $V(x)$ (left) is positive for $x < 0$. In this region the function $\frac{|\nabla V|}{V}$ (right) is bounded from below by the larger exponent λ_2.

C Extra Figures

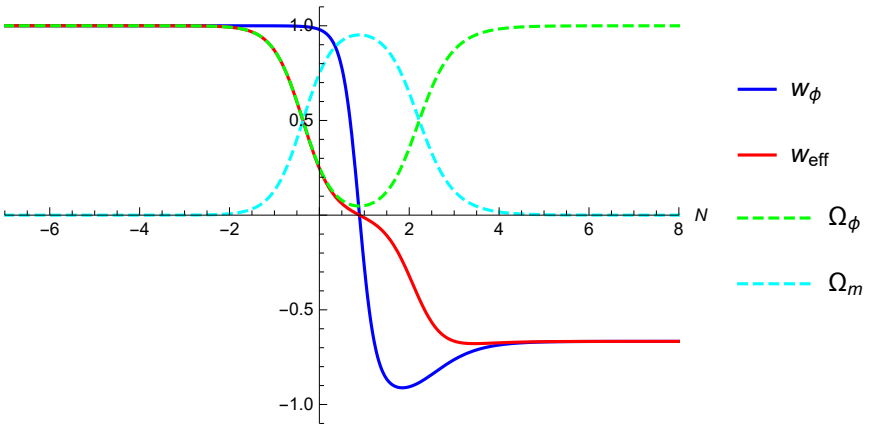

(a) $\lambda = 1$, $w = 0$; $x[N = 0] = 0.5$, $y[N = 0] = 0.05$.

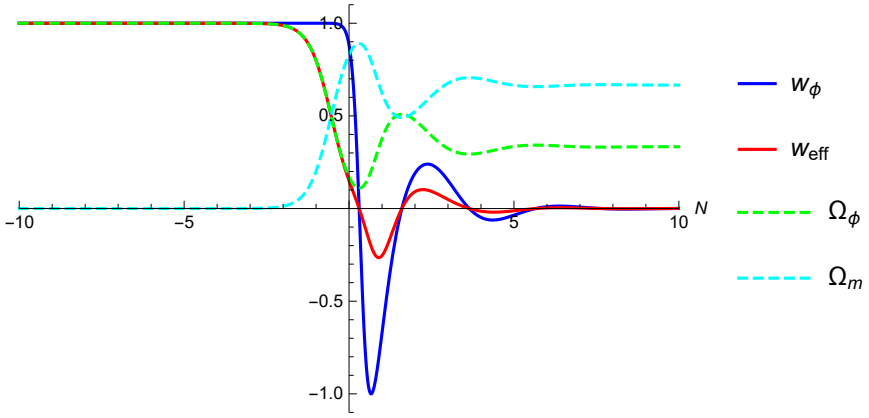

(b) $\lambda = 3$, $w = 0$; $x[N = 0] = 0.4$ $y[N = 0] = 0.1$.

Figure 19: (Single exponential potential Section 4.3). Evolution of cosmological parameters. If Subfigure (a) ($\lambda = 1$) the initial conditions have been displaced slightly from the y-axis and hence matter domination does not occur for a significant period of time before dark energy domination. In Subfigure (b) ($\lambda = 3$) we see the scaling solution effects, where the effective equation of state comes to $w_{eff} = w$ no matter the initial conditions.

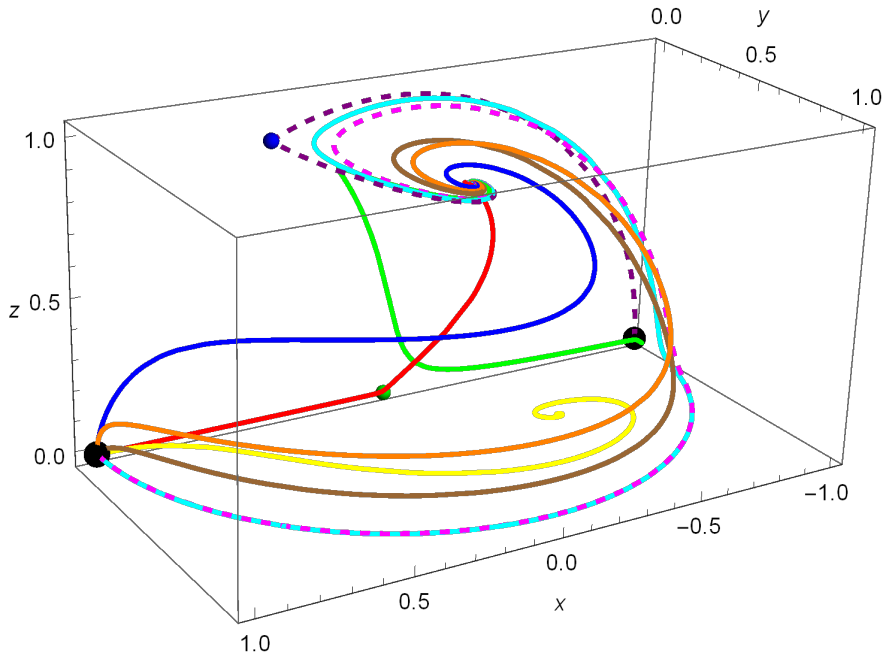

(a) Orbit of multiple trajectories through phase space. Point (i) is represented by the green ball, points $(ii)_{\pm}$ are represented by the black balls and point (vi) is represented by the blue ball. All of the trajectories, bar one, converge on the de-Sitter solution (vii) at late times. The yellow trajectory is confined the $z = 0$ plane.

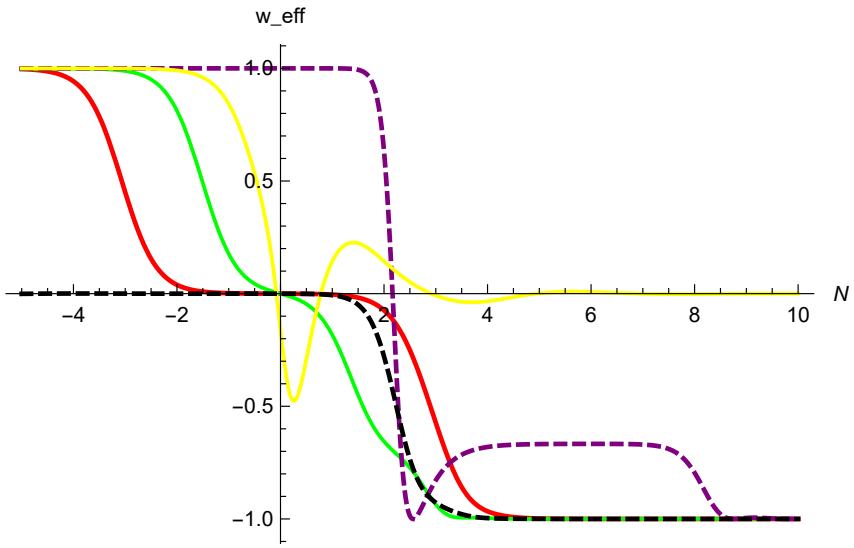

(b) Evolution of w_{eff} for some of the trajectories plotted above.

Figure 20: (Double exponential potential Section 4.4). Numerical solutions to the autonomous equations (5.35)-(5.37) for $\alpha = -3$, $\beta = 1$ and $w = 0$. Subfigure (a) shows multiple orbits with different initial conditions, whilst Subfigure (b) shows the corresponding evolution of w_{eff} for several of the orbits. All initial conditions with $z \neq 0$ end up at the de Sitter late-time attractor.

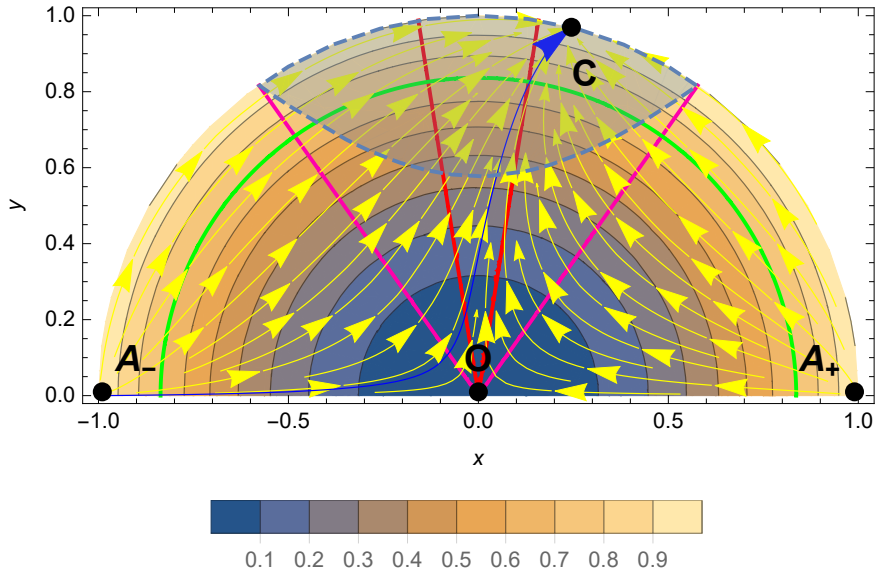

(a) Phase space for $\lambda = 0.6$ and $w = 0$. The blue orbit originates at the past attractor A_- and passes through a point $(-0.5, 0.01)$ at $N = 0$. The orbit is then attracted towards the Saddle O along the x-axis, before being attracted to the late-time accelerating attractor, point C.

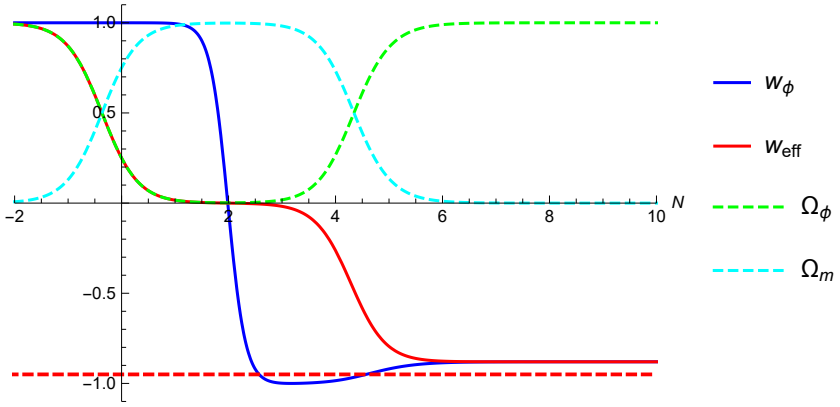

(b) Evolution of the cosmological parameters for the blue trajectory in the phase space above.

Figure 21: (Single exponential potential Section 6.3) Solutions for the single exponential potential along with the swampland constraints. he free parameters are set to $\lambda = 0.6$ and $w = 0$, and the initial conditions for the blue orbit are $(-0.5, 0.01)$ at $N = 0$. Here we sufficiently close to the x-axis so that the solution has enters a matter domination phase near point O. This orbit is not in conflict with the swampland constraints 1-4 (Section 6.4.1).

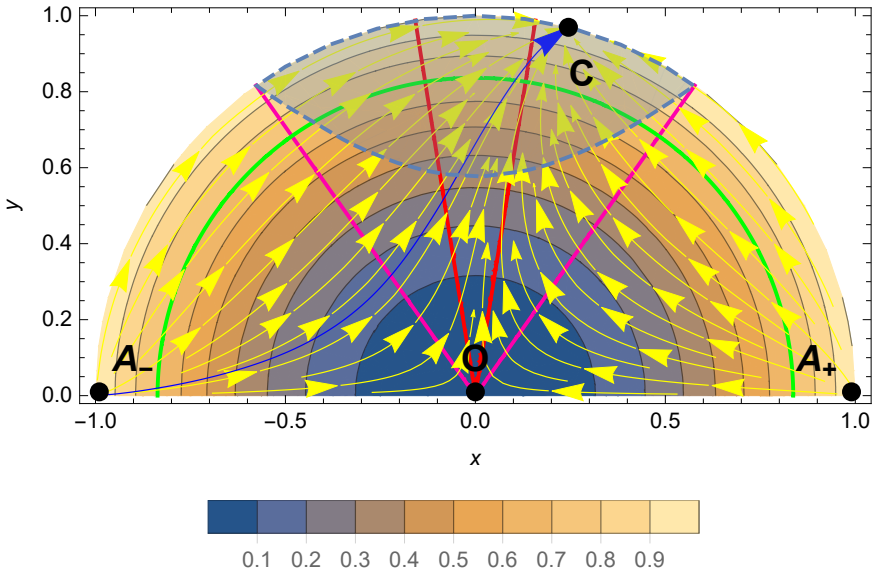

(a) Phase space for $\lambda = 0.6$ and $w = 0$. The blue orbit originates at the past attractor A_- and passes through a point $(-0.9, 0.01)$ at $N = 0$. The orbit is attracted to the late-time attractor C without passing close to point O at the origin.

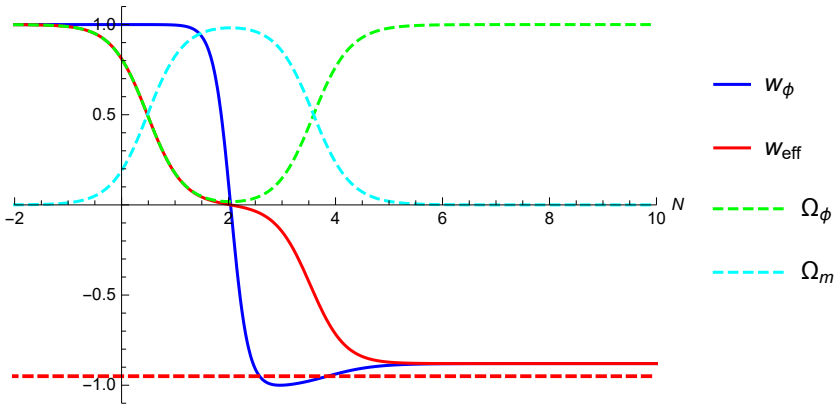

(b) Evolution of the cosmological parameters for the blue trajectory in the phase space above. The effective equation of state w_{eff} does not stay at

Figure 22: (Single exponential potential Section 6.3). Solutions for the single exponential potential along with the swampland constraints. The free parameters are set to $\lambda = 0.6$ and $w = 0$, and the initial conditions for the blue orbit are $(-0.9, 0.01)$ at $N = 0$. Despite beginning close to the x-axis, it is far enough away from the origin O that the orbit is in conflict with the swampland constraints 1-4 (Section 6.4.1).

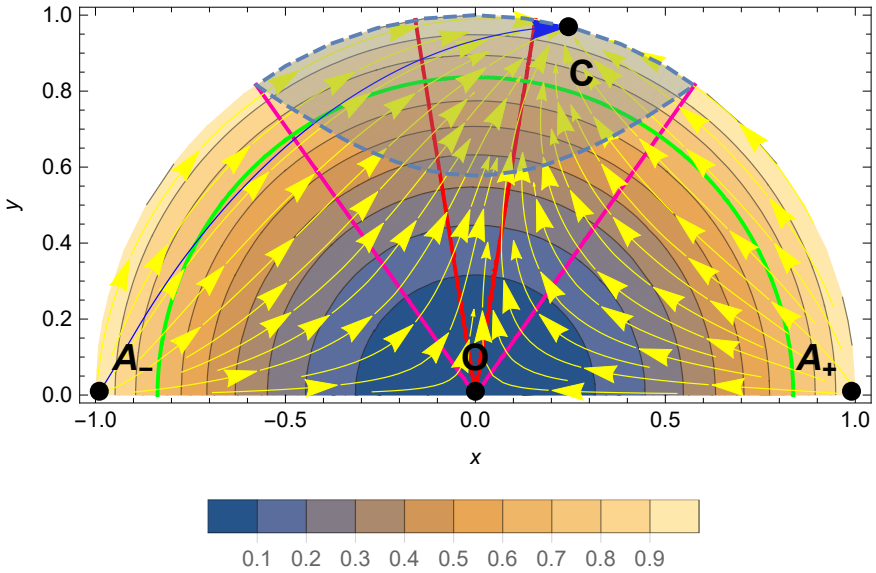

(a) Phase space for $\lambda = 0.6$ and $w = 0$. The initial conditions of the blue orbit, $(-0.99, 0.01)$ at $N = 0$, is now very close to the past attractor A_-. The trajectory is in major conflict with all cosmological observations.

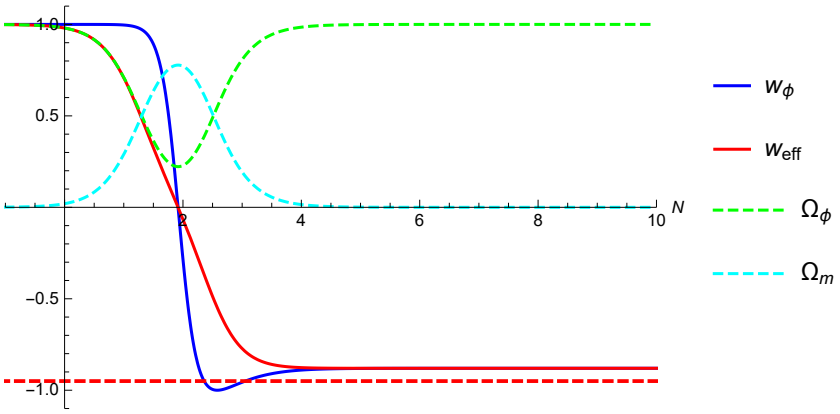

(b) Evolution of the cosmological parameters for the blue trajectory in the phase space above. The effective equation of state w_{eff} quickly comes to its final value at the critical point C (see table 2 for the exact value).

Figure 23: (Single exponential potential Section 6.3). Solutions for the single exponential potential along with the swampland constraints. The free parameters are set to $\lambda = 0.6$ and $w = 0$, and the initial conditions for the blue orbit are $(-0.99, 0.01)$ at $N = 0$. This solution, with an initial condition arbitrarily close to the past attractor A_-, is clearly not a viable trajectory and is in conflict with the swampland constraints 1-4 (Section 6.4.1).

References

[1] Collins, C.B., 1971. More qualitative cosmology. Communications in Mathematical Physics, 23(2), pp.137-158.

[2] Collins, C.B., 1972. Qualitative magnetic cosmology. Communications in Mathematical Physics, 27(1), pp.37-43.

[3] Bogoiavlenskii, O.I. and Novikov, S.P., 1973. Singularities of the cosmological model of the Bianchi IX type according to the qualitative theory of differential equations. Soviet Physics-JETP, 37, pp.747-755.

[4] Bahamonde, S., Boehmer, C.G., Carloni, S., Copeland, E.J., Fang, W. and Tamanini, N., 2017. Dynamical systems applied to cosmology: dark energy and modified gravity. arXiv preprint arXiv:1712.03107.

[5] Obied, G., Ooguri, H., Spodyneiko, L. and Vafa, C., 2018. De Sitter space and the Swampland. arXiv preprint arXiv:1806.08362.

[6] Agrawal, P., Obied, G., Steinhardt, P.J. and Vafa, C., 2018. On the cosmological implications of the string Swampland. Physics Letters B.

[7] Coley, A.A., 1999. Dynamical systems in cosmology. arXiv preprint gr-qc/9910074.

[8] Strogatz, S.H., 2018. Nonlinear dynamics and chaos: with applications to physics, biology, chemistry, and engineering. CRC Press.

[9] Glendinning, P., 1994. Stability, instability and chaos: an introduction to the theory of nonlinear differential equations (Vol. 11). Cambridge university press.

[10] Wiggins, S., 2003. Introduction to applied nonlinear dynamical systems and chaos (Vol. 2). Springer Science & Business Media.

[11] Wainwright, J. and Ellis, G.F.R. eds., 2005. Dynamical systems in cosmology. Cambridge University Press.

[12] Dahleh, M., Dahleh, M.A. and Verghese, G., 2004. Lectures on dynamic systems and control. A+ A, 4(100), pp.1-100.

[13] Charters, T.C., Nunes, A. and Mimoso, J.P., 2001. Stability analysis of cosmological models through Lyapunov's method. Classical and Quantum Gravity, 18(9), p.1703.

[14] Dodelson, S., 2003. Modern cosmology. Elsevier.

[15] Ryden, B., 2016. Introduction to cosmology. Cambridge University Press.

[16] Winberg, S., 1972. Gravitation and cosmology. ed. John Wiley and Sons, New York.

[17] Carroll, S.M., 2004. Spacetime and geometry. An introduction to general relativity.

[18] Perez, J., et al., 2014. The Jungle Universe: coupled cosmological models in a LotkaVolterra framework. General Relativity and Gravitation, 46(6), p.1753.

[19] Aghanim, N., et al., 2018. Planck 2018 results. VI. Cosmological parameters. arXiv preprint arXiv:1807.06209.

[20] Riess, A.G., et al., 1998. Observational evidence from supernovae for an accelerating universe and a cosmological constant. The Astronomical Journal, 116(3), p.1009.

[21] Riess, A.G., et al., 2016. A 2.4% determination of the local value of the Hubble constant. The Astrophysical Journal, 826(1), p.56.

[22] Riess, A.G., et al., 2018. Milky Way Cepheid standards for measuring cosmic distances and application to Gaia DR2: implications for the Hubble constant. The Astrophysical Journal, 861(2), p.126.

[23] Tegmark, M., et al., 2004. Cosmological parameters from SDSS and WMAP. Physical Review D, 69(10), p.103501.

[24] Koivisto, T. and Mota, D.F., 2006. Dark energy anisotropic stress and large scale structure formation. Physical Review D, 73(8), p.083502.

[25] Clifton, T., Ferreira, P.G., Padilla, A. and Skordis, C., 2012. Modified gravity and cosmology. Physics reports, 513(1-3), pp.1-189.

[26] Rugh, S.E. and Zinkernagel, H., 2002. The quantum vacuum and the cosmological constant problem. Studies In History and Philosophy of Science Part B: Studies In History and Philosophy of Modern Physics, 33(4), pp.663-705.

[27] Carroll, S.M., Press, W.H. and Turner, E.L., 1992. The cosmological constant. Annual review of astronomy and astrophysics, 30(1), pp.499-542.

[28] Padilla, A., 2015. Lectures on the cosmological constant problem. arXiv preprint arXiv:1502.05296.

[29] Steinhardt, P.J., Fitch, V.L. and Marlow, D.R., 1997. Critical problems in physics. edited by VL Fitch et al. DR Marlow & MAE Dementi (Princeton Univ. 1997).

[30] Susskind, L., 2007. The anthropic landscape of string theory. Universe or multiverse, pp.247-266.

[31] Linde, A., 2017. A brief history of the multiverse. Reports on Progress in Physics, 80(2), p.022001.

[32] Douglas, M.R., 2003. The statistics of string/M theory vacua. Journal of High Energy Physics, 2003(05), p.046.

[33] Carter, B., 1974. Large number coincidences and the anthropic principle in cosmology. In Symposium-international astronomical union (Vol. 63, pp. 291-298). Cambridge University Press.

[34] Efstathiou, G., 1995. An anthropic argument for a cosmological constant. Monthly Notices of the Royal Astronomical Society, 274(1), pp.L73-L76.

[35] Townsend, P.K., 2001. Quintessence from M-theory. Journal of High Energy Physics, 2001(11), p.042.

[36] Hellerman, S., Kaloper, N. and Susskind, L., 2001. String theory and quintessence. Journal of High Energy Physics, 2001(06), p.003.

[37] Schwarz, J.H., 2012. The early history of string theory and supersymmetry. arXiv preprint arXiv:1201.0981.

[38] Donoghue, J.F., 1994. General relativity as an effective field theory: The leading quantum corrections. Physical Review D, 50(6), p.3874.

[39] Shomer, A., 2007. A pedagogical explanation for the non-renormalizability of gravity. arXiv preprint arXiv:0709.3555.

[40] Becker, K., Becker, M. and Schwarz, J.H., 2006. String theory and M-theory: A modern introduction. Cambridge University Press.

[41] Polchinski, J., 1998. String theory: Volume 1 & 2, superstring theory and beyond. Cambridge university press.

[42] Zwiebach, B., 2004. A first course in string theory. Cambridge university press.

[43] McAllister, L. and Silverstein, E., 2008. String cosmology: a review. General Relativity and Gravitation, 40(2-3), pp.565-605.

[44] Lidsey, J.E., Wands, D. and Copeland, E.J., 2000. Superstring cosmology. Physics Reports, 337(4-5), pp.343-492.

[45] Kachru, S., et al., 2003. Towards inflation in string theory. Journal of Cosmology and Astroparticle Physics, 2003(10), p.013.

[46] Conlon, J.P. and Quevedo, F., 2006. Khler moduli inflation. Journal of High Energy Physics, 2006(01), p.146.

[47] Baumann, D. and McAllister, L., 2015. Inflation and string theory. Cambridge University Press.

[48] Kachru, S., et al., 2003. De Sitter vacua in string theory. Physical Review D, 68(4), p.046005.

[49] Ng, S.C.C., Nunes, N.J. and Rosati, F., 2001. Applications of scalar attractor solutions to cosmology. Physical Review D, 64(8), p.083510.

[50] Bousso, R. and Polchinski, J., 2000. Quantization of four-form fluxes and dynamical neutralization of the cosmological constant. Journal of High Energy Physics, 2000(06), p.006.

[51] Vafa, C., 2005. The string landscape and the swampland. arXiv preprint hep-th/0509212.

[52] Kaluza, T., 1921. Zum unittsproblem der physik. Sitzungsberichte der Kniglich Preuischen Akademie der Wissenschaften (Berlin), Seite p. 966-972, pp.966-972.

[53] Klein, O., 1926. Quantum Theory and Five-Dimensional Theory of Relativity.(In German and English). Surveys High Energ. Phys., 5, pp.895-906.

[54] Quevedo, F., Krippendorf, S. and Schlotterer, O., 2010. Cambridge lectures on supersymmetry and extra dimensions (No. MPP-2010-143).

[55] Duff, M.J. and Pope, C.N., 1985. Consistent truncations in Kaluza-Klein theories. Nuclear Physics B, 255, pp.355-364.

[56] Grana, M., 2006. Flux compactifications in string theory: A comprehensive review. Physics reports, 423(3), pp.91-158.

[57] Douglas, M.R. and Kachru, S., 2007. Flux compactification. Reviews of Modern Physics, 79(2), p.733.

[58] Denef, F., Douglas, M.R. and Kachru, S., 2007. Physics of string flux compactifications. Annu. Rev. Nucl. Part. Sci., 57, pp.119-144.

[59] Pilch, K., Van Nieuwenhuizen, P. and Sohnius, M.F., 1985. De Sitter superalgebras and supergravity. Communications in Mathematical Physics, 98(1), pp.105-117.

[60] Maldacena, J. and Nunez, C., 2001. Supergravity description of field theories on curved manifolds and a no go theorem. International Journal of Modern Physics A, 16(05), pp.822-855.

[61] Steinhardt, P.J., 2003. A quintessential introduction to dark energy. Philosophical Transactions of the Royal Society of London A: Mathematical, Physical and Engineering Sciences, 361(1812), pp.2497-2513.

[62] Copeland, E.J., Liddle, A.R. and Wands, D., 1998. Exponential potentials and cosmological scaling solutions. Physical Review D, 57(8), p.4686.

[63] Steinhardt, P.J., Wang, L. and Zlatev, I., 1999. Cosmological tracking solutions. Physical Review D, 59(12), p.123504.

[64] Ferreira, P.G. and Joyce, M., 1998. Cosmology with a primordial scaling field. Physical Review D, 58(2), p.023503.

[65] Velten, H.E.S., vom Marttens, R.F. and Zimdahl, W., 2014. Aspects of the cosmological coincidence problem. The European Physical Journal C, 74(11), p.3160.

[66] Azreg-Anou, M., 2013. Phase-space analysis of the cosmological 3-fluid problem: families of attractors and repellers. Classical and Quantum Gravity, 30(20), p.205001.

[67] Barreiro, T., Copeland, E.J. and Nunes, N.A., 2000. Quintessence arising from exponential potentials. Physical Review D, 61(12), p.127301.

[68] Li, X.Z., Zhao, Y.B. and Sun, C.B., 2005. The heteroclinic orbit and tracking attractor in a cosmological model with a double exponential potential. Classical and Quantum Gravity, 22(17), p.3759.

[69] Gonzalez, T., Leon, G. and Quiros, I., 2006. Dynamics of quintessence models of dark energy with exponential coupling to dark matter. Classical and Quantum Gravity, 23(9), p.3165.

[70] Ratra, B. and Peebles, P.J., 1988. Cosmological consequences of a rolling homogeneous scalar field. Physical Review D, 37(12), p.3406.

[71] Peebles, P.J.E. and Ratra, B., 1988. Cosmology with a time-variable cosmological'constant'. The Astrophysical Journal, 325, pp.L17-L20.

[72] Tamanini, N., 2014. Dynamical systems in dark energy models (Doctoral dissertation, UCL (University College London)).

[73] Carr, J., 2012. Applications of centre manifold theory (Vol. 35). Springer Science & Business Media.

[74] Caldwell, R.R. and Linder, E.V., 2005. Limits of quintessence. Physical review letters, 95(14), p.141301.

[75] Clemson, T.G. and Liddle, A.R., 2009. Observational constraints on thawing quintessence models. Monthly Notices of the Royal Astronomical Society, 395(3), pp.1585-1590.

[76] Copeland, E.J., Sami, M. and Tsujikawa, S., 2006. Dynamics of dark energy. International Journal of Modern Physics D, 15(11), pp.1753-1935.

[77] Danielsson, U.H. and Riet, T.V., 2018. What if string theory has no de Sitter vacua?. International Journal of Modern Physics D.

[78] Akrami, Y., et al. 2018. The landscape, the swampland and the era of precision cosmology, arXiv:1808.09440v1.

[79] Cicoli, M., et al., 2018. De Sitter vs Quintessence in String Theory, arXiv:1808.08967.

[80] Kachura, S., Trivedi,. S.P, 2018, A comment on effective field theories of flux vacua, arXiv:1808.08971.

[81] Andriot, D., 2018. On the de Sitter swampland criterion. arXiv preprint arXiv:1806.10999.

[82] Andriot, D., 2018. New constraints on classical de Sitter: flirting with the swampland. arXiv preprint arXiv:1807.09698.

[83] Dvali, G. and Gomez, C., 2018. On Exclusion of Positive Cosmological Constant. arXiv preprint arXiv:1806.10877.

[84] Colgin, E.., van Putten, M.H. and Yavartanoo, H., 2018. H_0 tension and the de Sitter Swampland. arXiv preprint arXiv:1807.07451.

[85] Ben-Dayan, I., 2018. Draining the Swampland. arXiv preprint arXiv:1808.01615.

[86] Lehners, J.L., 2018. Small-Field and Scale-Free: Inflation and Ekpyrosis at their Extremes. arXiv preprint arXiv:1807.05240.

[87] Heisenberg, L., et al. 2018. Dark Energy in the Swampland. arXiv preprint arXiv:1808.02877.

[88] Banerjee, S., et al., 2018. Emergent de Sitter cosmology from decaying AdS. arXiv preprint arXiv:1807.01570.

[89] Achcarro, A. and Palma, G.A., 2018. The string swampland constraints require multi-field inflation. arXiv preprint arXiv:1807.04390.

[90] Alvarez-Gaume, L., Ginsparg, P., Moore, G. and Vafa, C., 1986. An O (16) O (16) heterotic string. Physics Letters B, 171(2-3), pp.155-162.

[91] Karthauser, J.L. and Saffin, P.M., 2006. Scaling solutions and geodesics in moduli space. Classical and Quantum Gravity, 23(14), p.4615.

[92] Barreiro, T., De Carlos, B. and Copeland, E.J., 1998. Stabilizing the dilaton in superstring cosmology. Physical Review D, 58(8), p.083513.

[93] Scolnic, D.M., et al., 2017. The Complete Light-curve Sample of Spectroscopically Confirmed Type Ia Supernovae from Pan-STARRS1 and Cosmological Constraints from The Combined Pantheon Sample. arXiv preprint arXiv:1710.00845.

[94] Bean, R., Hansen, S.H. and Melchiorri, A., 2001. Early-universe constraints on dark energy. Physical Review D, 64(10), p.103508.

[95] Chiba, T., De Felice, A. and Tsujikawa, S., 2013. Observational constraints on quintessence: Thawing, tracker, and scaling models. Physical Review D, 87(8), p.083505.

[96] Akrami, Y., Kallosh, R., Linde, A. and Vardanyan, V., 2018. Dark energy, -attractors, and large-scale structure surveys. Journal of Cosmology and Astroparticle Physics, 2018(06), p.041.

[97] Peebles, P.J.E. and Vilenkin, A., 1999. Quintessential inflation. Physical Review D, 59(6), p.063505.

[98] Krippendorf, S., Quevedo, F. and Schlotterer, O., 2010. Cambridge Lectures on Supersymmetry and Extra Dimensions. arXiv preprint arXiv:1011.1491.

[99] Wald, R.M., 1984. General Relativity, Chicago, Usa: Univ. Pr. 491p.

[100] Kolb, E., 2018. The early universe. CRC Press.